Orthogonal Frequency Division Multiplexing for Next Generation Optical Networks

Colm Browning

B.A., B.A.I.

A Dissertation submitted in fulfilment of the

requirements for the award of

Doctor of Philosophy (Ph.D.)

to the

Dublin City University

Faculty of Engineering and Computing, School of Electronic Engineering

Supervisor: Prof. Liam P. Barry

1st October 2013

Declaration

I hereby certify that this material, which I now submit for assessment on the programme of study leading to the award of Doctor of Philosophy is entirely my own work, and that I have exercised reasonable care to ensure that the work is original, and does not to the best of my knowledge breach any law of copyright, and has not been taken from the work of others save and to the extent that such work has been cited and acknowledged within the text of my work.

Signed:

ID No.:

Date:

Contents

Abstract

Next generation optical networks will be required to provide increased data throughput on a greater number of optical channels and will also have to facilitate network flexibility in order to adapt to dynamic traffic patterns. Furthermore, the potentially wide deployment of optical Access and Metropolitan networks in particular require that these challenges are met in a cost effect manner.

This thesis examines the use of Orthogonal Frequency Division Multiplexing (OFDM) as a means of helping to meet these requirements for next generation optical systems with a high market volume. OFDM is a multi–carrier modulation technique which exhibits high spectral efficiency and a tolerance to chromatic dispersion making it an excellent candidate for use in next generation optical networks.

The work presented in this thesis shows how the use of OFDM in conjunction with novel laser devices and direct detection can be used to construct cost effective, low footprint optical systems. These systems are capable of providing $>$10Gb/s per optical channel and are suitable for implementation as optical access networks. Furthermore, OFDM is shown to be a realistic candidate for use in an optical switching environment where external modulation is employed and, as such, can be considered for use in next generation metropolitan networks.

Acknowledgements

Firstly, I would like to acknowledge the constant support of my parents, Frank and Úna, and my sister Heather throughout my entire education. Without their encouragement and guidance I certainly would not be in a position today to complete a Ph.D.

I would like to thank my supervisor Prof. Liam Barry both for the faith he showed in me by accepting me as his student and for the continual support and encouragement he provided throughout my time in DCU. I could not think of a better supervisor to have.

I would also like to acknowledge the enormous help I received from my colleagues at DCU; Prince, Frank, Sylwester, Rob, Karl, Josue, Eamonn, Vidak and Robert Clare. In particular I would like to thank my friend Kai Shi who has been so patient with me and from whom I have learned so much. His assistance throughout my research (and on the football pitch) has been nothing but absolutely invaluable.

A special thanks goes to my friend Paul Teahan who helped to facilitate my research/life balance, which is extremely important!

Lastly, I would like to thank Louise for helping me to keep a perspective on things and who made life so much easier throughout my studies.

A.I.C.

To Louise,

my great friend and companion,

miss you always.

Love,

Colm

List of Figures

List of Tables

List of Acronyms

ADC AnaloguetoDigital Converter

ADSL Asymmetric Digital Subscriber Line

AM–OFDM Adaptive Modulation Orthogonal Frequency Division Multiplexing

APD Avalanche Photo-detector

ASE Amplified Spontaneous Emission

ASK Amplitude Shift Keying

ATM Asynchronous Transfer Mode

AWG Arbitrary Waveform Generator, Arrayed Waveguide Filter

BER Bit Error Rate

BMRx Burst Mode Receiver

CO Central Office

CompSSB Compatible Single Sideband

CP Cyclic Prefix

CW Constant Wave

DAC Digital–to–Analogue Converter

DCF Dispersion Compensated Fibre

DFB Distributed Feedback

DM Discrete Mode

DMT Discrete MultiTone

DPSK Differential Phase Shift Keying

DQPSK Differential Quadrature Phase Shift Keying

DSB Double Sideband

DSL Digital Subscriber Line

DSP Digital Signal Processing

ECL External Cavity Laser

EDFA Erbium Doped Fibre Amplifier

EPON Ethernet Passive Optical Network

EQ Equalisation

EVM Error Vector Magnitude

FDM Frequency Division Multiplexing

FEC Forward Error Correction

FFT Fast Fourier Transform

FP Fabry Perét

FTTH Fibre-to-the-Home

GPON Gigabit Passive Optical Network

HDTV High Definition Television

HFC Hybrid Fibre–Co–axial

IDFT Inverse Discrete Fourier Transform

IFFT Inverse Fast Fourier Transform

IMD3 Third Order Inter-modulation Distortion

IP Internet Protocol

IPTV Internet Protocol Television

ISP Internet Service Provider

LC Levin–Campello

LO Local Oscillator

LTE Long Term Evolution

MAN Metropolitan Area Network

MCM Multi–Carrier Modulation

MMF Multi–Mode Fibre

MZM MachZehnder Modulator

NLSE Nonlinear Schrödinger Equation

OAN Optical Access Network

OBI Optical Beat Interference

OBPF Optical Bandpass Filter

OBS Optical Burst Switching

OECD Organisation for Economic Cooperation and Development

OFDM Orthogonal Frequency Division Multiplexing

OFDMA Orthogonal Frequency Division Multiple Access

OLT Optical Line Terminal

OMI Optical Modulation Index

ONU Optical Network Unit

OOK On–Off Keying

OPS Optical Packet Switching

PAPR Peak–to–Average Power Ratio

PLL Phase Locked Loop

POF Plastic Optical Fibre

PON Passive Optical Network

POTS Plain Old Telephone Service

PSK Phase Shift Keying

QAM Quadrature Amplitude Modulation

QPSK Quadrature Phase Shift Keying

RB Rayleigh Backscattering

RF Radio Frequency

RMS RootMeanSquare

RN Remote Node

ROADM Reconfigurable Optical Adddrop Multiplexers

ROF Radio–over–Fibre

RSOA Reflective Semiconductor Optical Amplifier

RTS Real Time Oscilloscope

SDH Synchronous Digital Hierarchy

SFP Slotted Fabry Perót

SG–DBR Sampled Grating Distributed Bragg Reflector

SMSR Side Mode Suppression Ratio

SNR Signal–to–Noise Ratio

SOA Semiconductor Optical Amplifier

SONET Synchronous Optical Networking

SSB Single Sideband

SSMF Standard Single Mode Fibre

TDM Time Division Multiplexing

TDMA Time Division Multiple Access

TIA Trans-Impedance Amplifier

TS Training Sequence

UDWDM Ultra Dense Wavelength Division Multiplexing

VOA Variable Optical Attenuator

VoIP Voice-over-IP

WDM Wavelength Division Multiplexing

WDM Wavelength Division Multiple Access

WiMAX Worldwide Interoperability for Microwave Access

WLAN Wireless Local Area Network

Introduction

The ever increasing demand for higher internet speeds, driven by media-rich applications such as on–demand HDTV, Voice over IP (VoIP), video conferencing and online gaming, will require Internet Service Providers (ISPs) to upgrade their existing networks to satisfy the needs of both residential and commercial customers as current Ethernet speeds of 10Gb/s will be upgraded to 100Gb/s. Current Core and Metropolitan Area Networks are employing optical multiplexing to help to meet increasing data rate requirements. The development of Wavelength Division Multiplexing (WDM) systems now allows multiple wavelengths to be propagated through fibres which in the past carried a single wavelength only. However, such a simplistic augmentation of network speeds does not account for the ever–changing bandwidth demand patterns and as such network flexibility and reconfigurability will need to be incorporated into future optical communications systems.

Although the capacity of Core and Metro networks have increased greatly through the use of WDM, a corresponding improvement in Access Networks (which provide the final connection to the end–user) has not occurred. This is due to the fact that these networks are primarily comprised of electrical cables (telephone or co–axial) and are therefore are limited in terms of data throughput and transmission distance. The natural solution to overcome this 'last–mile bottleneck' is to take advantage of the large bandwidths offered by optical fibres and to move the fibre network closer to the customer so as to eventually create an all optical communications network. This type of all optical access network has been termed Fibre–To–The–Home and is seen as a long term solution to meet growing bandwidth demands.

Unlike Core and Metro networks whose distance–bandwidth products are sufficiently large to justify high implementation costs, Access networks must be constructed in an extremely cost effective manner due to their potential for wide deployment in a price sensitive market. This presents significant financial and technical challenges in order to provide adequate data rates to each user.

Of utmost importance when designing next generation Access networks will be the selection of a highly efficient modulation format to provide maximum throughput on each optical channel. This has led to the emergence of Orthogonal Frequency Division Multiplexing (OFDM) as a candidate for use in future optical networks. OFDM is a modulation technique which is widely used in both wired and wireless radio communications and indeed has been specified for in radio communications standards such as WiMAX, LTE and ADSL. OFDM's high spectral efficiency is the main reason behind its use in current radio standards. However, what makes OFDM particularly attractive for use in optical communications is its inherent tolerance to chromatic dispersion. OFDM also offers the possibility of implementing dynamic bandwidth allocation (to subcarrier granularity) electronically, thereby reducing cost.

Main Contributions

The main contributions of this work are:

- ❏ Performance improvement of OFDM Passive Optical Networks using direct modulation of a laser by the reduction of nonlinearity – OFDM's relatively poor performance in nonlinear regimes is a hindrance to its use in optical channels which in general contain some level of nonlinearity. By using optical injection, the levels of nonlinearity introduced at the optical transmitter can be reduced allowing for improved performance of direct modulation OFDM Passive Optical Networks. This technique is shown to improve performance/increase throughput using both an external laser and a monolithically integrated device.
- ❏ Direct modulation of a tuneable laser with Adaptive Modulation AM-OFDM – A cost

effective novel tuneable laser is directly modulated with highly spectrally efficient Adaptive Modulation (AM) OFDM in order to construct a high data rate transmitter suitable for implementation with optical access networks such as PONs.

- ❏ Demonstration of optical burst mode OFDM – The performance of Single Sideband OFDM in a switching environment using an external modulator and a single switching laser at the transmitter is examined. The Wavelength Division Multiplexing grid size used is found to be a major factor influencing performance. Single Sideband modulation is used in order to overcome the effects of dispersive fading which can lead to a large degradation in the performance of OFDM signals.

Thesis Structure

This thesis is structured as follows:

Chapter 1 describes the evolution of optical communications networks as well as the motivation behind their continued growth in capacity today. The optical network topology is introduced with descriptions of each network layer given. Particular attention is given to the discussion of optical access networks with both current and future variants of these types of networks being presented. Key optical components which are used to construct optical communication systems are discussed along with advanced modulation formats which are used for the efficient transmission of data.

Chapter 2 provides a detailed discussion of the theory behind Orthogonal Frequency Division Multiplexing. The involvement of the Inverse Fast Fourier Transform in the generation of OFDM is examined and the subsequent mathematical relationships between sample rate, subcarrier spacing and signal bandwidth are explained. Crucial enabling techniques used with OFDM, such as the Cyclic Prefix, the facilitation of a simple channel estimation and the Levin–Campello algorithm are discussed. Important parameters used to measure the quality of OFDM signals, and their relationship to one another, are described mathematically. Lastly, the various types of OFDM implementations within optical systems are presented and discussed.

Chapter 3 focuses on the reduction of nonlinearity in direct modulation OFDM systems. The origin of nonlinearity in laser diodes and a means by which its level can be estimated are introduced. How optical injection can be employed to reduce this level of nonlinearity is also discussed. Both simulation and experimental demonstrations of the use of optical injections in an OFDM PON are presented with results given for non-injected and injected cases. This injection technique is demonstrated using an external laser diode as well as a novel monolithically integrated device.

Chapter 4 describes experimental work involving the direct modulation of a tuneable laser with Adaptive Modulation OFDM. The motivations behind, and the advantages of, using tuneable lasers in passive optical networks along with the types of network scenarios with which they can be employed are explored. The novel device, a discrete mode tuneable laser, is subject to detailed characterisation which is described in this chapter. The experimental setup of a PON structure incorporating this device and its direct modulation by high data rate AM–OFDM signals is explained and the performance on various optical channels in terms of achievable data rate is presented and discussed.

Chapter 5 examines the use of OFDM in a switching environment. Burst mode operation is discussed in terms of its suitability for use in next generation metropolitan area networks. The generation of optical Single Sideband is also outlined. The experimental demonstration of burst mode OFDM using a fast switching SG–DBR is described and performance is evaluated on a subcarrier basis at various times after a switching event. Static transmission of double sideband and single sideband OFDM signals over 180km of fibre is performed demonstrating the capability of single sideband modulation to overcome the effects of dispersive fading.

Chapter 6 gives a brief summary of conclusions that can be drawn from the results presented in this thesis. The potential for future work in the areas discussed throughout the thesis is outlined also.

Chapter 1

Optical Networks

This chapter presents an overview of past and present optical communications networks. The ever–increasing demand for greater network speeds is outlined and the challenges which this poses to next generation optical networks are discussed. Key technologies in the design of these networks such as direct and external modulation, and higher level modulation formats, are also discussed.

1.1 Introduction

The advent of optical amplifiers to commercial optical communication systems in 1989, resulting in extended transmission distance and increased data rates, led to an explosive growth in the capacity of our communications systems [1]. The internet, which was commercially deployed at around the same time, has evolved from a primarily text based platform to a position where it now provides a plethora of multimedia services and is in fact the main driver behind advances in today's optical communications systems [2].

Figure 1.1 shows estimated and projected growth in Internet Protocol (IP) traffic in North America since 1990 [3–6][1]. From 1990 to 1994 internet traffic doubled year on year. The

[1] Minnesota Internet Traffic Study (MINTS) provide high and low estimates for IP traffic growth. The line shown in figure 1.1 is the median of these values.

large–scale deployment of Wavelength Division Multiplexing (WDM) systems, allowing for increased data rates by using multiple optical channels, facilitated a rapid growth in traffic [1] with growth rates in North America from 1994 to 1996 increasing more than 90 fold to around 1.5 PB/month. Figure 1.1 also shows that since 1996 traffic growth has slowed with the rate increasing by a factor of about 100% for the years 1997 to 2002 and 50–60% from then up to the present. This period of growth comes as advances in WDM technology and the use of higher order modulation formats are commercially exploited.

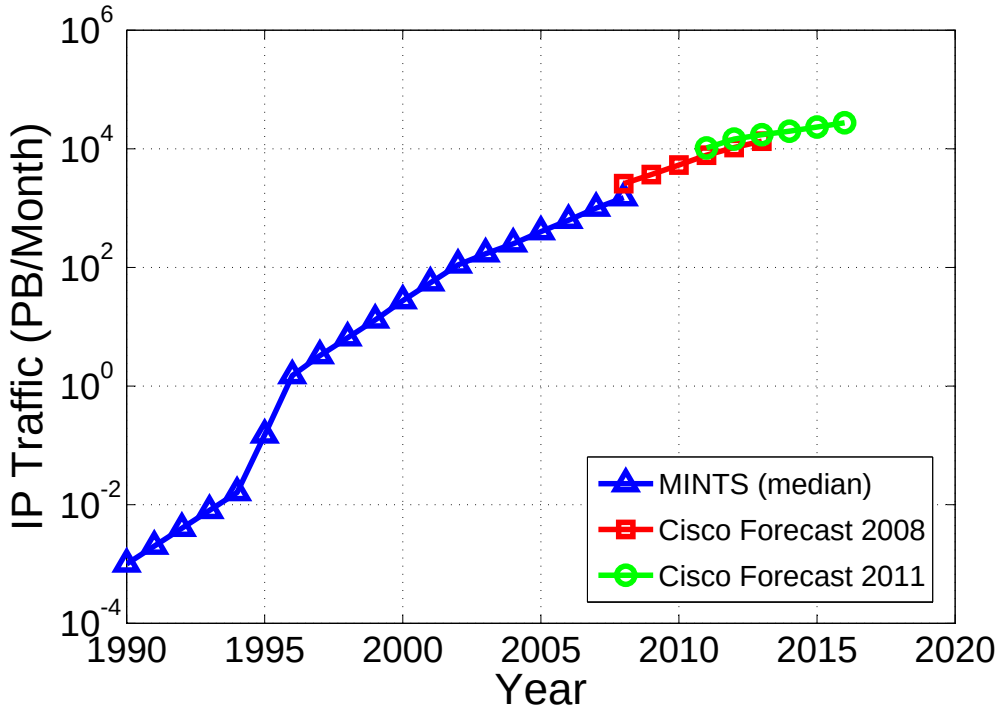

Figure 1.1: Estimated and projected growth in total IP traffic in North America

Today an increasing amount of internet traffic is generated by mobile devices such as smart phones, tablet computers and portable gaming devices. It is reported in [3] that by the end of 2014 traffic generated from wireless enabled devices will exceed that generated by wired devices, and will account for 61% of global traffic by 2016. This fact highlights both the increasing ubiquitousness of the internet today and the growing demand from customers for on–demand multimedia services.

The new ways in which consumers experience the internet coupled with the widespread adoption of wireless enabled mobile devices means that global IP traffic is expected to surpass 1 Zettabyte in 2015 [3]. This ever–increasing trend poses significant technological challenges to the telecommunications industry and the development of current optical communications systems will be of utmost importance in helping to meet these challenges.

1.2 Wavelength Division Multiplexing

Wavelength Division Multiplexing (WDM) is an optical multiplexing technique used currently in core and Metropolitan (metro) optical networks to help to increase system capacity. WDM provides an efficient means of utilising the large optical bandwidth available from a single optical fibre by transmitting multiple wavelengths with a given frequency separation. Similar to Frequency Division Multiplexing (FDM) in radio communications, WDM divides the optical spectrum into many channels with each optical carrier modulated independently either directly or externally. The received optical signal is passively demultiplexed into individual channels and distributed to the intended destination. A generic WDM system is depicted in figure 1.2.

The frequency gap between two adjacent WDM optical carriers is known as the channel spacing. Today's core and metro WDM systems typically use a channel spacing of 100GHz or 50GHz which is specified for by the International Telecommunication Union (ITU) and is referred to as Dense WDM (DWDM). In this case hundreds of optical carriers can be transmitted with typical data rates of 10Gb/s and 40Gb/s on each carrier using either Non Return–to–Zero (NRZ) or Differential Phase Shift Keyed (DPSK) modulation [1]. DWDM metro network designs which are employed today transmit 40Gb/s using DPSK on each optical carrier across a 50GHz grid [7]. Ultra Dense WDM (UDWDM) is used to refer to grid spacings as low as 25GHz and 12.5GHz and recommendations for their standardisation have already been published in ITU G.694.1 [8]. This is in anticipation of increased spectral efficiencies (*Bit Rate*/*Channel Spacing* measured in b/s/Hz [1]) offered by advanced mod-

ulation formats and the adaptation of WDM technology to access networks where a higher number of channels is desirable given the relatively large number of users [9, 10].

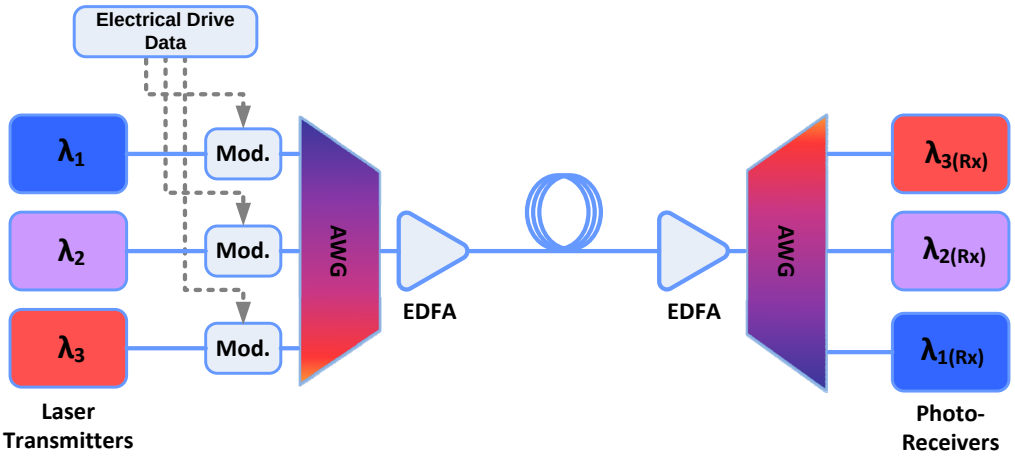

Figure 1.2: WDM downlink/uplink using an AWG as a (de)mux.

There are three main limitations to how many optical channels can be used:

- ❏ Erbium Doped Fibre Amplifiers (EDFAs) are the most commonly used amplifiers in optical communications systems. EDFAs are a critical part of all current WDM systems as they make long–haul transmission of many channels viable by ensuring sufficient received power for each channel. In this way EDFAs have facilitated rather than limited WDM networks, but clearly all WDM channels must be within the frequency range of operation of the amplifier which can span the C–band (1525nm–1565nm) or the L–band (1570nm–1610nm).

- ❏ The rate and spectral efficiency of the data carried by each WDM channel is also of critical importance when defining the number of available operational wavelengths. In many current metro networks 40Gb/s per channel is required with OOK modulation applied to each channel. Therefore a grid of 100GHz spacing must be used in order to avoid crosstalk and/or overlapping with neighbouring channels. As more advanced modulation formats with higher spectral efficiencies are introduced, lower grid spacing can be realised. The prospect of using advanced modulation in future WDM access networks, where the data rate required per channel is significantly

lower than that required for backbone networks, means that grid spacings as low as 12.5GHz can be realised [8]. This increase in the number of operational wavelengths would broaden the scope for optical networking and allow a greater number of users to be reached.

- The optical components used to multiplex and demultiplex WDM optical signals define the minimum grid size that can be employed in the system. A common component used for this purpose is the Arrayed Waveguide Grating (AWG) which uses precise phase shifts and free space propagation to direct each WDM channel to an individual fibre. The reverse effect can be used for multiplexing. The precise physical requirements of an AWG means that they are tailor made to operate on a given WDM grid. Those in use today typically operate with a spacing of 100GHz and 50GHz and so contribute to an inertia which impedes movements to smaller grid sizes. More recently reconfigurable (de)multiplxing components such as Wavelength Selective Switches have been proposed for use in WDM networks [11].

1.3 Network Topology

Figure 1.3 shows the optical network topology consisting of core, metro and access networks. Although the backbone of the topology (core and metro networks) have been in use for a relatively long time, due to increasing bandwidth demands next generation optical networks will need to evolve to become more reconfigurable so as to adapt to changing patterns of network traffic and also to be capable of providing an array of services such as On–Demand TV, IP–TV, video conferencing and online gaming [12]. Access networks which are comprised entirely of electrical cables in some cases, must undergo drastic change in order to meet these future requirements. The three layers of this topology are discussed below.

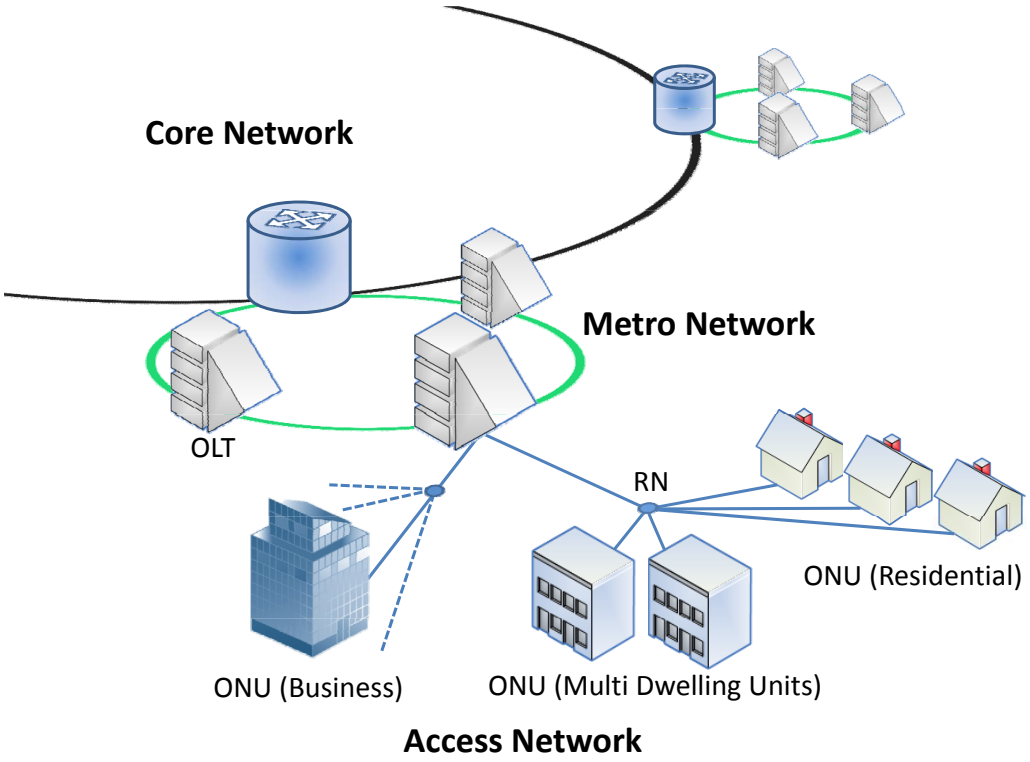

Figure 1.3: Network topology includes core, metro and access networks.

1.3.1 Core Networks

The core network is the backbone of the optical system. It consists of many nodes each interconnected by an amplified fibre link. The core network transports large amounts of aggregated data from one node to another over thousands of kilometres. These nodes (usually located in cities) pass data from the metro network to the core network or vice versa using either optical or electrical switching. Core networks employ WDM and must be capable of an overall an overall capacity of greater than 1Tb/s.

Early core networks consisted of up to 16 wavelengths, each carrying 2.5Gb/s using fixed transmitters/receivers (i.e. transmission and reception of one fixed wavelength only). Advances in optical amplification allowed for the total number of wavelengths used to be increased, with a line rate of 10Gb/s on each channel [13]. All of these legacy core networks were limited by their switching ability due to their use of Optical–Electrical–Optical (OEO) conversion. With this technique all traffic routed through a node, regardless of whether it is

destined for that node, is converted to an electrical signal, switched by an electrical switching module and regenerated in the optical domain. This approach limits the bandwidth to that of the electronics used and is costly due to the often unnecessary regeneration and amplification that is applied. As advances in the access network mean that fibre penetration is coming closer to the end user, with downstream speeds of 100Mb/s per user envisaged, the strain on the core network is expected to increase significantly in terms of both capacity and flexibility [14].

More recent core networks employ all–optical networking where switching at each node is carried out in the optical domain. These optical switching modules are known as optical bypass switches as traffic destined for another node can transition through the node without undergoing O–E–O. 'Bypassing' in this way has resulted in 90% reduction of required O–E–O regenerations compared to legacy networks [14]. Optical Bypass Switching has been made possible due to technological advances, which have lead to increased optical reach (i.e. the maximum distance the optical signal can travel while maintaining sufficient received optical power). The use of Raman amplification extends the optical reach and allows signals to bypass nodes, without undergoing electronic signal regeneration, and still reach their target destination [15]. The use of Dispersion Compensated Fibre (DCF) and Forward Error Correction (FEC) have also helped to extend the achievable optical reach in modern WDM core networks.

Today, with optical amplification extended to cover both the C and L wavelength bands and with the use of more efficient modulation formats, systems using 80 WDM channels, with each channel carrying 40Gb/s (giving an aggregate bit rate of 3.2Tb/s), are being deployed [16]. 100Gb/s per channel systems are envisaged for the near future and have been standardised already in IEEE 802.3ba.

1.3.2 Metropolitan Area Networks

Metropolitan Area Networks (MANs) or 'Metro' Networks provide the optical link between the core network and the access network which connects to the end user. These networks typically span 200km and are usually implemented with a ring topology [17]. Similar to adaptations that are required for core networks, metro networks must also be upgraded to support growing traffic levels in the access network.

Legacy metro networks employed WDM with a 200GHz grid spacing and 2.5Gb/s line rate on each channel [7]. The networks were aimed specifically at providing high speed Synchronous Optical Networking (SONET) and Synchronous Digital Hierarchy (SDH) services. Today's metro networks have not only evolved to support higher bit rates, but are also capable of supporting a range of traffic types such as Internet Protocol (IP), Asynchronous Transfer Mode (ATM) and, in particular, packet services such as Ethernet protocol [18]. ITU-T G.709 [19] standardises metro network operation to support these services, making them a true multi–service technology.

Like core networks, metro networks have evolved to avoid the use of OEO conversion. Optical Add–drop Multiplexers (OADMs) allow specific wavelengths to be added or dropped from the metro ring. In this way optical routing can be achieved whereby wavelengths allocated for downstream transmission to a specific access network can be dropped from the metro ring while others are allowed to propagate to their intended destination within the metro network. Increased reconfigurability and support for various services is achieved by integrating these components with reconfigurable optical switches to form reconfigurable OADMs (ROADMs) [20]. The introduction of advanced modulation formats (e.g. DQPSK) means that higher spectral efficiencies will soon be available and currently deployed metro networks are designed with a view to upgrading to 40Gb/s and 100Gb/s with a grid spacing of 50GHz and lower, facilitating their integration with current core networks standards [7].

1.3.3 Access Networks

Access networks are often referred to as the 'first/last' mile and they connect the customer to the first node on the metro network. Currently, optical access networks are not widely deployed. The main impediment to employing all optical access networks is cost. In general, copper wire currently connects each customer directly to the network, meaning an upgrade to an optical access network would incur a large deployment cost. To date, service providers have met the required increase in access network capacity (driven by new services such as VoIP and online gaming) by employing more efficient forms of digital modulation over the existing electrical cables. To meet future network speeds access networks will need to evolve, like core and metro networks before them, to be all optical networks. Proposed schemes for all optical access networks will be discussed in the following sections.

1.4 Optical Access Networks

New technologies have emerged as candidates for use in these future optical networks, but unlike the long haul core and metro networks, where the distance-bandwidth product make it feasible to employ expensive optical techniques and components, it is crucial, due to their high market volume, that next generation optical access networks are extremely cost effective. FTTH has experienced growth in recent years in several parts of Europe, the U.S and Asia [21]. Figure 1.4 shows the percentage of fibre broadband connections in Organisation for Economic Co–operation and Development (OECD) countries as of June 2012 [22].

1.4.1 Existing Access Networks

The most common broadband communication connections to the end user in place today consist of a twisted pair of copper wires. These wires were originally designed to carry 4kHz voice data referred to as Plain Old Telephone Service (POTS). Through the use of a

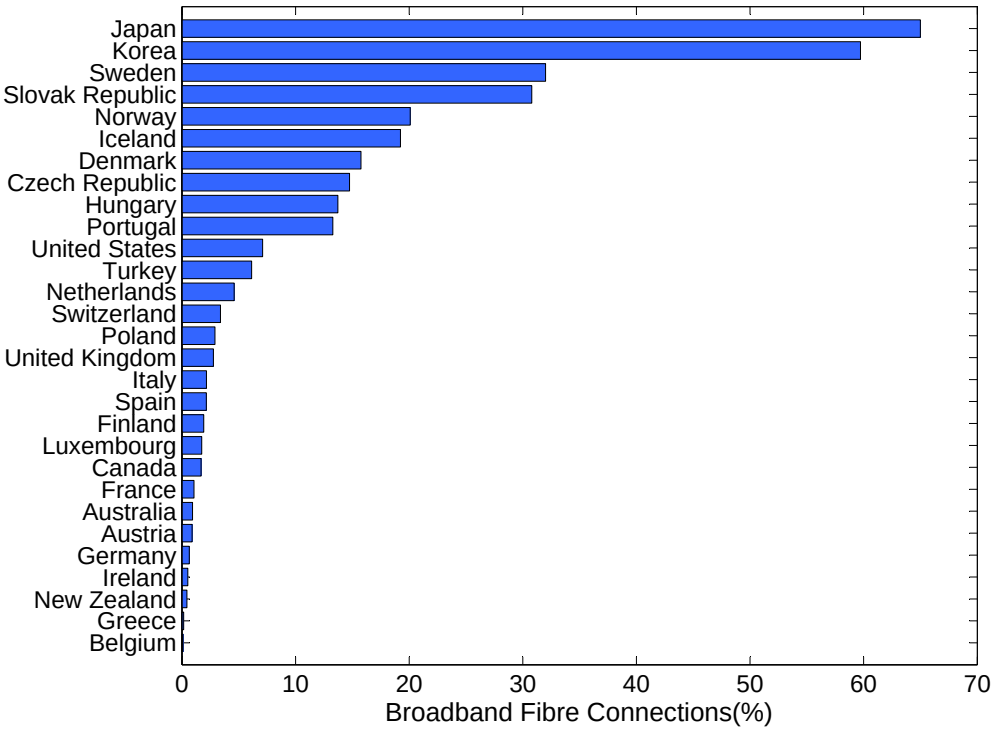

Figure 1.4: Broadband fibre connections as a percentage of all connections, OECD: June, 2012.

family of technologies known as the Digital Subscriber Line (DSL) more efficient use of the telephone network is made so as to provide broadband services to the end user. Telephone and broadband services are assigned a specific frequency sub–band from the available bandwidth and are separated by filtering at the subscriber end. Upstream data (sent from the user) is transmitted along the copper wire to a DSL Access Multiplexer (DSLAM) located at the Central Office (CO). This is used to multiplex multiple lower data rate upstream signals from many users into one higher speed signal for onward transmission. Asymmetric DSL is a variant of DSL which provides higher downstream data rates than upstream data rates. Today the term DSL is used interchangeably with ADSL and downstream data rates to each subscriber of about 8Mb/s can be achieved [23].

Another method of providing broadband communication services today is by using co–axial cables originally deployed to homes to facilitate the transmission of analogue TV signals. The 8MHz bandwidth per channel required to transmit analogue TV cannot be

provided by the copper twisted pair and so co–axial cable has been installed in many urban areas. The greater bandwidth provided by co-axial cables facilitates the provision of higher upstream and downstream broadband data rates compared to the telephone network. The disadvantage of co–axial cables lies in the fact that electrical amplifiers are needed every 100–200m in order to ensure sufficient received power. This is not only energy inefficient but limits transmission distance. A solution to this problem is to use a Hybrid Fibre–Co-axial (HFC) network. In these types of networks, optical fibre is deployed from the service provider's CO to a Remote Node (RN). At the RN the optical to electrical conversion takes place and the downstream data is transmitted to each user via the co–axial cable. In this way the use of the co–axial cable is minimised and the superior transmission characteristics of optical fibres are exploited. The data rates provided by such a system to each user depends greatly on how close to the home the optical–electrical conversion takes place. This has given rise to many forms of network implementation such as Fibre–to–the–Node (FTTN), which brings the fibre to within 1.5km of the user, Fibre–to–the–Cabinet (FTTC) which brings the fibre to a cabinet within 150m of the user or Fibre–to–the–Basement (FTTB), which runs the fibre to a cabinet within a large commercial or residential premises. Due to the many acronyms used to describe the iterative advances in HFC fibre penetration, the term FTTx can be used to refer to these technologies collectively. Current FTTx access networks are capable of providing downstream speeds of up to 100Mb/s to each user with between 10–50 residential units per optical unit (RN) [24].

Although it is currently commercially advantageous to make use of legacy networks such as copper twisted pair or co–axial cables, more advanced technologies such as higher order modulation formats will be required to meet the continued growth in demand for bandwidth in the near future. This not only decreases the financial incentive to continue using such infrastructures (as operation costs rise), but is also unsustainable given projections for future bandwidth demands [25]. The next step in the evolution of access networks will be to create an all optical access network by providing Fibre–to–the–Home (FTTH).

1.4.2 Passive Optical Networks

A Passive Optical Network (PON) is the network architecture which is seen as the most promising, 'future-proof' candidate for use in next generation optical access networks [26]. In this architecture a feeder fibre runs from the central office (CO) to a remote node. The remote node contains a passive optical device which connects this fibre to multiple users. In the CO an Optical Line Terminator (OLT) manages the transmissions from each subscriber. An Optical Network Unit (ONU) is used at the subscriber end to convert the incoming optical signal into the electrical domain. The ONU then transmits data back to the OLT at the CO, this being referred to as upstream data. There are a number of candidate PON technologies that have attracted much attention within the research community [27]. These will be discussed in the following sections.

1.4.2.1 Time Division Multiple Access PON

Current PON standards Ethernet PON (EPON) IEEE 802.3ah [28] and Gigabit PON (GPON) ITU-T G.984 [29] both use Time Division Multiple Access (TDMA). A typical TDMA PON layout is shown in figure 1.5. In this type of architecture each subscriber is allocated a time slot in which they can access available bandwidth. The passive power splitter shown is also used to couple the upstream data from each subscriber into the feeder fibre and back to the OLT. The OLT assigns the time slots used by each subscriber in such a way so that there is no overlap of data streams. This introduces difficulty as, to achieve this, the OLT requires precise time–delay information which is usually supplied by a probe signal. Another challenge associated with TDMA–PONs is the requirement for a Burst Mode Receiver (BMRx) at the OLT [30]. As packets of data arrive at different times, from various users at different distances from the OLT, clock synchronisation and receiver gain equalisation for each received packet from an ONU must be performed by the BMRx. Dynamic bandwidth allocation is possible, but adds a high level of complexity to the control algorithm.

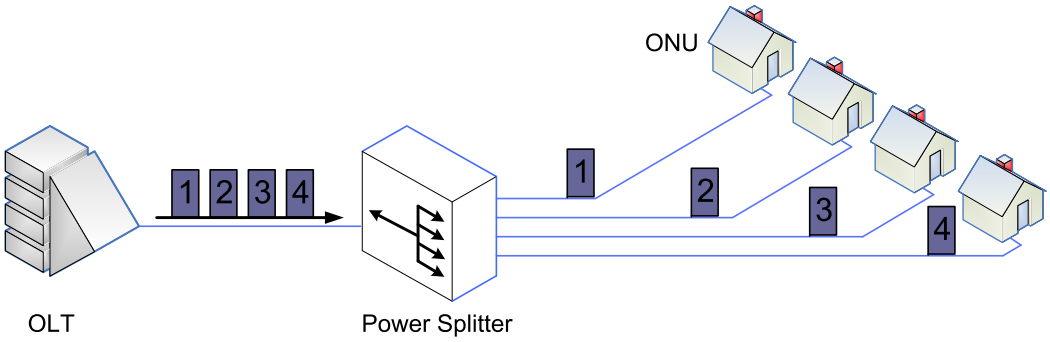

Figure 1.5: TDM–PON architecture.

1.4.2.2 Wavelength Division Multiplexing PON

The complex management issues associated with TDMA can be avoided using Wavelength Division Multiplexing (WDM), which assigns a pair of dedicated wavelengths to each subscriber (for upstream and downstream data); as a result users are independent of each other and can transmit without interference [31]. Furthermore, as WDM is the technology of choice for both core and metro networks, its adoption in access networks would facilitate simpler integration with the higher layer systems.

Instead of a power splitter at the RN, WDM employs a passive wavelength (de)multiplexer such as an Arrayed Waveguide Grating (AWG), see figure 1.6. Problems arise with WDM PONs when it comes to low cost implementation. It is necessary that the source wavelength at each ONU matches the wavelength profile of the AWG (which may change due to environmental conditions) and this may be difficult to implement in a cost effective manner. Also, for each subscriber, a separate transceiver at the OLT is required, which raises cost. The addition of tunable optical devices allows for network reconfigurability [9] but again it is currently difficult to implement this in a cost effective manner.

1.4.2.3 Orthogonal Frequency Division Multiplexing PON

An Orthogonal Frequency Division Multiplexing (OFDM) PON layout is shown below in figure 1.7. In this structure a large bandwidth OFDM signal is transmitted from the CO to

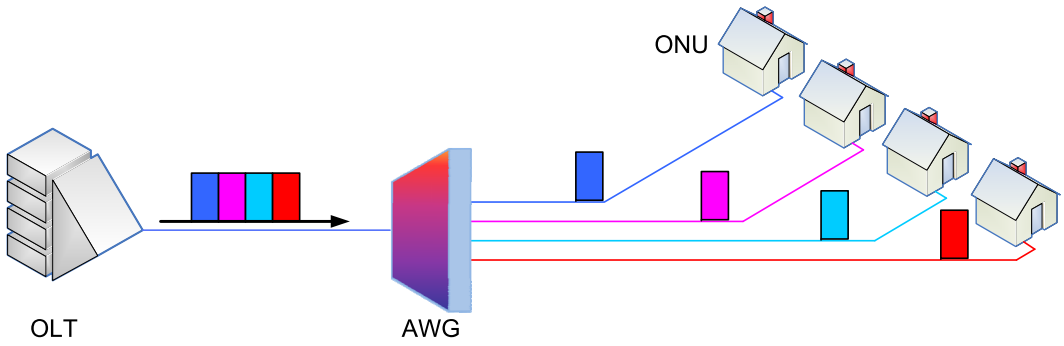

Figure 1.6: WDM–PON architecture

each subscriber. At the ONU the optical signal is detected and converted to the electrical domain. A specific potion (e.g. a single subcarrier) of the data carries information about which other subcarriers are designated to a particular ONU, and the relevant subcarriers can be processed accordingly. For upstream transmission each ONU uses the same designated RF OFDM subcarrier frequencies as for the downstream data. The upstream OFDM signals from each ONU are modulated onto an optical carrier, combined with other upstream ONU data signals at the remote node and then sent to the OLT through the feeder fibre. This type of architecture has been the subject of much research [32–36] and is referred to as OFDM Access (OFDMA). Indeed, 108Gb/s downstream transmission has been demonstrated using polarization multiplexing [37].

There has also been a considerable amount of research carried out on WDM–OFDM–PONs which employ a WDM–PON architecture as shown in figure 1.6 and use OFDM as the data modulation format on each WDM channel [38–40]. In this way reconfigurability can be achieved using a combination of techniques in both the electronic and optical domains.

These architectures lend themselves well to network reconfigurability as, through DSP, users can be dynamically assigned more or less OFDM subcarriers depending on dynamic traffic patterns [41]. As will be discussed later in section 2.2.3, dispersion is also easily dealt with through DSP by exploiting OFDMs' cyclic prefix. The transfer of complexity from optics to low cost electronics to address these key issues in future optical access networks

is the key differentiator between OFDM PON and other potential technologies [12].

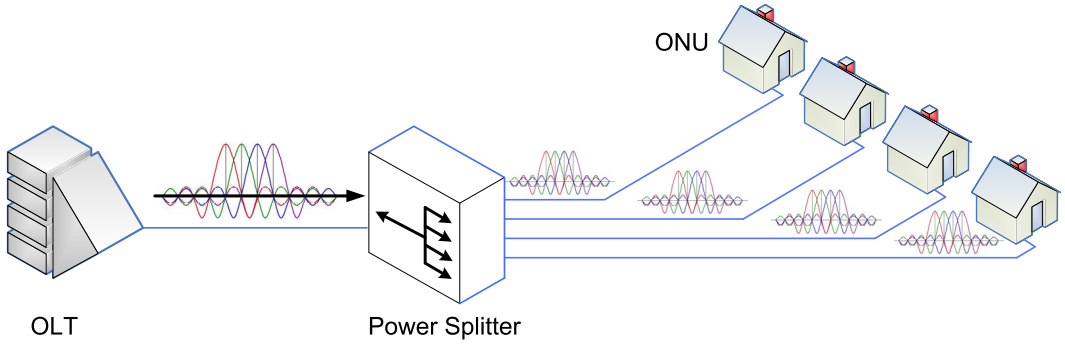

Figure 1.7: OFDM–PON architecture

1.4.3 Requirements for Next Generation Access

Current PON deployments (EPON and GPON) offer aggregate 1.25/2.5Gb/s upstream/-downsteam data rates through the use of TDMA. Next generation PONs can be broken doen into two stages as defined by the Full Service Access Network (FSAN) community. NG-PON stage 1 (NG-PON1) and NG-PON stage 2 (NG-PON2). NG-PON1 targets an aggregate downstream data rate of 10Gb/s and an upstream rate of with 2.5 or 10Gb/s. The XG-PON standardised by ITU-T is an example of such a PON architecture.

NG-PON2 technologies target a total downstream data rate of 40Gb/s with at least 1Gb/s in the upstream direction. The required reach for NG-PON2 is 40km with a splitter ratio of 1:64. TDM, WDM, OFDM, and TWDM have all been proposed for use in such PONs.

Although the use of TDM would offer a simple migration from current PON deployments, the burst mode reception required for TDM operation becomes increasingly difficult as line rates increase. Furthermore, the downstream data rate is limited to that which can be provided on a single optical carrier. One way to overcome this problem is to use a hybrid of TDM and WDM (TWDM) where multiple optical carriers are used to carry TDM data each. Each ONU in the system is equipped with a tuneable transceiver. This technique exploits the advantages of WDM while reducing the requirements on the components necessary for

TDM operation. However, the passive routing and tuneable optics required for WDM are still necessary with this type of network configuration. This technique appears to be the current front-runner for NG-PON2.

Ultra Dense WDM (UdWDM) has also been proposed for use in NG-PON2 [42]. This method makes use of coherent detection both at the OLT and at the ONU. In such a case, very low channel spacings could be employed (as low as 2.8GHz) with each optical channel carrying 1.25Gb/s DQPSK data. This technique would offer excellent receiver sensitivity but the deployment of coherent receivers as well as tuneable lasers at every ONU, in a cost effective manner, remains a major challenge if this technique is to be a realistic candidate for future PONs.

Finally, OFDM based solutions, much like that presented in section 1.4.2.3, have also been investigated. The key advantage of OFDM is that channel impairments can be overcome in the electrical domain. Furthermore, OFDM's tightly packed subcarriers offer good spectral efficiency and the potential for dynamic bandwidth allocation, again in the electrical domain. OFDM's high Peak-to-Average Power Ratio (PAPR) (discussed in section 2.4) can lead to low signal powers which impacts reach/splitter ratio. However, the avoidance of both a burst mode receiver and expensive tuneable optics makes OFDM based solutions an excellent candidate to provide 40Gb/s (aggregate) data rates and beyond, for future PONs.

1.5 Key Components and Technologies

It is clear from the above discussion regarding the requirements and composition of potential next generation optical networks, that the development of optical components as well as communication technologies will have a major role to play in terms of how easily current networks will be upgraded. In the case of Metro and Access networks it is critical that technological advances allowing for the scaling of these networks take place in a cost effective manner. The next sections discuss key optical components as well as optical and

electrical techniques, some of which are currently utilised but may be adapted to enable more spectrally efficient, higher bit rate optical networks to emerge.

1.5.1 Direct Modulation

Above the threshold value of the laser diode, the emitted light intensity is directly proportional to the bias current. As current is varied temporally so too is the output power from the laser diode. In this way light from the diode can be varied in accordance with, or *modulated* by, a multilevel data signal known as the drive signal. This technique is known as Direct Modulation. Figure 1.8 shows a typical measured Output Optical Power Vs. Bias Current plot for a Distributed Feedback (DFB) laser. A linear relationship between output power and bias current is displayed for values above the threshold current, I_{th}.

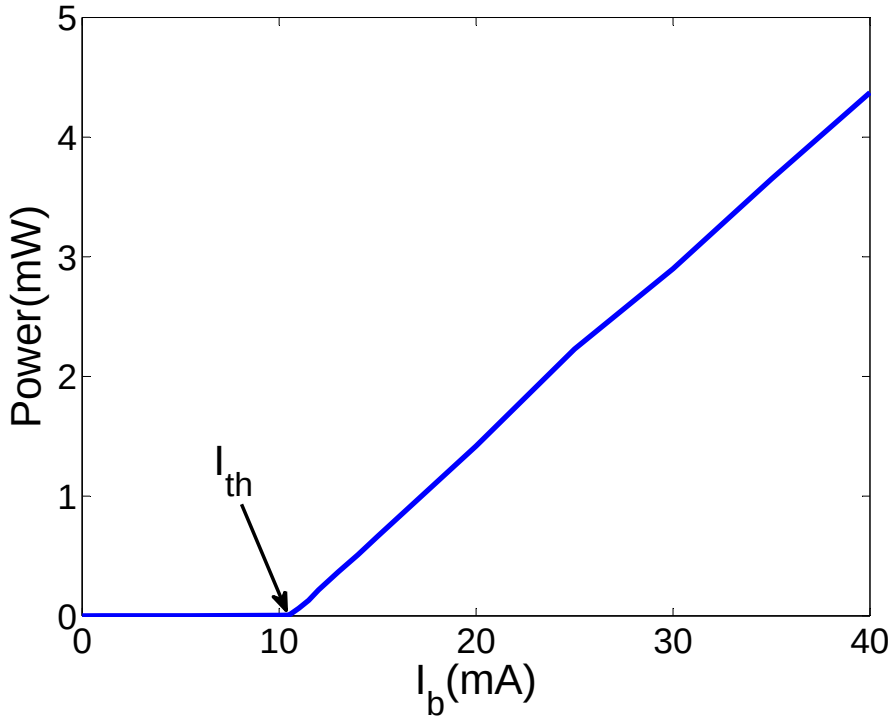

Figure 1.8: Measured PI curve of a DFB laser.

An important parameter when considering direct modulation of a laser is how quickly the driving current can be modulated before the laser stops responding to current variations.

This information can be inferred from the laser's modulation response. The 3dB bandwidth of this response is one of the main limitations of direct modulation as it places a restriction of usable frequencies for driving data signals. An estimate for the 3dB bandwidth can be derived from the laser rate equations [1].

$$f_{3dB} \approx \left[\frac{3G_N}{4\pi^2 q}(I_b - I_{th})\right]^{\frac{1}{2}} \tag{1.1}$$

where G_N is the optical gain coefficient, q is the electron charge, I_b is the bias current and I_{th} is the threshold current. From the expression we can see that f_{3dB} increases with bias level as $\sqrt{I_b - Ith}$. Figure 1.9 shows the typical modulation response of a DFB laser for various bias current values.

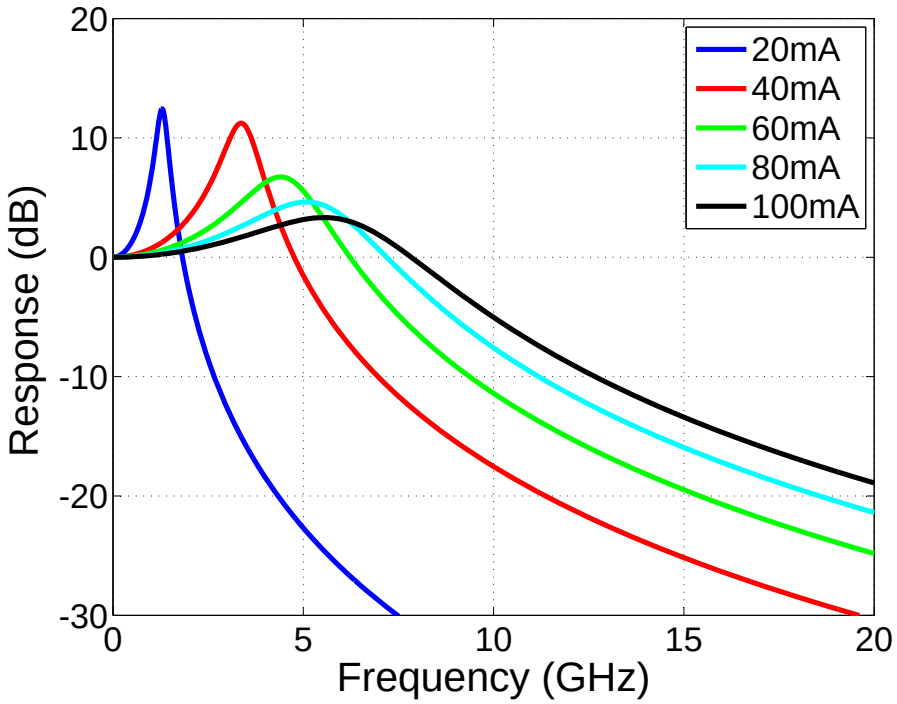

Figure 1.9: Modulation response of a modelled laser diode at various bias currents.

Another effect that occurs with direct modulation is frequency chirp. Amplitude modulation of a semiconductor laser is always accompanied by phase modulation of the output light–wave. A time varying change in phase is equivalent to a change in frequency. The resultant

broadening in frequency of the output optical signal in this way is known as chirp. This is undesirable, particularly in long-haul communications as it limits the transmission distance before dispersive effects in optical fibre begin to degrade the signal [1].

The problems associated with direct modulation are more sharply felt for longer-haul transmission systems. In access networks, where transmission distances are generally less than 100km, frequency chirp does not contribute to a major degradation in system performance. Furthermore, through the use of more spectrally efficient digital modulation formats and higher speed electronics, direct modulation bandwidths can be used to provide 10+Gb/s data rates required for future systems. These factors, coupled with the lower cost and footprint of direct modulation transmitters compared to transmitters employing external modulators, makes direct modulation transmitters the transmitters of choice for optical access networks.

1.5.2 External Modulation

To increase modulation bandwidth and overcome the frequency chirp associated with direct modulation, external optical modulators can be employed. For transmitters employing these modulators the laser bias current is held constant and so Constant Wave (CW) light is output from the laser diode. This CW output is coupled to a modulator which manipulates either the phase or amplitude of the light in proportion to an electrical drive signal which is also applied to the modulator.

An optical phase modulator can be constructed by embedding an optical waveguide in an electro-optical substrate, most commonly $LiNbO_3$. By applying a voltage across the substrate material the refractive index of that material and hence the effective refractive index of the waveguide can be altered, which in turn alters the phase of the incoming optical signal [43]. So by controlling the external voltages applied, the phase of the incoming optical field can be modulated. This phase modulation can be converted to amplitude modulation using a Mach–Zehnder interferometer structure [1].

Phase modulation is converted to amplitude modulation using the principle of interferometry. The Dual Drive Mach–Zehnder Modulator (DD–MZM) structure which consists of two phase modulators and two light paths is shown in figure 1.10. Incoming light from a laser diode operating in CW mode is split into two paths each containing a phase modulator. An independent drive voltage is applied across each phase modulator and so the optical signals in either path are subjected to a different changes in phase. Having acquired a relative phase difference between the two optical signals they are then recombined. The interference between the two signal varies from constructive to destructive depending on the relative phase shift and so the output signal can be modulated in terms of optical intensity.

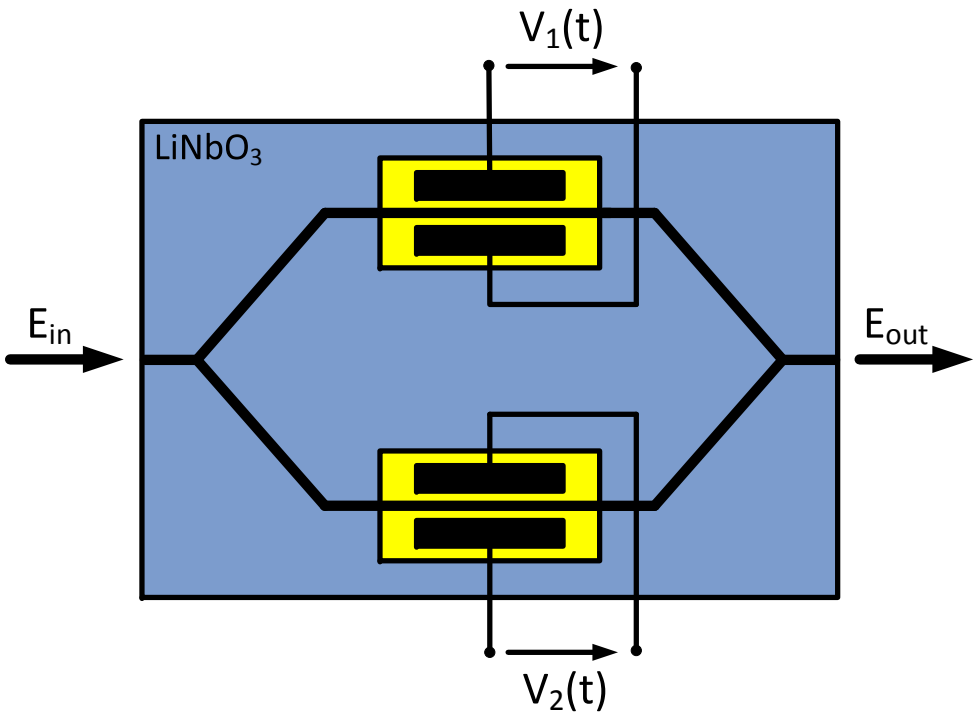

Figure 1.10: $LiNbO_3$ Mach–Zehnder Modulator.

Figure 1.11 shows the ideal DD–MZM characteristic where ΔV represents the difference between the two external drive voltages. This transfer function is expressed mathematically as

$$\frac{E_o(t)}{E_i(t)} = \frac{1}{2} \cdot (\exp^{j\varphi_1(t)} + \exp^{j\varphi_2(t)}) \tag{1.2}$$

where $E_i(t)$ is the input optical field, $E_o(t)$ is the output optical field and $\varphi_1(t)$ and $\varphi_2(t)$ are the phase shifts applied to the upper and lower paths of the modulator. The voltage swing required to change the relative phase difference between the two optical paths from zero radians to π radians is known as V_π. Therefore, in the ideal case, a shift of V_π in the voltage difference between the two arms of the modulator is capable of changing the output optical intensity from minimum to maximum. To achieve a linear relationship between driving voltages and optical intensity, the modulator is typically biased by ΔV to be halfway between these points. This point is known as the quadrature point. A time varying voltage data signal whose amplitude is less than V_π is then added to the bias and so the output optical intensity is linearly proportional to ΔV.

It is also possible to achieve a linear relationship between the drive voltages and the optical field by biasing the modulator at the minimum of its intensity characteristic (the null point). Biasing in this way is typically employed in systems which are capable of detecting changes in optical phase at the receiver. Again, a time varying drive signal is added to the bias whose peak–to–peak amplitude is tailored to remain within the linear region of the field characteristic. It is clear to see from figure 1.11 that this linear region is larger than that of the intensity characteristic and so driving voltages are not limited to a maximum amplitude of less than V_π. However, biasing at this point leads to a large insertion loss as the mean intensity, and hence the optical carrier, is minimised and of course the requirement for phase coherence at the receiver is introduced.

1.5.3 Advanced Modulation

Progress in optical filtering has allowed optical communications systems to move towards employing WDM as a means to achieve true optical networking [44]. Due to advances in electronic and optoelectronic components, available electronic bandwidth has grown greatly. This, coupled with the desire to maximise the efficiency on each optical channel, has given rise to the implementation of digital modulation formats, most of which have been successfully adopted from the Radio Frequency (RF) communications to help maxim-

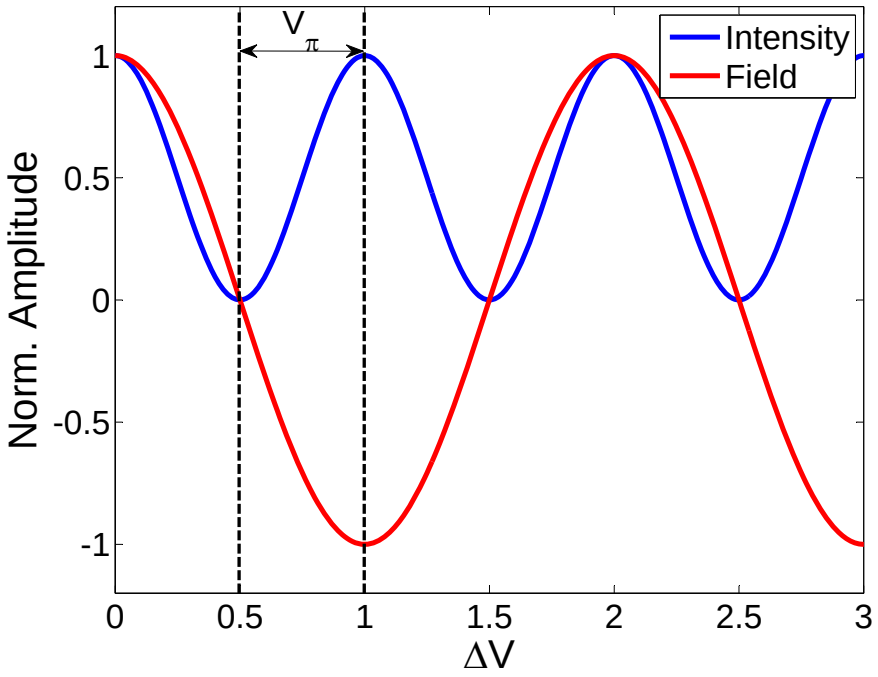

Figure 1.11: Transfer function of a Dual Drive MZM showing optical intensity and field for various voltage bias values.

ise throughput and bandwidth efficiency.

The idea behind using advanced modulation formats, both in the optical and RF world, is to increase the number of bits transmitted per symbol from one, which is the case for optical systems employing On-Off Keying (OOK), to the maximum number of bits per symbol the signal-to-noise ratio of the optical link with allow, thereby increasing spectral efficiency. The simplest way to do this is to transmit multiple bits per symbol using multilevel amplitude modulation. This is known as Amplitude Shift Keying (ASK). Another degree of freedom is added when the phase of the carrier is also used for encoding data, where multiple phase shifts are used to represent data symbols which are each assigned a unique pattern of bits. Modulating the phase alone is known as Phase Shift Keying (PSK). Using a combination of these carrier variables, multilevel amplitude and phase modulation, increases the symbol size and allows a greater number of bits per symbol to be transmitted. This technique is referred to as Quadrature Amplitude Modulation (QAM). For any modulation format the relationship between the number of available symbols, M, and allowable

number of bits transmitted per symbol, m, is given by:

$$m = \log_2(M) \tag{1.3}$$

Although these advanced modulation formats (which modulate both amplitude and phase) can be adapted for implementation with an optical carrier through the use of external optical amplitude and phase modulators, the requirement in many cases for an optical coherent receiver to detect optical phase changes, coupled with their associated cost and complexity, makes this type of implementation feasible only for Core and Metro networks. Nevertheless, advanced modulation formats have received attention for use in Access networks, in the form of RF data which is typically multiplexed using OFDM [38, 45]. Instead of encoding the information using only the optical carrier, data signals are generated digitally in the RF domain i.e. the phase and amplitude of the RF carrier or subcarriers are modulated. These RF data signals are then used to modulate only the amplitude of the optical carrier by either direct or external modulation. This approach not only allows for the use of direct detection, it also avoids high insertion loss associated with external optical modulators when they are biased at, or close to, their intensity null point (i.e. to modulate optical phase as discussed in section 1.5.2).

1.5.3.1 Quadrature Phase Shift Keying

Quadrature Phase Shift Keying (QPSK) is a form of PSK which encodes data onto four discrete phase angles of the carrier. Each symbol is represented by one of four phase values, each separated by 90°. In this way each QPSK symbol can convey 2 bits of information, doubling the spectral efficiency compared to OOK. A reference signal is needed at the receiver to detect these phase values. The amplitude of the carrier is not varied. Figure 1.12 shows the symbol mapping or constellation diagram on the complex plane for QPSK. Each symbol has a distinct phase value, but has the same amplitude.

The requirement for a Local Oscillator (LO) or reference signal at the receiver for QPSK is

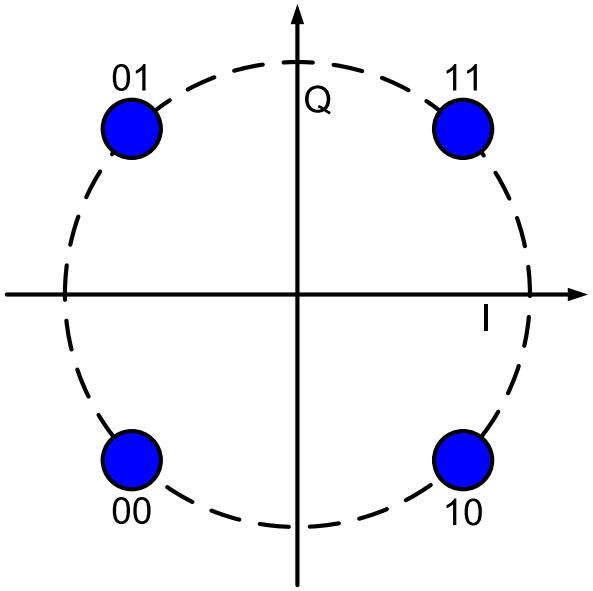

Figure 1.12: QPSK Constellation

a drawback as phase locking must be performed in order to ensure correct detection. This is a problem for optical systems employing optical QPSK (i.e. the phase of the optical carrier is modulated) due to the complexities associated with optical LOs and Optical Phase Locked Loops (PLLs). This has led to the emergence of Differential QPSK (DQPSK) which negates the requirement for a LO at the receiver by encoding data using phase shifts relative to the phase of the previous symbol at the transmitter. In this way the data can be decoded at the receiver by comparing the phase of the carrier during the current symbol period to that of the previous symbol period. This is carried out optically using a Delay Interferometer (DI) whose delay is set to equal the symbol period. The phase difference between the two represents the data symbol. In practice, two binary signals known as the In-phase (I) and Quadrature (Q) signals are used to independently modulate the optical field and a version of the optical field which is π/2 radians out of phase, respectively. These optical signals are combined so that four relative phase shifts are achieved 0, $+\frac{\pi}{2}$, $-\frac{\pi}{2}$ and π enabling two bits per symbol to be encoded. Two DIs are required to recover the I and Q data signals at the receiver.

This approach not only simplifies receiver design but, as it is not the absolute phase value

which is of importance, overcomes any ambiguity that may arise due to constellation rotation through the channel.

1.5.3.2 Quadrature Amplitude Modulation

Quadrature Amplitude Modulation (QAM) is a very popular RF modulation technique due to its potential to provide high spectral efficiencies. In RF communications this scheme typically involves the multilevel Amplitude Modulation (AM) of two carriers with two bit streams respectively. The carriers are 90° out of phase with each other and so are said to be in *quadrature*. The two carriers are then summed and the resultant waveform is both amplitude and phase modulated.

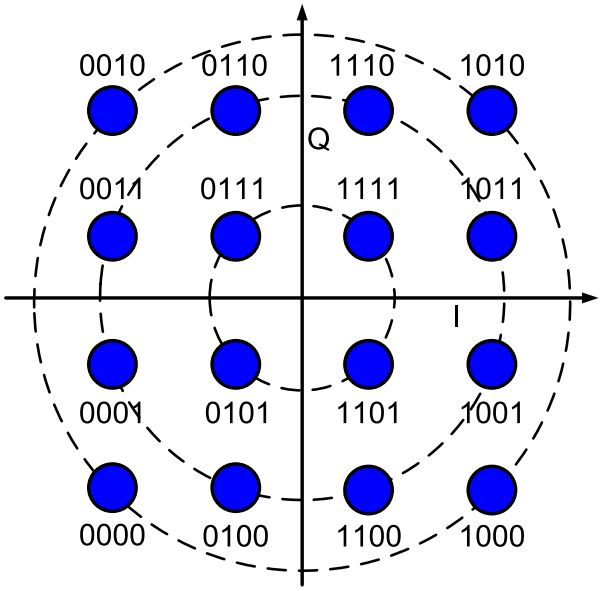

Figure 1.13: 16–QAM Constellation

Of course, it is possible to simply increase the number of levels (phase shifts) employed by PSK, but this brings the symbol values, or constellation points, closer together, making them less distinguishable and hence more susceptible to being decoded erroneously at the receiver. QAM increases the distance between constellation points by introducing multiple amplitude levels which are used for symbol mapping. Increasing the level of amplitude modulation of the two carriers therefore increases the constellation size and so very high

spectral efficiency can be achieved by using 16–QAM (4 bits per symbol), 32–QAM (5 bits per symbol) or 64–QAM (6 bits per symbol) for example. Of course, there is still a trade off to be considered as increasing the QAM constellation size increases the required SNR for a given level of performance. Figure 1.13 shows the constellation diagram for 16–QAM. Each symbol, or constellation point, has a unique combination of amplitude and phase. Bits are assigned to symbols such that each adjacent QAM symbol on the constellation diagram differs by only one bit. This is know as Gray Coding and it minimises bit errors in the case where a symbol is erroneously decoded as an adjacent symbol.

QAM can be achieved with an optical carrier by the simultaneous modulation of both the carrier amplitude and phase by an external complex modulator. Again, a coherent receiver with a LO is required in order to retrieve the optical phase information.

1.6 Conclusion

The continuous growth in demand for higher data rates, fuelled by on–demand and interactive internet services, will drive the development of optical communications networks. The relatively low market volume and enormous throughput of core networks justify high expenditure on new advanced technologies to help to meet future capacity needs. Planning and deploying the next generation of metro, and to a greater extent, access networks will prove to be a difficult task given the required reconfigurability and inherent cost sensitivity of these networks.

To overcome the bottleneck that exists in access networks, legacy copper and co–axial cables are being replaced by fibre as FTTH systems are deployed. FTTH has already been specified in the context of a Passive Optical Network which uses TDM technology. Next generation access networks will need to provide greater downstream data rates and a greater level of reconfigurability while remaining low cost. OFDM is a promising technology for use in next generation PONs due to its bandwidth efficiency, robustness to optical channel effects such as dispersion and, given is multicarrier composition, its wide scope for

providing network reconfigurability using low cost electronics rather than complex optical components.

This thesis explores ways in which OFDM can be integrated into cost effective optical systems so as to provide the data rates and reconfigurability required for next generation optical access and metro networks.

References

[1] G. Agrawal, *Fiber–Optic Communication Systems*. Wiley, New York, 2010.

[2] C. Qiao and M. Yoo, "Recommendation G.709/y.1331 (02/12)," *, Journal of High Speed Networks*, vol. 8, pp. 69–84, 1999.

[3] Cisco Systems, "Cisco visual networking index: Forecast and methodology, 2011–2016," *White Paper*, May 2012. [Online]. Available: http://www.cisco.com/en/US/solutions/collateral/ns341/ns525/ns537/ns705/ns827/white_paper_c11-481360.pdf

[4] ——, "Cisco visual networking index: Forecast and methodology, 2008–2013," *White Paper*, June 2009. [Online]. Available: http://www.cisco.com/web/BR/assets/docs/whitepaper_VNI_06_09.pdf

[5] R. Tkach, "Scaling optical communications for the next decade and beyond," *Bell Labs Technical Journal*, vol. 14, no. 4, pp. 3–9, 2010.

[6] University of Minnesota, "Minnesota internet traffic studies (mints)," 2013. [Online]. Available: http://www.dtc.umn.edu/mints/home.php

[7] J. Elbers and K. Grobe, "Optical metro networks 2.0," in *Proceedings of SPIE (invited paper)*, 2010.

[8] International Telecommunications Union, "G.694.1 spectral grids for WDM applications: DWDM frequency grid," *Series G: Transmission Systems and Media, Digital Systems and Networks*, 2012.

[9] N. Froberg, S. Henion, H. Rao, B. Hazzard, S. Parikh, B. Romkey, and M. Kuznetsov, "The NGI ONRAMP test bed: Reconfigurable WDM technology for next generation regional access networks," *Journal of Lightwave Technology*, vol. 18, no. 12, pp. 1697–1708, Dec. 2000.

[10] K. Iwatsuki, J. ichi Kani, H. Suzuki, and M. Fujiwara, "Access and Metro networks based on WDM technologies," *Journal of Lightwave Technology*, vol. 22, no. 11, pp. 2623–2630, Nov. 2004.

[11] A. Sano, H. Masuda, E. Yoshida, T. Kobayashi, E. Yamada, Y. Miyamoto, F. Inuzuka, Y. Hibino, Y. Takatori, K. Hagimoto, T. Yamada, and Y. Sakamaki, "30 x 100Gb/s all–optical OFDM transmission over 1300km SMF with 10 ROADM nodes," *33rd European Conference on Optical Communication (ECOC)*, pp. 1–2, Sept. 2007.

[12] N. Cvijetic, D. Qian, and J. Hu, "100Gb/s optical access based on optical Orthogonal Frequency-Division Multiplexing," *IEEE Communications Magazine*, vol. 48, no. 7, pp. 70–77, July 2010.

[13] A. Saleh and J. Simmons, "All-optical networking – evolution, benefits, challenges, and future vision," *Proceedings of the IEEE*, vol. 100, no. 5, pp. 1105–1117, May 2012.

[14] ——, "Evolution toward the next-generation core optical network," *Journal of Lightwave Technology*, vol. 24, no. 9, pp. 3303–3321, Sept. 2006.

[15] M. El-Sayed and J. Jaffe, "A view of telecommunications network evolution," *IEEE Communications Magazine*, vol. 40, no. 12, pp. 74–81, Dec. 2002.

[16] J. Berthold, A. Saleh, L. Blair, and J. Simmons, "Optical networking: Past, present, and future," *Journal of Lightwave Technology*, vol. 26, no. 9, pp. 1104–1118, May 2008.

[17] J. Baliga, K. Hinton, and R. Tucker, "Energy consumption of the internet," in *32nd Australian Conference on Optical Fibre Technology (ACOFT)*, June 2007, pp. 1–3.

[18] R. Alferness, "The evolution of configurable wavelength multiplexed optical networks; a historical perspective," *Proceedings of the IEEE*, vol. 100, no. 5, pp. 1023–1034, May 2012.

[19] International Telecommunications Union, "Recommendation G.709/y.1331 (02/12)," Feb. 2012. [Online]. Available: http://www.itu.int/rec/T-REC-G.709-201202-I/en

[20] M. Mezhoudi, R. Feldman, R. Goudreault, B. Basch, and V. Poudyal, "The value of multiple degree ROADMs on metropolitan network economics," in *2006 Optical Fiber Communication Conference (OFC)*, Mar. 2006, p. NThA4.

[21] J. Park, G. Y. Kim, H. Park, and J. Kim, "FTTH deployment status and strategy in korea," in *Globecom 2008*, 2008.

[22] OECD, "OECD broadband portal: Percentage of fibre connections in total broadband (june 2012)," Jun 2012. [Online]. Available: http://www.oecd.org/sti/broadband/oecdbroadbandportal.htm#Penetration

[23] Y. M. Yoon, S.H. and J. Lee, "On selecting a technology evolution path for broadband access networks," *Technological Forecasting and Social Change*, vol. 72, no. 4, pp. 449–470, 2005.

[24] S. Gupta, "Residential broadband technologies for high-speed internet access," in *IET International Conference on Wireless, Mobile and Multimedia Networks*, Jan. 2008, pp. 279–282.

[25] E. Desurvire, "Capacity demand and technology challenges for lightwave systems in the next two decades," *Journal of Lightwave Technology*, vol. 24, no. 12, pp. 4697–4710, Dec 2006.

[26] J. Kani, F. Bourgart, A. Cui, A. Rafel, M. Campbell, R. Davey, and S. Rodrigues, "Next-generation PON–Part I: Technology roadmap and general requirements," *IEEE Communications Magazine*, vol. 47, no. 11, pp. 43–49, Nov. 2009.

[27] R. Davey, J. Kani, F. Bourgart, and K. McCammon, "Options for future optical access networks," *IEEE Communications Magazine*, vol. 44, no. 10, pp. 50–56, Oct. 2006.

[28] IEEE, "IEEE standard for information technology telecommunications and information exchange between systems – local and metropolitan area networks," Sept. 2004. [Online]. Available: http://www.ieee802.org/21/doctree/2006_Meeting_Docs/2006-11_meeting_docs/802.3ah-2004.pdf

[29] International Telecommunications Union, "G.984.1 gigabit-capable passive optical networks (GPON): General characteristics," *Series G: Transmission Systems and Media, Digital Systems and Networks*, 2008.

[30] X. Qiu, C. Melange, T. De Ridder, B. Baekelandt, J. Bauwelinck, X. Yin, and J. Vandewege, "Evolution of burst mode receivers," in *35th European Conference on Optical Communication (ECOC)*, Sept. 2009, p. 7.5.1.

[31] A. Banerjee, Y. Park, F. Clarke, H. Song, S. Yang, G. Kramer, K. Kim, and B. Mukherjee, "Wavelength-Division-Multiplexed Passive Optical Network (WDM-PON) technologies for broadband access: A review [invited]," *Journal of Optical Networking*, vol. 4, no. 11, pp. 737–758, Nov. 2005.

[32] C. Chow, C. Yeh, C. Wang, C. Wu, S. Chi, and C. Lin, "Studies of OFDM signal for broadband optical access networks," *IEEE Journal on Selected Areas in Communications*, vol. 28, no. 6, pp. 800–807, 2010.

[33] D. Qian, J. Hu, P. N. Ji, and T. Wang, "10.8Gb/s OFDMA-PON transmission performance study," in *National Fiber Optic Engineers Conference*. Optical Society of America, 2009, p. NME6.

[34] B. Zhao and X. Chen, "A 40Gbps SSB-OFDMA-PON architecture using direct-detection and source-free ONUs supporting dynamic bandwidth allocation," in *Third International Conference on Communications and Mobile Computing (CMC)*, Apr. 2011, pp. 223–225.

[35] C.-H. Yeh, C.-W. Chow, and H.-Y. Chen, "Adaptive 6.25-40Gb/s downstream rate using four-band OFDM channels within 10GHz bandwidth for long-reach PON," in *2012 Optical Fiber Communication Conference (OFC)*. Optical Society of America, 2012, p. JTh2A.51.

[36] K. Kanonakis, I. Tomkos, T. Pfeiffer, J. Prat, and P. Kourtessis, "ACCORDANCE: A novel OFDMA-PON paradigm for ultra-high capacity converged wireline-wireless access networks," in *Transparent Optical Networks (ICTON), 2010 12th International Conference on*, 2010, pp. 1–4.

[37] D. Qian, N. Cvijetic, J. Hu, and T. Wang, "108Gb/s OFDMA-PON with polarization multiplexing and direct detection," *Journal of Lightwave Technology*, vol. 28, no. 4, pp. 484–493, Feb. 2010.

[38] L. Chen, J. G. Yu, S. Wen, J. Lu, Z. Dong, M. Huang, and G. Chang, "A novel scheme for seamless integration of ROF with centralized lightwave OFDM-WDM-PON system," *Journal of Lightwave Technology*, vol. 27, no. 14, pp. 2786–2791, Jul 2009.

[39] X. Hu, L. Zhang, P. Cao, K. Wang, and Y. Su, "Energy-efficient WDM-OFDM-PON employing shared OFDM modulation modules in optical line terminal," *Optics Express*, vol. 20, no. 7, pp. 8071–8077, Mar 2012.

[40] D. Qian, T. Kwok, N. Cvijetic, J. Hu, and T. Wang, "41.25Gb/s real-time ofdm receiver for variable rate WDM-OFDMA-PON transmission," in *2010 Optical Fiber Communication Conference (OFC)*. Optical Society of America, 2010, p. PDPD9.

[41] K. Kanonakis, E. Giacoumidis, and I. Tomkos, "Physical-layer-aware MAC schemes for dynamic subcarrier assignment in OFDMA-PON networks," *Journal of Lightwave Technology*, vol. 30, no. 12, pp. 1915–1923, Jun 2012.

[42] Y. Luo, X. Yan, and F. Effenberger, "Next generation PON offering 40G or more bandwidth," in *Asia Communications and Photonics Conference*. Optical Society of America, 2012, p. ATh3C.2.

[43] M. Seimetz, *High–Order modulation for Optical Fiber Transmission Systems*. Springer, Atlanta, GA, 2009.

[44] P. Winzer and R.-J. Essiambre, "Advanced modulation formats for high-capacity optical transport networks," *Journal of Lightwave Technology*, vol. 24, no. 12, pp. 4711–4728, Dec. 2006.

[45] B. Liu, X. Xin, L. Zhang, K. Zhao, and C. Yu, "Broad convergence of 32QAM-OFDM ROF and WDM-OFDM-PON system using an integrated modulator for bidirectional access networks," in *National Fiber Optic Engineers Conference*. Optical Society of America, 2010, p. JThA26.

Chapter 2

Orthogonal Frequency Division Multiplexing

This chapter discusses the theory behind and the applications of Orthogonal Frequency Division Multiplexing (OFDM) as well as important metrics for measuring its signal quality. OFDM's recent adaptation to the world of optical communications is examined and the reasons behind its excellent performance in optical channels are explained. Various implementations of OFDM in next generation optical communications are presented.

2.1 Introduction

Orthogonal Frequency Division Multiplexing (OFDM) is a Multi–Carrier Modulation (MCM) technique which transmits data on many subcarriers which are harmonically related. The key differentiator between OFDM and regular Frequency Division Multiplexing (FDM) is that subcarrier spectra overlap, but do not interfere due to their harmonic relationship (known as orthogonality), allowing for an increased number of subcarriers to be transmitted in a given bandwidth.

The first proposal to use orthogonal frequencies for data transmission was made in 1966 by

Chang at Bell Labs [1]. This system used information about the channel characteristics and a bank of electrical filters at the transmitter to realise the harmonic relationship between subcarriers required for orthogonality. The next major step in the development of OFDM was made when Weinstein *et. al.* first proposed the use of a Fast Fourier Transform (FFT) as an efficient means to generate orthogonal subcarriers in publications in 1969 and 1971 [2], making OFDM viable for electronic communications at the time.

It was not until 1990 that OFDM was incorporated into a major consumer application, the wireline protocol Asymmetric Digital Subscriber Line (ADSL). Cioffi *et. al.* at Stanford University first demonstrated the suitability of Discrete Multi–Tone (DMT) – essentially the same as OFDM – for DSL systems [3, 4] which they attributed to its provision of relatively high data rates and efficiency in terms of spectral power distribution [5].

The first application of OFDM to optical communications was shown by Pan and Green in 1996 [6]. They demonstrated the direct modulation of a laser diode with a RF OFDM signal which they called a 'Lightwave Hybrid AM/OFDM system'. In 2001 Dixon *et. al.* proposed the use of OFDM to mitigate the effects of modal dispersion in a Multi–Mode Fibre (MMF) [7]. This tolerance to dispersion in an optical channel has since been recognised as one of the key attributes for making OFDM an excellent candidate for use in future optical networks. Research on this topic has grown rapidly with the use of OFDM in many types of optical systems, from Plastic Optical Fibre (POF) applications [8], to Hybrid wireline/wireless Access Networks [9], to Optical Super–Channels [10].

2.2 OFDM Principles

OFDM is a highly popular technique in both wired and wireless radio communications and has been specified in many radio standards such as WiFi, WiMAX, LTE, UWB, VDSL and ADSL as well as TV and radio broadcasting protocols such as DAB+, DRM and DVB. As stated above, only recently has OFDM been the subject of much research as a modulation technique for use in optical communication systems. The idea behind MCM techniques,

such as OFDM, is that one high data rate stream is split into multiple lower data rate streams and these streams are transmitted in parallel, giving longer symbol periods than single carrier techniques. In OFDM these parallel streams are typically modulated with Quadrature Amplitude Modulation (QAM). OFDM's compact arrangement of subcarriers, which are orthogonal to each other in the frequency domain, ensures high spectral efficiency and is the main reason behind OFDM's use in current radio standards. However, as previously stated, what makes OFDM particularly attractive for use in optical communications is its inherent tolerance to chromatic dispersion [11]. These key attributes will be discussed in the following sections.

2.2.1 Inverse Fast Fourier Transform

Shown in figures 2.1a and 2.1b below are the typical spectra of a FDM and an OFDM signal respectively. Like FDM, OFDM subcarriers each have a different frequency, but the difference is that individual OFDM subcarrier spectra overlap in the frequency domain. If each subcarrier is made to be orthogonal to all other subcarriers then they can be transmitted in parallel without interference. In OFDM, subcarriers are chosen to be orthogonal to each other in frequency. This is achieved by the implementation of an Inverse Fast Fourier Transform (IFFT) at the transmitter. In practice, as OFDM signals are created digitally, an Inverse Discrete Fourier Transform (IDFT) is implemented.

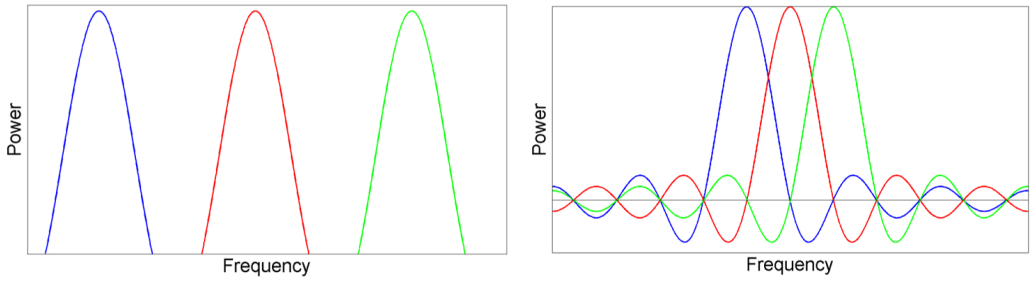

(a) (b)

Figure 2.1: OFDM (a) and FDM (b) subcarriers.

$$x_m = \frac{1}{\sqrt{N}} \sum_{k=0}^{N-1} X_k exp\left(\frac{j2\pi km}{N}\right) \text{ for } 0 \leq m \leq N-1 \tag{2.1}$$

Equation 2.1 gives the discrete form of the IFFT where N is the number of IFFT inputs (equals the number of resultant subcarriers), X refers to the frequency domain inputs or Fourier coefficients and x is the time domain output arising from the IFFT. It is important to note that each output x contains information about all X coefficients i.e. X_k for $0 \leq k \leq N-1$. On inspection of equation 2.1 it can be seen that output frequencies vary as $\frac{k}{N} = \frac{0}{N}, \frac{1}{N} \ldots \frac{N-1}{N}$ and as such each subcarrier frequency is an integer multiple of a fundamental frequency, in this case $\frac{1}{N}$. Since the area under the product of two sinusoids with frequency of an integer number of a fundamental frequency (ω) is 0,

$$\frac{1}{T} \cdot \int_{\frac{-T}{2}}^{\frac{T}{2}} \sin(p\omega t) \cdot \sin(q\omega t)\, dt = 0$$

$$p, q \epsilon \mathbb{Z}, \;\; p \neq q$$

the sinusoids, or subcarrier frequencies, assigned by the IFFT are said to be orthogonal over one IFFT operation i.e. they do not interfere and are therefore uniquely detectable by the inverse receiver function, the Fast Fourier Transform (FFT). In the frequency domain, it can be seen in figure 2.1b that at the peak of one particular subcarrier all other subcarriers pass through 0. Practically, this point corresponds to the ideal sampling instant at the receiver required for unique detection.

Figure 2.2 gives a conceptual diagram of the IFFT. The transform can be seen as a bank of mixers whose respective sinusoidal inputs, frequencies f_1 to f_{N-1}, are orthogonal. The output x_m is the summation of all orthogonal sinusoids. Each IFFT operation results in an output x_m and this is referred to as an OFDM symbol. The following analysis shows the relationship between the input QAM symbol stream and the resulting OFDM symbol rate and subcarrier spacing.

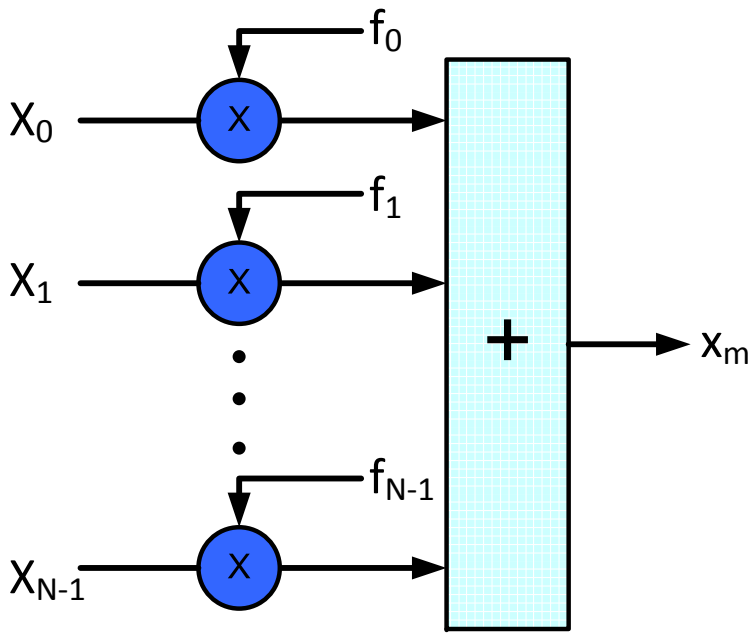

Figure 2.2: Conceptual diagram of the discrete IFFT

2.2.2 OFDM Symbol Rate and Subcarrier Spacing

Figure 2.3 shows a trivial example of the conversion of data from a serial bit stream to an OFDM symbol. The bit stream is divided into groups of bits which will each be assigned a specific QAM symbol. As 16–QAM is used in the example in figure 2.3, 4 bits are allocated to each QAM symbol. Serial to parallel conversion also takes place as the QAM symbols are arranged as inputs to the 6–point IFFT shown in the figure. The QAM inputs are processed by the IFFT as discussed in the previous section and the resultant output symbol, the OFDM symbol, is 6 times longer in time than each input QAM symbol.

More generally, if N parallel streams of QAM data are fed to the IFFT, then the OFDM symbol period, T_{ofdm}, is set to the original QAM stream symbol period, T_{data}, multiplied by N (since an OFDM symbol contains information about all input QAM symbols over one IFFT operation from equation 2.1).

$$T_{ofdm} = T_{data} \times N \tag{2.2}$$

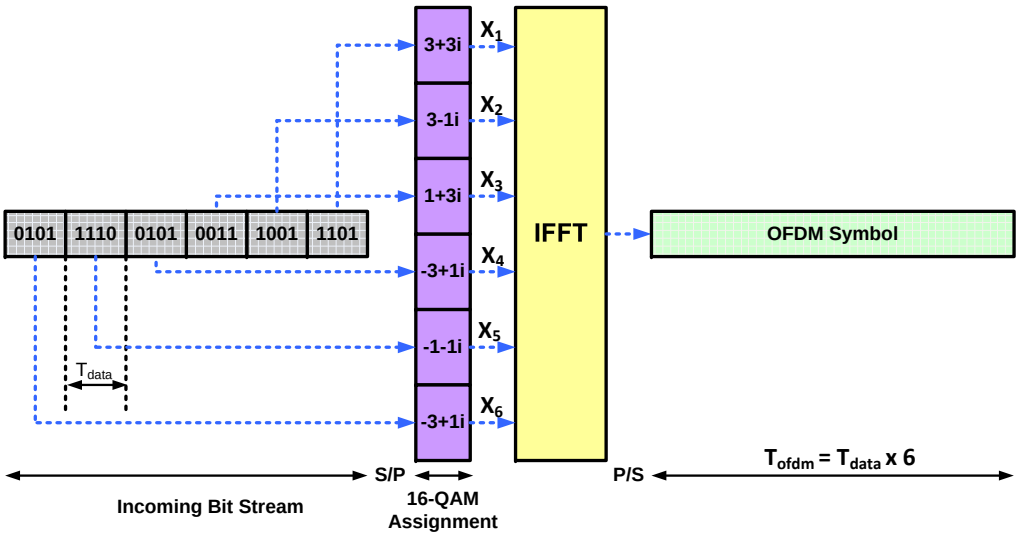

Figure 2.3: IFFT inputs (QAM symbols) and summed output (an OFDM symbol).

This gives an OFDM symbol rate of

$$R_{ofdm} = \frac{1}{(T_{data} \times N)}$$

$$= \frac{R_{data}}{N} \tag{2.3}$$

Now we can evaluate the subcarrier spacing in terms of the OFDM symbol rate. From equation 2.1 subcarrier frequencies vary from

$$f_0 = \frac{0}{N}, f_1 = \frac{1}{N} \ldots f_{N-1} = \frac{(N-1)}{N} \quad \text{cycles/sample} \tag{2.4}$$

and it can be seen that the subcarrier spacing is set by the IFFT to

$$f_p - f_q = \frac{1}{N} \quad \text{cycles/sample} \tag{2.5}$$

where p and q are consecutive integers and $0 \leq p, q \leq N-1$.

Given an input sample[1] rate to the IFFT of R_{data} samples/s, equation 2.5 can be scaled by to give a subcarrier spacing of

$$R_{data} \times \frac{1}{N} = \frac{R_{data}}{N} \quad \text{Hz} \tag{2.6}$$

which means, from equation 2.3, that the OFDM subcarrier spacing is equal to the OFDM symbol rate because

$$\frac{R_{data}}{N} = R_{ofdm} \quad \text{Hz} \tag{2.7}$$

The extremely low subcarrier spacing facilitated by the fact that subcarriers can overlap and still be uniquely detectable, is one of that major advantages of OFDM and is the main reason for its popularity in RF communications. Spectral efficiency can be even further increased my maximising the level of QAM used on each subcarrier. Another key advantage of OFDM, particularly for applications in optical communications, is its tolerance to large amounts of chromatic dispersion which is discussed in the following section.

2.2.3 Cyclic Prefix

One of the enabling techniques for OFDM is the insertion of a Cyclic Prefix [12]. Let us consider one OFDM symbol. We have seen in section 2.2.1 that each OFDM symbol contains N orthogonal subcarriers. As each subcarrier is at a different frequency the effect of dispersion is to introduce a delay spread across all transmitted subcarriers. The receiver FFT window size is the same as the transmitted IFFT size (i.e. the size of one OFDM symbol).

Consider just two subcarriers within an OFDM symbol which are aligned in time at the transmitter as per figure 2.4A. Assume, for simplicity, that one subcarrier arrives at the receiver exactly within the FFT window. Therefore the other (lower frequency) subcarrier has been delayed due to dispersion by a time t_d, see figure 2.4B. It is clear from the diagram

[1] Here 'sample' refers to one discrete element of the input data stream to the IFFT, which most commonly happens to be a stream of QAM symbols.

that the received version of Subcarrier 1 is a truncated version of the original transmitted subcarrier. Note also that inter (OFDM) symbol interference has occurred. As a full copy of Subcarrier 1 is not received, the subcarriers can no longer be described as orthogonal.

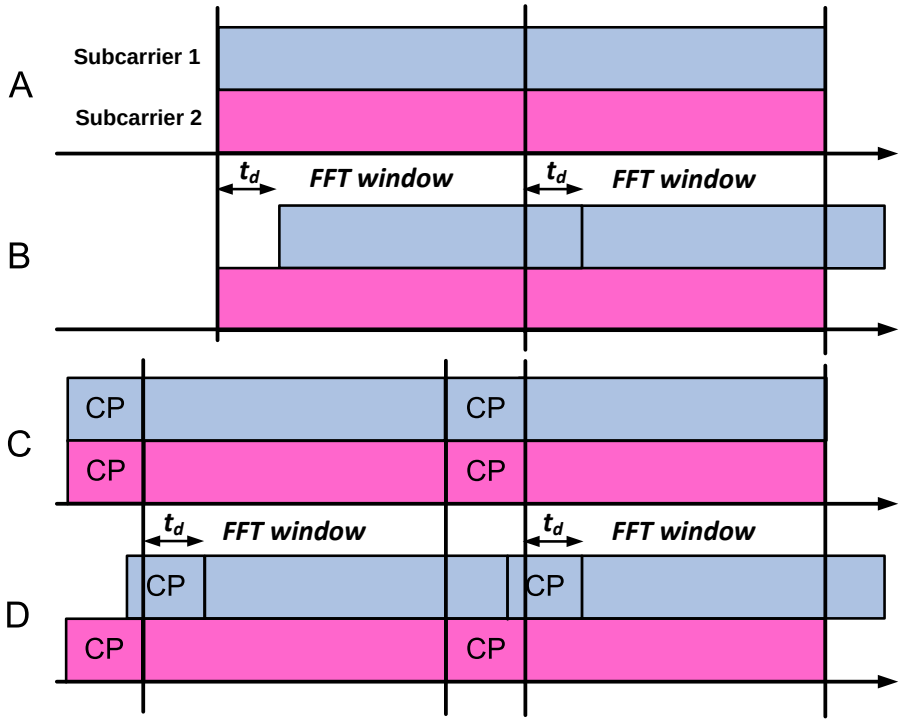

Figure 2.4: A. Transmitted subcarriers, B. Received subcarriers, C. Transmitted subcarriers with a CP and D. Received subcarriers with a CP.

The solution to this problem is to append a portion from the end of each subcarrier (within each OFDM symbol) to the start of it as shown in figure 2.5. This is known as the Cyclic Prefix (CP) and once the length of the CP is greater than the maximum delay spread caused by dispersion, t_{max}, then a complete copy of every subcarrier will be received and orthogonality is preserved. The addition of a CP at the transmitter is shown in figure 2.4C and reception after propagation through a dispersive channel is shown in figure 2.4D. Figure 2.5 shows the CP being added to an entire OFDM subcarrier containing N subcarriers.

When the CP is employed at the receiver to ensure a full copy of a particular subcarrier is obtained it can be seen in figure 2.4D that the received version is a time shifted version of the transmitted subcarrier. In essence, the received subcarrier is a copy of the transmitted

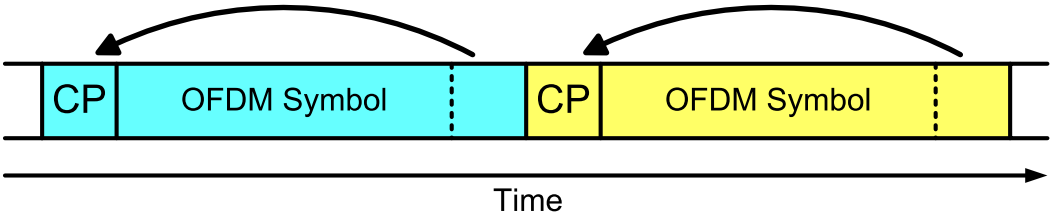

Figure 2.5: OFDM Cyclic Prefix implementation.

subcarrier with an added phase shift. As each subcarrier is delayed by a different amount of time it follows that each received subcarrier, in one OFDM symbol, has a different phase shift relative to the corresponding transmitted subcarrier. This phase shift, as well as other frequency selective effects caused by the channel, affect the received data and need to be accounted for.

2.2.4 Channel Estimation and Equalisation

As stated previously, IFFT parallel input data is typically data that has been modulated using QAM. One QAM symbol is described by one complex number. This QAM data is in turn modulated onto OFDM subcarriers by the IFFT. The phase shifted versions of the original transmitted subcarriers at the receiver are processed using the FFT and the output is the transmitted QAM data with channel effects. The relative change in phase caused by dispersion manifests itself as a shift in phase of each QAM symbol. The channel frequency response causes different subcarriers to have different channel gains and this affects the magnitudes of the QAM symbols. Therefore, in order to retrieve the QAM data correctly, it is necessary to estimate these channel effects and account for them by equalising the data accordingly.

The solution to this particular problem is to use a Training Sequence (TS). This is a known sequence of complex numbers that is used as the input to the N dimensional IFFT and therefore results in one OFDM symbol. It is common to transmit this sequence more than once throughout an entire OFDM signal. As the training sequence constitutes one entire OFDM symbol, and therefore contains every subcarrier, information about the channel ef-

fect on every subcarrier can be obtained by comparing the transmitted and received training sequences. This is known as channel estimation. This can be described simply in mathematical terms. For a given channel response H and known input X the output is

$$Y = H \times X$$

Since in this case the input and the output are both known, we can estimate the channel as:

$$H_{est} = \frac{Y}{X}$$

Now we have a channel estimation H_{est} that describes the effect of the channel on every OFDM subcarrier. To reverse the channel effect on all subsequent data we simply invert the channel estimation H_{est} and apply the resulting equalizer to all subsequent data. The practical implementation of this in DSP is also straightforward. Since both the transmitted and received training sequences consist simply of a vector of N complex numbers, so too does the channel estimation, H_{est}. It follows that this equaliser vector can be seen as a bank of N equalisers which is used to reverse the channel effects of each subsequent corresponding N QAM symbols, following receiver demodulation by the FFT as illustrated in figure 2.6.

In optical systems this technique can be used to overcome chromatic dispersion which is a linear impairment. For simplicity, consider the effect of a dispersive channel on a single subcarrier in an OFDM symbol which is in the range $0 \leq k \leq N-1$. The time domain OFDM symbol associated with the k^{th} subcarrier at the transmitter can be described as

$$x(k,t) = \frac{1}{\sqrt{N}} X_k exp\left(\frac{j2\pi kt}{T}\right) \tag{2.8}$$

where T is the OFDM symbol duration and $0 \leq t \leq T$. Ignoring the effects of noise, the received version of the signal will experience a certain amount of gain, g_k and a time shift

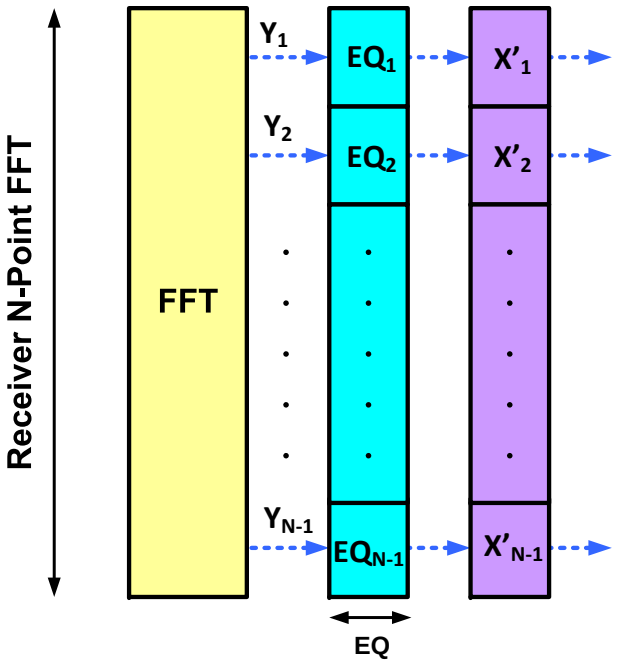

Figure 2.6: Channel equalisation after receiver FFT.

due to dispersion τ_k associated with the k^{th} subcarrier frequency.

$$y(k,t) = g_k \cdot \frac{1}{\sqrt{N}} X_k exp\left(\frac{j2\pi k(t-\tau_k)}{T}\right) \tag{2.9}$$

Rearranging equation 2.9,

$$y(k,t) = \frac{1}{\sqrt{N}} X_k exp\left(\frac{j2\pi kt}{T}\right) \cdot \left[g_k \cdot exp\left(\frac{-j2\pi k\tau_k}{T}\right)\right] \tag{2.10}$$

After FFT demodulation at the receiver and adding the effects of noise we receive

$$Y_k = X_k \left[g_k \cdot exp\left(\frac{-j2\pi k\tau_k}{T}\right)\right] + W_k \tag{2.11}$$

$$Y_k = X_k \cdot H_k + W_k \tag{2.12}$$

So the transmitted symbol X_k can be recovered from the received symbol Y_k using only one complex multiplication: Y_k multiplied by $1/H_k$, the k^{th} equaliser in the bank of N equalisers which corrects for phase shifts and attenuation on the k_{th} subcarrier after it has propagated

through the optical channel.

This is referred to as one–tap equalisation (EQ) because it requires only one complex multiplication. This operation takes place after the receiver FFT and as such is implemented in the frequency domain. This simple channel EQ is a major advantage of OFDM over other multiplexing techniques such as TDM, which require complicated time domain algorithms. Figures 2.7a, 2.7b and 2.7c show transmitted and received constellations (before and after EQ) obtained from the simulation of several OFDM symbols propagating through standard single mode fibre (SSMF). The effect of dispersion on the phase of the QAM symbols is clearly shown in the 'rotated' received constellation before EQ (figure 2.7b).

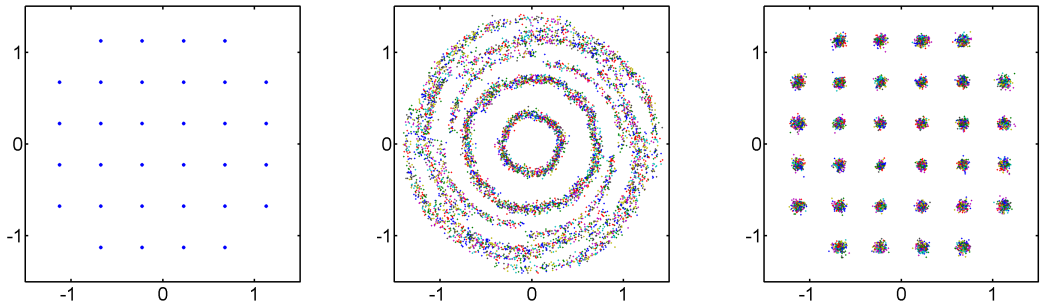

(a) Transmitted. (b) Received. (c) Estimated.

Figure 2.7: Various 32-QAM constellations.

2.3 Error Vector Magnitude

Error Vector Magnitude (EVM) is a common measure for expressing the quality of a measured digitally modulated signal. It is defined as the vector subtraction of a reference signal from a measured signal and so it quantifies by how much a received symbol has deviated from the ideal symbol point [13]. When observing BER, fluctuations, in amplitude and phase are not detected until they are large enough to cause a bit error. EVM rises and falls in proportion to these fluctuations providing a measure of signal quality for all received signals. Furthermore, to process received advanced modulation format signals, most laboratory experiments make use of receivers employing offline DSP with reduced clock rates.

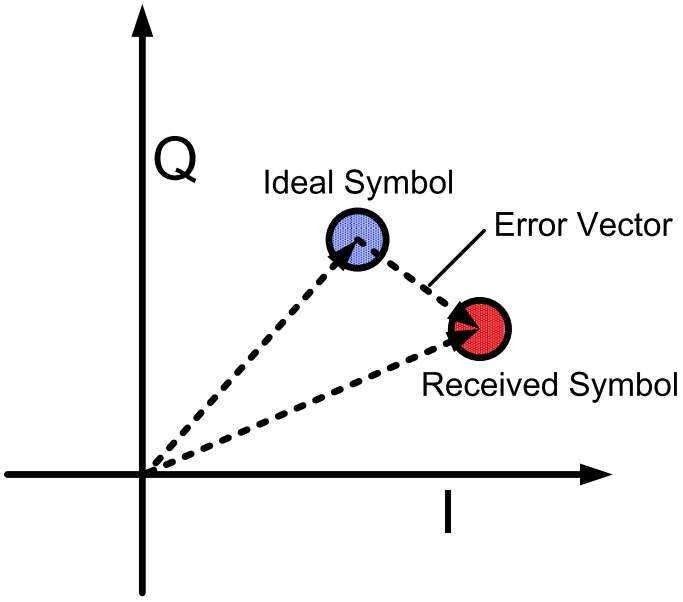

Figure 2.8: Error Vector Magnitude for one transmitter/received QAM symbol.

In this case it can be very time consuming to compute a reliable BER, particularly if the signal quality is high [14]. Consequently, EVM is used to provided a fast, yet reliable, method for gauging received signal quality. For OFDM systems, EVM is calculated by examining transmitted and received QAM constellations i.e. the input symbols to the IFFT (transmitted) and the demodulated symbols after the FFT (received).

Figure 2.8 shows the error vector for a single transmitted and received QAM symbol. The magnitude of this vector is calculated by subtracting the ideal and received vector magnitudes and taking the absolute value. EVM values are typically given as a percentage of the ideal transmitted vector magnitude. For the case where many symbol values (constellation points) are transmitted and received, the EVM is equal to the sum of the magnitude of error vectors, for all of the received symbols, divided by the total number of transmitted/received symbols. This average value can then be expressed as a percentage of the average ideal vector magnitude. From [15] Root–Mean–Square (RMS) EVM can be calculated as

$$EVM_{rms} = \left[\frac{\frac{1}{N} \sum_{p=1}^{N} |S_{p,i} - S_{p,m}|^2}{\frac{1}{N} \sum_{p=1}^{N} |S_{p,i}|^2} \right]^{\frac{1}{2}} \tag{2.13}$$

where S_i and S_m are the ideal and measured symbol (or constellation) points respectively and N is the number of unique symbols in the constellation (e.g. $N = 16$ for 16–QAM).

2.3.1 Constellation Normalisation

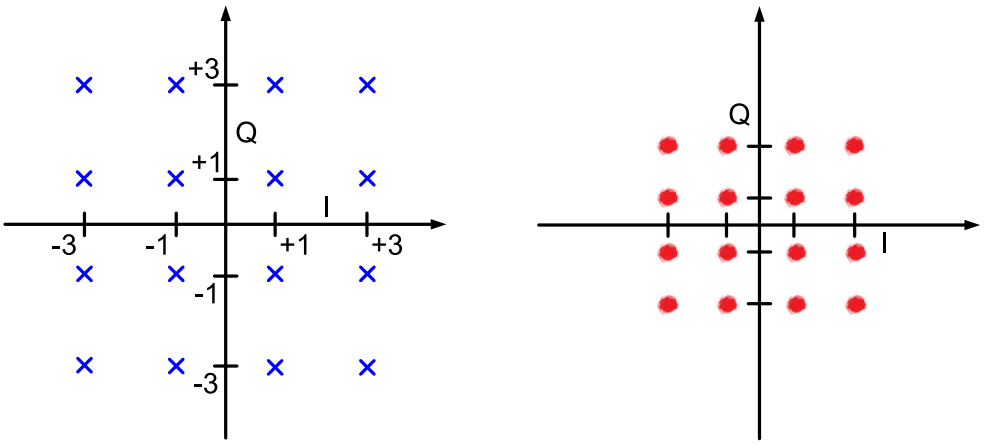

(a) (b)

Figure 2.9: Ideal (a) and received (b) constellations.

In order to correctly calculate EVM it is necessary to scale transmitted and received constellation diagrams so that a direct comparison can be made. Ideal QAM constellation points, like those shown in figure 2.9a, are represented by symbols at integer levels e.g. $3 + 1i$. However, received constellations, as shown in figure 2.9b, are quantified using measured signal voltage levels which depend greatly on the system transmitter and receiver components. Both ideal and received constellation diagrams must be scaled to give a normalised constellation diagram so that the ideal symbol values can be compared to arbitrary voltage values [16].

A common normalisation process for constellations is to normalise the transmitted (ideal)

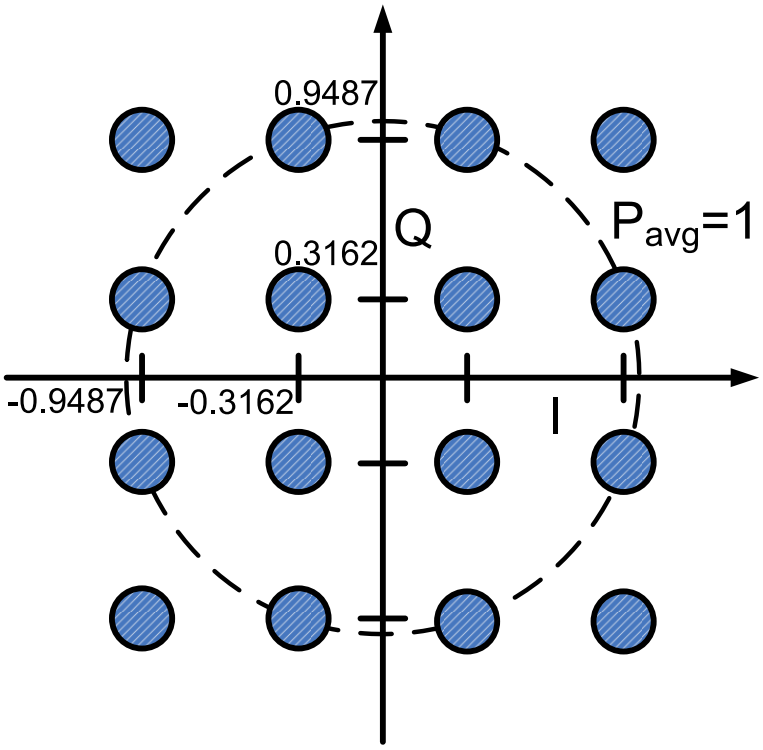

Figure 2.10: Normalised 16–QAM constellation.

and received constellation powers to 1, as shown in figure 2.10 [16]. For the received constellation this can be achieved by dividing the power in each symbol, P_{sym} by the average symbol power calculated over all received symbols N_{total} to obtain P_{norm}. Hence, this method assumes that each constellation point is equally likely to be received.

$$P_{norm} = \frac{P_{sym}}{P_{total}/N_{total}} \tag{2.14}$$

where P_{total} is the total power of all received symbols

$$P_{total} = \sum_{n=1}^{N_{total}} \left[(V_{I,t})^2 + (V_{Q,t})^2\right] \text{ W} \tag{2.15}$$

and $V_{I,t}$ and $V_{Q,t}$ are the measured in–phase and quadrature voltage level components of the received QAM symbols. P_{norm} represents the normalised symbol powers. It is dimensionless and has a mean value of 1.

An amplitude scaling factor can be obtained in order to implement this normalisation easily, with the EVM calculation in equation 2.13. From equation 2.14

$$|A_m| = \sqrt{\frac{1}{P_{total}/N_{total}}} \tag{2.16}$$

So $|A_m|$ is the amplitude scaling factor that must be applied to each received constellation symbol in order to normalise the average symbol power to 1 as shown in figure 2.10. A similar analysis is used to obtain the normalisation factor for the ideal case $|A_i|$, the difference being that this is carried out in an integer space rather than a voltage space. Adding these normalising terms to equation 2.13 we obtain an expression for EVM which is agnostic to transmitted ideal integer symbol points and received voltage symbol levels.

$$EVM_{rms} = \left[\frac{\frac{1}{N_{total}} \sum_{n=1}^{N_{total}} \left\{ |V_{I,t} \cdot |A_m| - Z_{I,t} \cdot |A_i||^2 + |V_{Q,t} \cdot |A_m| - Z_{Q,t} \cdot |A_i||^2 \right\}}{P_{avg}} \right]^{\frac{1}{2}} \tag{2.17}$$

where P_{avg} is the average power of the normalised constellation and is therefore always equal to 1 as in figure 2.10

2.3.2 EVM, SNR and BER

Signal–to–Noise Ratio (SNR) and, as stated previously, BER are metrics which are commonly used to evaluate system performance. EVM is essentially a relationship between the average ideal signal magnitude and the average error (or noise) magnitude as shown by equation 2.13 and so it is intuitive that EVM can easily be related to SNR. SNR is defined as

$$\begin{aligned} SNR &= \frac{\text{Signal Power}}{\text{Noise Power}} \\ &= \frac{E_s}{N_0} \end{aligned} \tag{2.18}$$

assuming a Gaussian noise model and where E_s/N_0 is the energy per symbol to noise spectral density for systems which are sampled at the symbol rate. Assuming a large number of transmitted symbols with each symbol equally likely to occur, for QAM systems, where $N_{total} >> M$ (the number of unique symbols in the constellation), this ratio can be expressed as

$$SNR = \left[\frac{\frac{1}{N_{total}} \sum_{n=1}^{N_{total}} \left\{ (V_{I,t})^2 + (V_{Q,t})^2 \right\}}{\frac{1}{N_{total}} \sum_{n=1}^{N_{total}} \left\{ (N_{I,t})^2 + (N_{Q,t})^2 \right\}} \right] \tag{2.19}$$

where $V_{I,t}$ and $V_{Q,t}$ are the in–phase and quadrature signal components respectively and $N_{I,t}$ and $N_{Q,t}$ are the in–phase and quadrature complex noise amplitudes [17]. Considering a Gaussian noise model, equation 2.17 can expressed with the in–phase and quadrature noise components $N_{I,t}$ and $N_{Q,t}$ as

$$EVM_{rms} = \left[\frac{\frac{1}{N_{total}} \sum_{n=1}^{N_{total}} \left\{ (N_{I,t})^2 + (N_{Q,t})^2 \right\}}{P_{avg}} \right]^{\frac{1}{2}} \tag{2.20}$$

and comparing equations 2.19 and 2.20 it follows that

$$\begin{aligned} EVM_{rms} &\approx \left[\frac{1}{SNR} \right]^{\frac{1}{2}} \\ &= \left[\frac{N_0}{E_s} \right]^{\frac{1}{2}} \end{aligned} \tag{2.21}$$

and SNR and be expressed in terms of EVM as

$$SNR \approx \frac{1}{EVM_{rms}^2} \tag{2.22}$$

where EVM_{rms} and hence SNR are calculated from the normalised constellations.

The relationship between SNR and BER is well known. The above analysis will allow BER to be expressed in terms of EVM. The probability of symbol error P_e for M–ary QAM in a

Gaussian noise channel can be expressed as [18][2]

$$P_e \approx 2 \cdot \left(1 - \frac{1}{\sqrt{N}}\right) \cdot erfc\left(\sqrt{\frac{3}{2(N-1)} \cdot \frac{E_s}{N_0}}\right) \tag{2.23}$$

where $erfc$, the Complimentary Error Function is given as

$$erfc(x) = \frac{2}{\sqrt{\pi}} \int_x^\infty e^{-t^2} dt$$

Combining equations 2.21 and 2.23, P_e can be expressed as

$$P_e \approx 2 \cdot \left(1 - \frac{1}{\sqrt{N}}\right) \cdot erfc\left(\sqrt{\frac{3}{2(N-1)} \cdot \frac{1}{EVM_{rms}^2}}\right) \tag{2.24}$$

P_e, the probability of *symbol* error for M–ary QAM systems, can be approximated to equal the probability of bit error in the case where Gray coding is used (see section 1.5.3.2). This is because in the presence of relatively low levels of noise, QAM symbols are most likely to be erroneously detected as an adjacent QAM symbol which only differs by one bit. i.e. one symbol error equals one bit error. Clearly this approximation decreases in accuracy as the levels of noise introduced increases.

2.4 OFDM Peak–to–Average Power Ratio

OFDM has many advantageous such as high spectral efficiency, resilience to dispersion and ease of channel equalisation. However, the main disadvantage of OFDM is its inherent high Peak–to–Average–Power Ratio (PAPR). Radio systems typically employ a high power amplifier at the transmitter which is operated in saturation for power efficiency. Amplifying a large PAPR signal in this way leads to non–linear distortion and so the amplifier must be operated in a 'back–off' region, leading to inefficient amplification and insufficient range [19, 20]. In optical communications systems high PAPR also affects the output signal

[2]M–ary QAM refers to QAM schemes which have an alphabet size of M where M is a power of 2 (e.g. 4, 16, 32 etc.). This gives the number of bits transmitted on each symbol equal to $\log_2(M)$.

power at the transmitter. Modulating laser diodes and external modulators with high PAPR signals provides maximum extinction only when the peaks of the driving signal occur. This occurrence can be rare and the peaks can have significantly higher power than the average power of the signal. In this case the laser diode or external modulator must be under–driven for the vast majority of the signal duration. Simply increasing the drive signal's amplitude can lead to modulating below threshold in the case of direct modulation, or non–linear distortion when using external modulators.

The composition of OFDM symbols from the summation of many subcarriers can lead to very high sample values at points where subcarrier peaks coincide. The summation of subcarrier modulated signals in this way leads to an approximately Gaussian distributed waveform [21].

From Equation 2.1 for the IFFT we can express a single OFDM symbol as

$$s(t) = \frac{1}{\sqrt{N}} \sum_{k=0}^{N-1} X_k exp\left(\frac{j2\pi kt}{T_s}\right) \text{ for } 0 \leq t \leq T_s \tag{2.25}$$

where T_s is the OFDM symbol period, N is the number of subcarriers and X_k are the input QAM symbols (of which there are N). PAPR is given by

$$PAPR = \frac{P_{max}}{P_{av}} \tag{2.26}$$

$$PAPR = \frac{\max(|s(t)|^2)}{E(|s(t)|^2)} \text{ for } 0 \leq t \leq T_s \tag{2.27}$$

$$PAPR = \frac{\max(|s(t)|^2)}{\frac{1}{N}\sum_{k=0}^{N-1} E(|X_k|^2)} \text{ for } 0 \leq t \leq T_s \tag{2.28}$$

where $E(\cdot)$ is the expected value. For simplicity, consider the case where $|X_k|$ is restricted to having the value 1 (e.g. 8–PSK modulation). Setting $|X_k| = 1$, $N = 256$ and setting

$t = 0$, the theoretical maximum PAPR can be calculated.

$$PAPR = \frac{\frac{1}{256} \cdot (256)^2}{\frac{1}{256} \cdot \frac{(256)^2}{256}} = 256 \tag{2.29}$$

$$PAPR_{dB} = 10 \log_{10}(256) = 24\text{dB} \tag{2.30}$$

Fortunately such a high PAPR is a rare event; however the more OFDM symbols that are transmitted in one signal the more likely it is for a very high PAPR to be observed. Many approaches have been taken to try to reduce PAPR, some more complex than others. These include clipping [22], constellation modification [23], pre–coding [24] and partial transmit sequence [25]. The most common form of PAPR reduction, hard clipping, is discussed in the following section.

2.4.1 Clipping

Hard clipping is a simple form of PAPR reduction whereby the OFDM signal to be transmitted is restricted to be within a given amplitude level. If signal peaks exceed this level they are simply reset to the maximum allowable level. There is clearly a trade off between the amount of noise introduced by clipping and the performance improvement gained due to the higher optical extinction which is achieved by employing a reduced PAPR signal. The optimum level of clipping which should be employed is dependant on the P–I curve of the laser diode or the characteristic of the external modulator used, as well as the voltage swing available from the driving electronics.

An issue posed by high PAPR signal which affects all systems using digitally generated OFDM signals is quantisation noise introduced by the Digital–to–Analogue Converter (DAC) at the transmitter and the Analogue–to–Digital Converter (ADC) at the receiver. In analogue to digital conversion, the difference between the actual analogue value and the sampled digital value is known as quantisation noise. ADCs and DACs have a given resolution to which they can operate and the presence of rare high peaks in a signal to be

processed by these electronic converters ensures that for the majority of the signal length the OFDM signal is quantised by only a fraction of the available levels, introducing increased quantisation noise. In order to overcome this problem clipping can be used. For ADCs/DACs of a given resolution it is possible to calculate an optimum clipping level such that maximum use is made of the electronics, while as little noise as possible is introduced due to clipping.

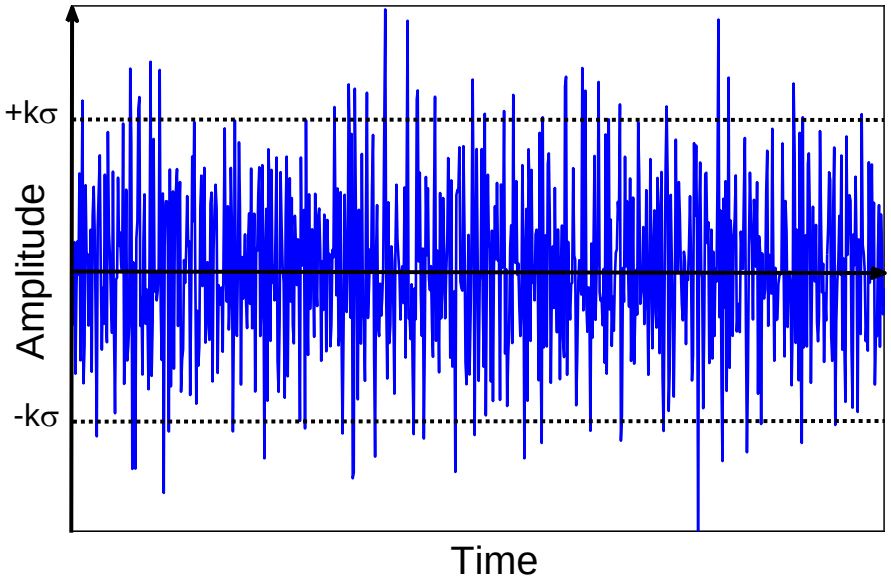

Figure 2.11: Hard clipping levels for a high PAPR OFDM signal.

Consider a clipping factor k where the OFDM signal is clipped at $+k\sigma$ at the upper boundary and $-k\sigma$ at the lower boundary, as in figure 2.11, where σ is the standard deviation of the OFDM signal samples $x[n]$. For ≥ 10 subcarriers the ensemble average of the amplitudes $x[n]$ can be modelled as a Gaussian Random Process [12]. So the Probability Density Function $p(x)$, which describes the relative likelihood of $x[n]$ to take on a particular value, can be written as

$$p(x) = \frac{1}{\sqrt{2\pi\sigma^2}} e^{-\frac{x^2}{2\sigma^2}} \tag{2.31}$$

The noise due to clipping can be estimated as the power lost due to clipping [22]. Summing

up the power of the signal above and below $+k\sigma$ and $-k\sigma$ respectively.

$$n_c^2 = 2 \cdot \int_{k\sigma}^{\infty} (x - k\sigma) \frac{1}{\sqrt{2\pi\sigma^2}} e^{\frac{x^2}{2\sigma^2}} dx \tag{2.32}$$

$$\approx 2 \cdot \sqrt{\frac{2}{\pi}} \cdot \sigma^2 k^{-3} e^{\frac{-k^2}{2}} \tag{2.33}$$

Quantization noise for a q bit ADC is given by [22]

$$n_q^2 = \frac{(k\sigma)^2 \cdot 2^{-2q}}{3} \tag{2.34}$$

and so the SNR, considering only digital distortion (clipping and quantisation noise), can be expressed as

$$SNR = \frac{\sigma^2}{n_c^2 + n_q^2} \tag{2.35}$$

$$= \left(2\sqrt{\frac{2}{\pi}} \cdot k^{-3} e^{\frac{-k^2}{2}} + \frac{k^2 2^{-2q}}{3} \right)^{-1} \tag{2.36}$$

So for a given bit resolution q an optimum clipping factor k can be chosen so that the value for SNR can be maximised. Figure 2.12 shows SNR as a function of clipping level for various ADC/DAC resolutions indicating optimum clipping factors in each case.

2.5 Adaptive Modulation OFDM

Errors due to transmission of an OFDM signal (with a fixed modulation scheme on each subcarrier) are dominated by the subcarriers with the smallest SNR, so simply increasing the transmit power signal may not necessarily have a large impact with regard to reducing the observed BER. This is in contrast to single–carrier modulation schemes, where the energy of a single bit is distributed across the bandwidth of the signal and so the frequency selective response of a channel results in far less errors when compared to OFDM [26].

To overcome this problem Adaptive Modulation OFDM (AM–OFDM) can be used. This

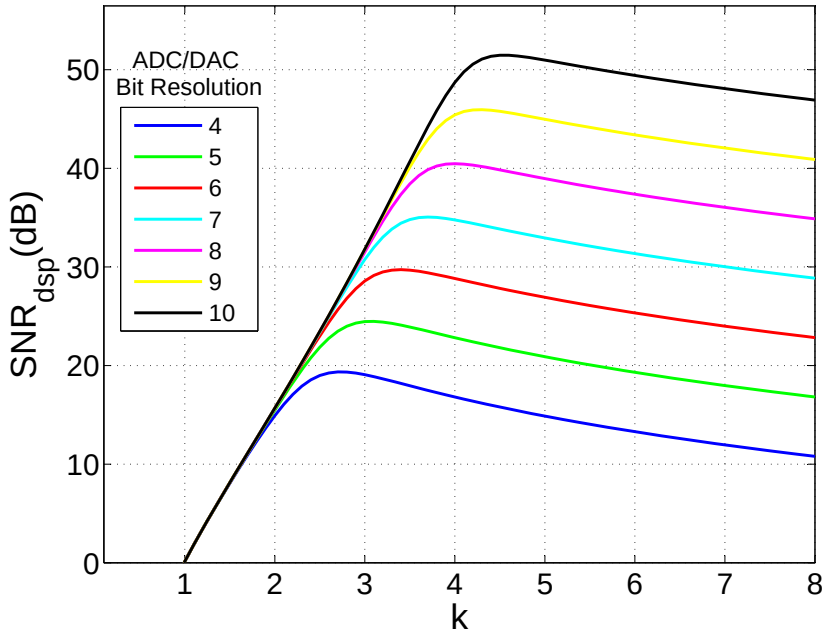

Figure 2.12: Clipping factor vs. SNR for various ADC/DAC resolutions.

differs to regular OFDM as the modulation format on each subcarrier is adjusted according to the characteristics of the transmission channel. In doing so, overall throughput and robustness to the channel can be improved [27]. As channel characteristics are needed in order to choose a suitable modulation format for each subcarrier, it is necessary to transmit a pilot signal so that channel information can be fed to the transmitter. Adaptive modulation in this way can be considered to be both a bit loading and power loading scheme as constellation sizes (and hence both bit/symbol and signal power) on each subcarrier can be either increased or decreased.

AM–OFDM, also known as Discrete Multi–Tone (DMT), was first proposed for use with DSL/ADSL services as a means of increasing data rates and robustness to channel impairments over the copper twisted pair cables [28–30]. The use of AM–OFDM was then demonstrated for wideband radio channels exhibiting a large improvement over a frequency selective, time variant channel when compared to regular OFDM [31]. More recently AM–OFDM has been the subject of research for optical communications systems [32–34]. AM–OFDM naturally lends itself to overcoming the frequency selective fading channel re-

sponses of direct modulation systems in particular, which are dominated by the modulation response of the laser diode [35, 36].

2.5.1 The Levin–Campello Algorithm

Each OFDM subcarrier can be considered as an independent sub–channel, with each experiencing a different SNR after transmission through a channel. In optical communications this channel is typically time invariant. In order to maximise the throughput for a given total allowable transmit power, a mapping needs to be derived which assigns the optimum modulation order to each subcarrier taking into account SNR experienced by those subcarriers respectively. This mapping is known as the bit distribution. The algorithm used to optimise this bit distribution is known as the Levin–Campello (LC) algorithm [37]. This was chosen over other algorithms such as Chow's algorithm [28] as it converges on an efficient bit distribution without violating the total allowable energy constraint.

Starting with a sub–optimal bit distribution $b = [b_1, b_2 \dots b_N]$ where N is the number of subcarriers, the algorithm exploits the fact that for a given set of subcarrier Gain-to-Noise Ratios(GNRs) and margin (this is also known as the gap–to–capacity and it measures the proximity of data rates to the highest theoretically available data rate – the channel capacity), the energy required on each subcarrier, $\varepsilon_n(b_n)$ can be calculated [38]. Furthermore, it is also possible to calculate the change in energy required to alter the constellation size on a subcarrier by β bits/symbol. This is known as the incremental energy.

The LC algorithm works in two steps.

Step 1 Efficientizing: The LC algorithm uses the incremental energy information to search for the subcarrier for which *increasing* the constellation size by 1 bit/symbol (therefore granularity β = 1) incurs the *least* amount of energy cost while simultaneously searching for the subcarrier for which *decreasing* the constellation by 1 bit/symbol saves the *most* energy. The relevant constellation sizes are updated and this process is continued until the maximum saving in energy gained by decreasing a subcarrier constellation by 1 bit/symbol

is *less than or equal to* the minimum energy required to increase a subcarrier constellation by 1 bit/symbol i.e.

$$\max_{1\leq n\leq N} e_n(b_n) \leq \min_{1\leq m\leq N} e_m(b_m+\beta) \tag{2.37}$$

Practically this condition means that even though the constellation size can be decreased by 1 bit/symbol on the subcarrier which provides the maximum saving in energy in doing so, this saving in energy is not sufficient to increase the constellation size (by 1 bit/symbol) on any other subcarrier. This step is known as the 'efficientizing' algorithm, as it converges on the most efficient bit distribution. A distribution is said to be efficient when it has the lowest total power of all bit distributions with the same bit rate.

Step 2 E–Tightness: Next the LC algorithm takes the 'efficient' bit distribution from step 1 and forces it to be constrained by the total allowable energy ε_T. While the sum of the subcarrier energies exceeds the total allowable energy, the algorithm searches for the subcarrier for which reducing the constellation size by 1 bit/symbol saves the most energy. Again, the constellation size on the subcarrier in question is decreased accordingly. This iterative process continues until the total allowable energy minus the sum of the subcarrier energies is *less than or equal to* the minimum energy required to increase the constellation size on a subcarrier by 1 bit/symbol. i.e.

$$0 \leq \varepsilon_T - \sum_{n=1}^{N} \varepsilon_n(b_n) \leq \min_{1\leq i\leq N}[e_i(b_i+\beta)] \tag{2.38}$$

This ensures that no additional unit of information can be carried without violation of the total allowable energy constraint.

2.5.1.1 Discrete Implementation

Although the algorithm is somewhat complex to describe, its implementation in a digital system is straightforward. In order to complete steps 1 and 2, the subcarrier energies must be calculated. Subcarrier energies for M–QAM, with a granularity of $\beta = 1$ are given

by [39]

$$\varepsilon_n(b_n) = 2 \cdot \frac{\Gamma}{g_n}(2^{b_n} - 1) \tag{2.39}$$

Again, where n is the subcarrier index ($n \, \epsilon \, [1, N]$), g_n is the subcarrier GNR and b_n is the number of bits per symbol carried by the modulation format on each subcarrier. Γ is the gap–to–capacity for M–QAM (see appendix B) which is calculated by specifying a desired probability of error. This allows the bit distribution to be optimised for a desired BER. Knowing the total subcarrier energies, the incremental energies $e_n(b_n)$ can be calculated for all subcarriers, for all levels of modulation, where

$$e_n(b_n) = \varepsilon_n(b_n) - \varepsilon_n(b_n - \beta) \tag{2.40}$$

Step 1: Deriving an efficient distribution. Assign the index of the minimum incremental energy required to add an extra bit/symbol to a subcarrier to variable m.

$$m \leftarrow \arg \min_{1 \leq i \leq N} \; e_i(b_i + 1) \tag{2.41}$$

Now assign the index of the maximum incremental energy which would be saved by taking away 1 bit/symbol from a subcarrier to variable n.

$$n \leftarrow \arg \max_{1 \leq j \leq N} \; e_j(b_j) \tag{2.42}$$

While the minimum increase in energy required is less than the maximum energy saved the following actions must be performed.

`WHILE` $e_m(b_m + 1) < e_n(b_n)$

1. $b_m \leftarrow b_m + 1$ `(add 1 bit/symbol)`
2. $b_n \leftarrow b_n - 1$ `(take away 1 bit/symbol)`
3. $m \leftarrow \arg \min_{1 \leq i \leq N} e_i(b_i + 1)$ `(re-assign index)`
4. $n \leftarrow \arg \max_{1 \leq j \leq N} e_j(b_j)$ `(re-assign index)`

Step 2: This step enforces the energy constraint (equation 2.38) while maintaining an 'efficient' distribution. Let $S = \sum_{n=1}^{N} \varepsilon_n(b_n)$, the sum of the subcarrier energies. The following sets of actions must be performed depending on whether the total allowable energy is exceeded or not.

WHILE $(\varepsilon_T - S) < 0$ or $(\varepsilon_T - S) \geq \min_{1 \leq i \leq N} e_i(b_i + 1)$

IF $(\varepsilon_T - S) < 0$ (exceed energy limit)

1. $n \leftarrow \arg \max_{1 \leq j \leq N} e_j(b_j)$ (assign index of maximum energy saving)
2. $S \leftarrow S - e_n(b_n)$ (update value of S)
3. $b_n \leftarrow b_n - 1$ (take away 1 bit/symbol)

ELSE

1. $m \leftarrow \arg \min_{1 \leq i \leq N} e_i(b_i{+}1)$ (assign index of minimum energy required)
2. $S \leftarrow S + e_m(b_m + 1)$ (Update value of S)
3. $b_m \leftarrow b_m + 1$ (add 1 bit/symbol)

2.6 OFDM for Optical Communications

For the reasons outlined in this chapter, OFDM has recently become of great interest to the optical communications research community. Access, Metro and Core networks employing OFDM have all been proposed [40–42] and due to this variation in system implementation many 'flavours' of optical OFDM systems have evolved. However, the vast majority of proposed OFDM systems employ digital OFDM generation.

Figure 2.13 shows the basic building blocks of a digital OFDM transmitter which are required for all systems employing digital generation. Also shown is digital I/Q modulation onto an RF subcarrier which is required for optical systems where the optical phase is not modulated, i.e. mixing the real and imaginary components of the complex valued output

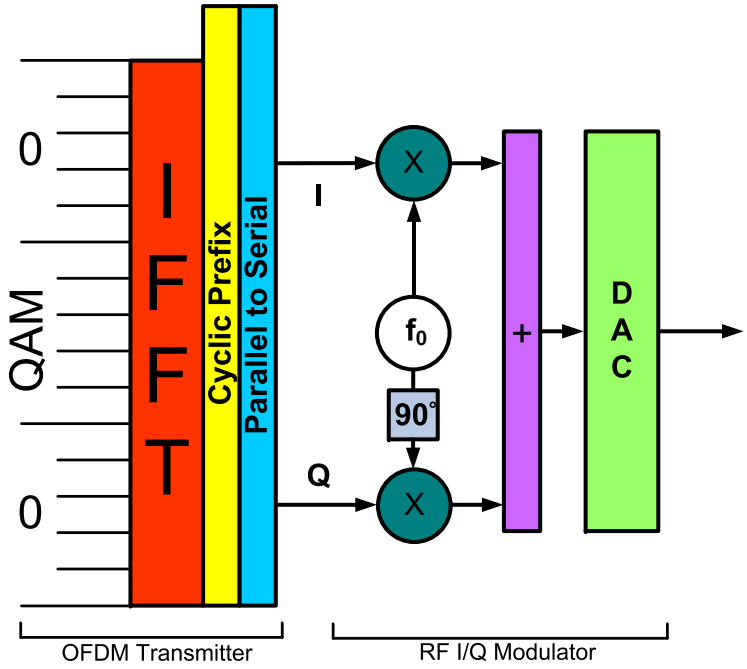

Figure 2.13: Electrical RF OFDM transmitter.

OFDM signal with the in–phase and quadrature components of an RF carrier. This produces a 'real' OFDM signal centred at the RF carrier frequency. An alternative to this technique is to arrange the QAM inputs to the IFFT to construct either a Hilbert transform (generating a real signal valued offset from baseband) or Hermettian symmetry (generating a real valued signal around baseband) [43]. Figure 2.14 shows the associated receiver consisting of an ADC, digital I/Q demodulator (using an RF Local Oscillator) and digital OFDM reception. It is worth noting that I/Q (de)modulation can also be carried out in the analogue domain where high RF carrier frequencies are required.

Although proposed optical OFDM systems architectures vary greatly, they can be broken down into three broad categories. Opto–Electrical OFDM, Coherent OFDM and All–Optical OFDM.

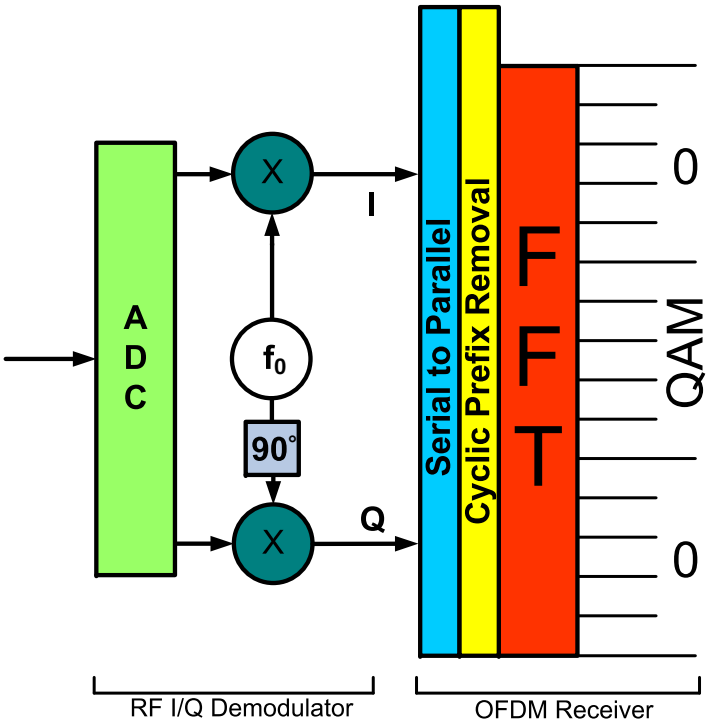

Figure 2.14: Electrical RF OFDM receiver.

2.6.1 Opto–Electrical OFDM

Opto–Electrical OFDM involves the modulation of a 'real' valued electrical OFDM signal onto an optical carrier. This can be achieved by driving a laser diode directly (as shown in figure 2.15), driving a single armed MZM or using the OFDM signal and its complement to drive a DD–MZM. In all cases the phase of the optical carrier is not modulated and so direct detection can be employed at the receiver. Either RF I/Q (de)modulation or the associated Hilbert transform/Hermettian symmetric IFFT are used to generate a real valued output and so the RF OFDM transmitter and receiver blocks shown in figure 2.15 consist of all the components shown in figures 2.13 and 2.14 respectively. Due to the low complexity and facilitation of the use of direct detection, optical OFDM systems employing this type of architecture are typically proposed for use in Access networks (mainly as PONs) [44] or sometimes for cost–effective long–haul applications [45].

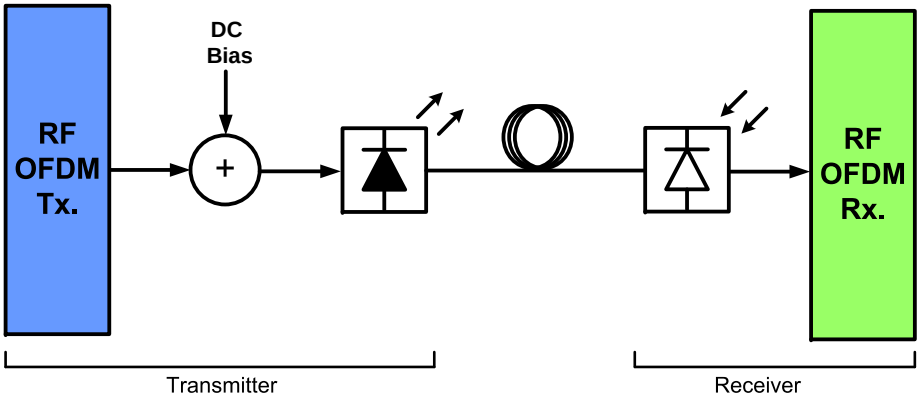

Figure 2.15: Electrical OFDM modulation onto an optical carrier.

2.6.2 Coherent Optical OFDM

In Coherent Optical OFDM the real and imaginary components of the output OFDM signal are used to modulate both the amplitude and phase of an optical carrier. Digital OFDM generation is employed, but rather than RF mixing, the complex baseband OFDM signal is used to drive an optical I/Q modulator as shown in figure 2.16. In order to retrieve both the optical amplitude and phase information, an optical Coherent Receiver (Co. Rx.) must be used. These types of receivers require that the in–phase and quadrature components of an optical Local Oscillator (LO) (with a known phase relationship to the transmitter optical source) beat with the received signal before being detected by a series of photo–detectors.

Although very high data throughput can be achieved, due to the increased amount of optical components used and the complexity associated in dealing with optical phase tracking/locking at the receiver [46], coherent Optical OFDM systems are typically proposed for Metro and Core applications [47]. Nevertheless, UdWDM schemes employing coherent detection, both at the OLT and the ONU, have been proposed for access networks. This would allow for excellent receiver sensitivity and close optical carrier spacings [48].

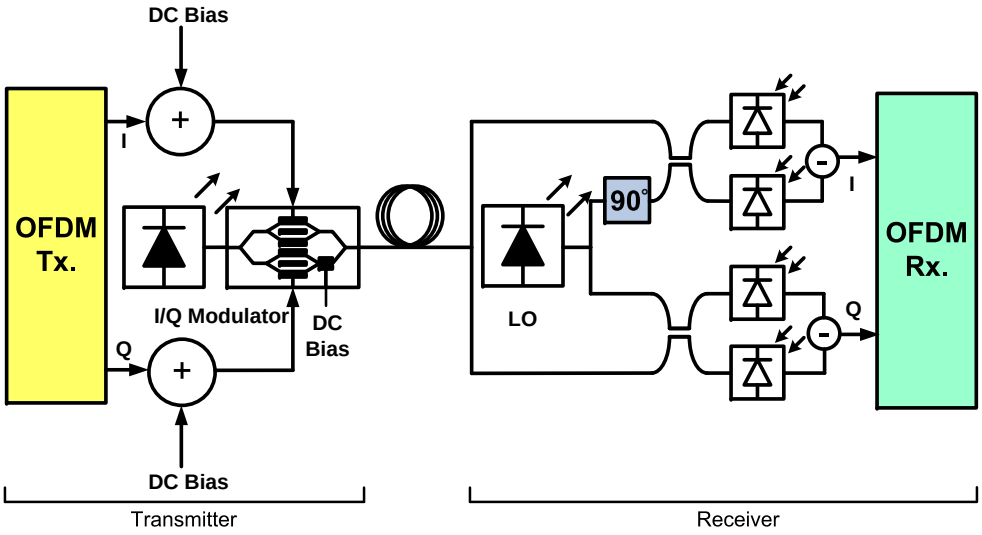

Figure 2.16: Coherent Optical OFDM.

2.6.3 All–Optical OFDM

Unlike the previous two architectures, All–Optical OFDM does not use digital OFDM generation or reception. In order to overcome electronic bandwidth limitations, some systems have been proposed which implement IFFT and FFT functionalty in the optical domain. The types of All–Optical OFDM systems proposed so far [10, 49, 50] differ greatly, but all have some characteristics in common.

Figure 2.17 shows phase and amplitude modulation of discrete laser sources by complex electrical QAM signals. Here each optical source is considered to be an OFDM subcarrier and as such the QAM symbol rate on each is set to equal the constant frequency separation between each adjacent optical source in order to satisfy the orthogonality condition. Furthermore, a phase correlation (known as coherence) is required between all of the optical subcarriers so as to mitigate cross talk between optical subcarriers [51]. To help to achieve this condition a ‘comb’ of optical carriers generated by a single laser diode (known as an optical comb source) can be used [52]. As all carriers come from the same laser cavity, they have an inherent phase correlation or coherence. After the optical OFDM subcarriers are generated, they are then aggregated by an optical passive combiner and transmitted

through the channel. Again, as both the phase and amplitude of the QAM modulated optical subcarriers need to be retrieved, coherent detection is required after passive splitting. FFT–like optical processing at the receiver is typically achieved using a combination of optical splitter, delay lines and phase shifters [53].

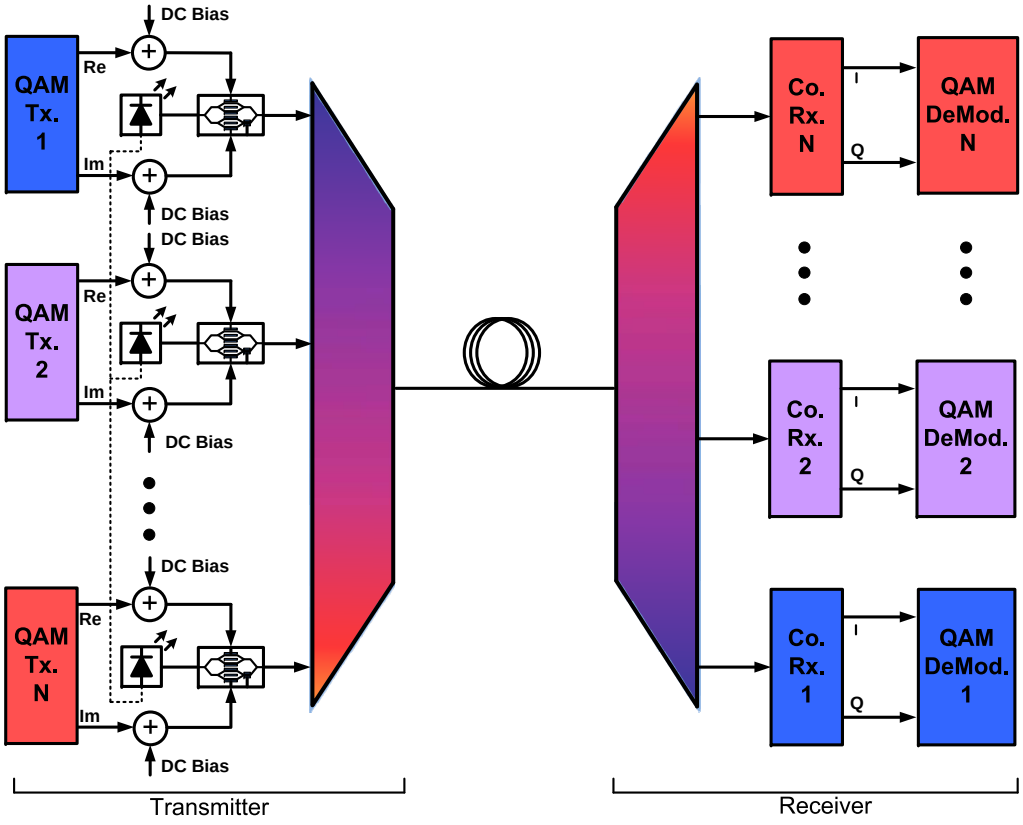

Figure 2.17: All optical OFDM.

The cost of so many optical components, coupled with the complexity associated with generating coherent optical subcarriers and coherent reception, means that All–Optical OFDM has only been considered so far as a viable option for ultra high bit rate long–haul optical communications known as optical super channels. Recently, the highest bit rate optical super channel ever experimentally demonstrated was presented in [10]. In this paper the authors use a form of All–Optical OFDM to achieve a data rate of 26Tb/s, employing matched symbol rates/subcarrier spacing with a passive optical combiner at the transmitter and optical splitters and cascaded delay interferometers at the receiver in order to synthesise an

optical receiver FFT.

2.7 OFDM for Optical Access Networks

2.7.1 Electronic Implementation

OFDM's inherent implementation in the digital domain allows for excellent flexibility with regard to the allocation of network resources. This will be an important part of managing NG-PONs and the fact that is can be handled electronically is a major advantage. Section 2.5 shows how the power and bit loading of each subcarrier can be achieved electronically so as to maximise efficiency given a finite allowable transmit power. Furthermore, the existence of large numbers of subcarriers provides a platform for dynamic bandwidth allocation, again maximising the use of the available bandwidth dependent on the users' needs.

2.7.2 Drawbacks

2.7.2.1 PAPR Induced Limitations

OFDM does exhibit some drawbacks which can impact on its performance in a PON configuration. Section 2.4 describes OFDM's large PAPR. Aside from impacting on performance in terms of ADC/DAC quantisation, high PAPR also leads to a small signal power and high carrier power in intensity modulated systems. Low signal power is undesirable in access networks as it limits reach/splitter ratio in the PON. A common way of overcoming this issue is to use an optical filter at the OLT to suppress one OFDM sideband and the optical carrier befire the signal is amplified by an EDFA. Another method which leads to greater OFDM signal power is that presented in [54]. It uses and complex modulator (biased close to its null point) to modulate the OFDM signal onto the optical field. A virtual carrier, offset from the OFDM data is added by coupling a RF sinusoid with the OFDM data before modulation onto the optical carrier. This method relies in the beating of the OFDM data

and the virtual carrier at the receiver photodiode in order to recover the phase information. A consequence of the large signal power attained by using this method is the high levels of signal x signal mixing which occurs at the photodiode. This is known as Optical Beat Interference (OBI) and leads to unwanted products close to DC. A frequency guard band must be used to avoid these products, reducing spectral efficiency.

2.7.2.2 Frequency Offset and Timing Errors

Another drawback associated with OFDM is its intolerance to frequency and timing errors. Due to the strict requirements for orthogonality, a small timing or frequency error in the received signal can lead to incorrect demodulation and subsequent loss of orthogonality. This issue has long been investigated in the RF world and many approaches have been taken to address this issue. A common method used to estimate frequency offset and timing errors is the Schmidl and Cox algorithm [55] which is based on the correlation of known training sequences within the OFDM frame.

2.7.3 Rayleigh Backscattering

Rayleigh Backscattering (RB) in optical fibres refers to the reflection, or scattering, of a light signal back to the direction from which it came. It is caused by the interaction with another light signal travelling in the opposite direction in the fibre. As PONs will have both downstream and upstream transmission over the same optical fibre, RB can be a major impairment to system performance. This problem is experienced for all modulation formats but, due to its potential for implementation in future PONs, OFDMs performance in the presence of RB has been investigated and quantified in a PON scenario [56] where it is found to exhibit similar performance to NRZ light signals which have experienced RB. Many techniques have been proposed to mitigate the effects of RB, particularly in WDM based PON solutions where many wavelengths are transmitted in the upstream and downstream direction. These methods include the use of new advanced modulation formats,

modulator phase or bias-current dithering and wavelength shifting at the ONU [57].

2.7.4 Fast OFDM

Fast OFDM is a variant of OFDM proposed in [58] which is computationally less complex than regular OFDM (by its use of a Inverse Discrete Cosine Transform (IDCT) rather than an IFFT) and so could be suitable for implementation in access networks. It achieves a subcarrier spacing equal to half of the symbol rate at the expense of the use of the subcarrier phase for modulation. This means that although subcarriers can be packed twice at tightly as regular OFDM, only amplitude modulation formats can be used on each subcarrier. For this reason Fast OFDM is not considered in the experiments presented in the following chapters.

2.8 Conclusion

OFDM is shown to be a highly spectrally efficient modulation format. This property has aided its adoption in many of today's radio standards. Through the use of a Cyclic Prefix, OFDM facilitates the construction of a simple maximum likelihood equaliser in the frequency domain which provides an effective means for overcoming linear channel impairments including, importantly from the point of view of optical communications, chromatic dispersion. It is this property in particular which has lead to much research into OFDM as a modulation format in practically all facets of optical communications systems; from short reach Plastic–Optical–Fibre applications to All–Optical OFDM superchannels.

OFDM is particularly attractive for use in optical access networks as it allows for high data rate transmission despite the limited bandwidth of cost effective components, while also providing a platform for network reconfigurability through digital bit/power loading or user assignment of individual OFDM subcarriers. Drawbacks associated with OFDM include its relatively high PAPR, resulting from the summation of OFDM subcarriers. For systems

employing intensity modulation at the transmitter, more commonly associated with access networks, this limits both optical reach and the number of potential users. Nevertheless, OFDM has been shown to be a realistic option for providing 10+Gb/s speeds required for next generation access networks and this is demonstrated in the following chapters which present experimental demonstrations of OFDM's use in such system configurations.

References

[1] R. Chang, "Orthogonal Frequency Multplex Data Transmission System," Jan. 1970.

[2] S. Weinstein and P. Ebert, "Data transmission by frequency division multiplexing using the Discrete Fourier Transform," *IEEE Transactions on Communication Technology*, vol. 19, no. 5, pp. 628–634, 1971.

[3] J. A. C. Bingham, "Multicarrier modulation for data transmission: An idea whose time has come," *IEEE Communications Magazine*, vol. 28, no. 5, pp. 5–14, 1990.

[4] J. Chow, J. Tu, and J. Cioffi, "A Discrete Multitone transceiver system for HDSL applications," *IEEE Journal on Selected Areas in Communications*, vol. 9, no. 6, pp. 895–908, 1991.

[5] S. Weinstein, "The history of Orthogonal Frequency Division Multiplexing [History of Communications]," *IEEE Communications Magazine*, vol. 47, no. 11, pp. 26–35, 2009.

[6] Q. Pan and R. Green, "Bit-Error-Rate performance of lightwave hybrid AM/OFDM systems with comparison with AM/QAM systems in the presence of clipping impulse noise," *IEEE Photonics Technology Letters*, vol. 8, no. 2, pp. 278–280, 1996.

[7] B. Dixon, R. Pollard, and S. Iezekiel, "Orthogonal Frequency Division Multiplexing in wireless communication systems with Multimode Fiber feeds," *IEEE Transactions on Microwave Theory and Techniques*, vol. 49, no. 8, pp. 1404–1409, 2001.

[8] B. Cardiff, M. Flanagan, F. Smyth, L. Barry, and A. Fagan, "On bit and power loading for OFDM over SI-POF," *Journal of Lightwave Technology*, vol. 29, no. 10, pp. 1547–1554, 2011.

[9] K. Kanonakis, I. Tomkos, H. Krimmel, F. Schaich, C. Lange, E. Weis, J. Leuthold, M. Winter, S. Romero, P. Kourtessis, M. Milosavljevic, I. Cano, and O. Prat, "An OFDMA-based optical access network architecture exhibiting ultra-high capacity and wireline-wireless convergence," *IEEE Communications Magazine*, vol. 50, no. 8, pp. 71–78, 2012.

[10] D. Hillerkuss, R. Schmogrow, T. Schellinger, M. Jordan, M. Winter, G. Huber, T. Vallaitis, R. Bonk, P. Kleinow, F. Frey, M. Roeger, S. Koenig, A. Ludwig, A. Marculescu, J. Li, M. Hoh, M. Dreschmann, J. Meyer, S. Ben Ezra, N. Narkiss, B. Nebendahl, P. F., P. Petropoulos, B. Resan, A. Oehler, K. Weingarten, T. Ellermeyer, J. Lutz, M. Moeller, M. Huebner, J. Becker, C. Koos, W. Freude, and J. Leuthold, "26Tbit s^1 line-rate super-channel transmission utilizing all-optical fast fourier transform processing," *Nature Photonics*, vol. 5, no. 6, pp. 364–371, 2011.

[11] J. Armstrong, "OFDM for Optical Communications," *Journal of Lightwave Technology*, vol. 27, no. 3, pp. 189–204, 2009.

[12] W. Sheih and I. Djordjevic, *OFDM for Optical Communications*. Academic Press, USA, 2010.

[13] R. Hassun, M. Flaherty, R. Matreci, and M. Taylor, "Effective evaluation of link quality using Error Vector Magnitude techniques," in *1997 Wireless Communications Conference*, Aug. 1997, pp. 89–94.

[14] R. Schmogrow, B. Nebendahl, M. Winter, A. Josten, D. Hillerkuss, S. Koenig, J. Meyer, M. Dreschmann, M. Huebner, C. Koos, J. Becker, W. Freude, and J. Leuthold, "Error Vector Magnitude as a performance measure for advanced modulation formats," *IEEE Photonics Technology Letters*, vol. 24, no. 1, pp. 61–63, Jan. 2012.

[15] S. Forestier, P. Bouysse, R. Quere, A. Mallet, J.-M. Nebus, and L. Lapierre, "Joint optimization of the power-added efficiency and the error-vector measurement of 20Ghz pHEMT amplifier through a new dynamic bias-control method," *IEEE Transactions on Microwave Theory and Techniques*, vol. 52, no. 4, pp. 1132–1141, Apr. 2004.

[16] M. McKinley, K. Remley, M. Myslinski, J. Kenney, D. Schreurs, and B. Nauwelaers, "EVM calculation for broadband modulated signals," in *2004 Automatic RF Techniques Group Conference*, Dec. 2004, pp. 45–52.

[17] R. Shafik, S. Rahman, and R. Islam, "On the extended relationships among EVM, BER and SNR as performance metrics," in *2006 International Conference on Electrical and Computer Engineering (ICECE)*, Dec. 2006.

[18] S. Haykin, *Communication Systems, 4th Edition*. Wiley, 2001, ch. Passband Data Transmission, p. 372.

[19] S. Han and J. Lee, "An overview of Peak-to-Average Power Ratio reduction techniques for multicarrier transmission," *IEEE Wireless Communications*, vol. 12, no. 2, pp. 56–65, 2005.

[20] T. Jiang and Y. Wu, "An overview: Peak-to-Average Power Ratio reduction techniques for OFDM signals," *IEEE Transactions on Broadcasting*, vol. 54, no. 2, pp. 257–268, 2008.

[21] S.-K. Deng and M.-C. Lin, "OFDM PAPR reduction using clipping with distortion control," in *2005 IEEE International Conference on Communications (ICC)*, 2005.

[22] D. Mestdagh, P. Spruyt, and B. Biran, "Effect of amplitude clipping in DMT-ADSL transceivers," *Electronics Letters*, vol. 29, no. 15, pp. 1354–1355, 1993.

[23] J. Tellado and J. Cioffi, "Peak power reduction for multicarrier transmission," in *Proceedings of IEEE GLOBECOM Conference*. Citeseer, 1998.

[24] N. Prasad, S. Wang, and X. Wang, "Efficient receiver algorithms for DFT-spread OFDM systems," *IEEE Transactions on Wireless Communications*, vol. 8, no. 6, pp.

3216–3225, 2009.

[25] S. Muller and J. Huber, "OFDM with reduced Peak-to-Average Power Ratio by optimum combination of partial transmit sequences," *Electronics Letters*, vol. 33, no. 5, pp. 368–369, 1997.

[26] A. Czylwik, "Comparison between Adaptive OFDM and single carrier modulation with frequency domain equalization," in *IEEE 47th Vehicular Technology Conference*, vol. 2, 1997, pp. 865–869.

[27] J. Tang and K. A. Shore, "30Gb/s signal transmission over 40km directly modulated DFB-laser-based single-mode-fiber links without optical amplification and dispersion compensation," *Journal of Lightwave Technology*, vol. 24, no. 6, p. 2318, Jun. 2006.

[28] P. Chow, J. Cioffi, and J. A. C. Bingham, "A practical Discrete Multitone transceiver loading algorithm for data transmission over spectrally shaped channels," *IEEE Transactions on Communications*, vol. 43, no. 234, pp. 773–775, 1995.

[29] A. Ruiz, J. Cioffi, and S. Kasturia, "Discrete Multiple Tone modulation with coset coding for the spectrally shaped channel," *IEEE Transactions on Communications*, vol. 40, no. 6, pp. 1012–1029, 1992.

[30] G. Dudevoir, J. Chow, J. Cioffi, and S. Kasturia, "Combined equalization and coding for T1 data rates on carrier serving area subscriber loops," in *1989 IEEE International Conference on Communications (ICC)*, vol. 1, 1989, pp. 536–540.

[31] A. Czylwik, "Adaptive OFDM for wideband radio channels," in *1996 Global Telecommunications Conference,*, vol. 1, 1996, pp. 713–718.

[32] E. Giacoumidis, J. L. Wei, X. L. Yang, A. Tsokanos, and J. M. Tang, "Adaptive-Modulation-Enabled WDM impairment reduction in multichannel optical OFDM transmission systems for Next-Generation PONs," *IEEE Photonics Journal*, vol. 2, no. 2, pp. 130–140, 2010.

[33] T. Duong, C. Milion, N. Genay, E. Grard, V. Rodrigues, J.-R. Burie, M. do Nascimento, K. Bougueroua, F. van Dijk, B. Charbonnier, J. Le Masson, M. Ouzzif, P. Chanclou, and A. Gharba, "Very high bit rate transmission for NGPON using AMOOFDM direct modulation of a linear laser," in *2010 Conference on Optical Fiber Communication (OFC)*, March 2010, p. OTuO3.

[34] J. Lee, F. Breyer, S. Randel, J. Zeng, F. Huijskens, H. P. van den Boom, A. M. Koonen, and N. Hanik, "24Gb/s transmission over 730m of Multimode Fiber by direct modulation of an 850-nm VCSEL using Discrete Multi-Tone modulation," in *2007 Optical Fiber Communication Conference (OFC)*. Optical Society of America, 2007, p. PDP6.

[35] C. Browning, K. Shi, S. Latkowski, P. Anandarajah, F. Smyth, B. Cardiff, and L. Barry, "Increased bit rate direct modulation AMO-OFDM transmission by optical injection using monolithically integrated lasers," *IEEE Photonics Technology Letters*, vol. 24, no. 11, pp. 879–881, 2012.

[36] L. Neto, P. Chanclou, B. Charbonnier, A. Gharba, N. Genay, R. Xia, M. Ouzzif, C. Aupetit-Berthelemot, J. Le Masson, D. Erasme, E. Grard, and V. Rodrigues, "On the interest of chirped lasers for AMOOFDM transmissions in long distance PON networks," in *2011 Optical Fiber Communication Conference (OFC)*, 2011, p. OWK4.

[37] J. Campello, "Optimal discrete bit loading for multicarrier modulation systems," in *1998 IEEE International Symposium on Information Theory*, Aug. 1998, p. 193.

[38] B. Cardiff, "Detection techniques for vector systems in communications," Ph.D. dissertation, University College Dublin, 2011.

[39] G. Li and G. Stuber, *Orthogonal Frequency Division Multiplexing for Wireless Communications*. Springer, New York, 2006.

[40] N. Cvijetic, "Optical OFDM for Next-Generation PON," in *Signal Processing in Photonic Communications*. Optical Society of America, 2010, p. SPTuB6.

[41] D. Qian, M. Cvijetic, J. Hu, and T. Wang, "Optical OFDM transmission in Metro/Access networks," in *2009 Optical Fiber Communication Conference (OFC)*, 2009, p. OMV1.

[42] A. Lowery, L. Du, and J. Armstrong, "Performance of optical OFDM in ultralong-haul WDM lightwave systems," *Journal of Lightwave Technology*, vol. 25, no. 1, pp. 131–138, 2007.

[43] B. Schmidt, A. Lowery, and J. Armstrong, "Experimental demonstrations of electronic dispersion compensation for long-haul transmission using direct-detection optical OFDM," *Journal of Lightwave Technology*, vol. 26, no. 1, pp. 196–203, 2008.

[44] C. Chow, C. Yeh, C. Wang, C. Wu, S. Chi, and C. Lin, "Studies of OFDM signal for broadband optical access networks," *IEEE Journal on Selected Areas in Communications*, vol. 28, no. 6, pp. 800–807, 2010.

[45] I. Djordjevic and B. Vasic, "Orthogonal Frequency Division Multiplexing for high-speed optical transmission," *Optics Express*, vol. 14, no. 9, pp. 3767–3775, May 2006.

[46] W. Shieh, H. Bao, and Y. Tang, "Coherent optical OFDM: theory and design," *Optics Express*, vol. 16, no. 2, pp. 841–859, 2008.

[47] P. Winzer, "Beyond 100G ethernet," *IEEE Communications Magazine*, vol. 48, no. 7, pp. 26–30, 2010.

[48] Y. Luo, X. Yan, and F. Effenberger, "Next generation PON offering 40G or more bandwidth," in *Asia Communications and Photonics Conference*. Optical Society of America, 2012, p. ATh3C.2.

[49] K. Yonenaga, A. Sano, E. Yamazaki, F. Inuzuka, Y. Miyamoto, A. Takada, and T. Yamada, "100Gbit/s all-optical OFDM transmission using 4x25Gbit/s optical duobinary signals with phase-controlled optical sub-carriers," in *National Fiber Optic Engineers Conference*. Optical Society of America, 2008, p. JThA48.

[50] A. Sano, H. Masuda, E. Yoshida, T. Kobayashi, E. Yamada, Y. Miyamoto, F. Inuzuka, Y. Hibino, Y. Takatori, K. Hagimoto, T. Yamada, and Y. Sakamaki, "30 x 100Gb/s all–optical OFDM transmission over 1300km SMF with 10 ROADM nodes," *33rd European Conference on Optical Communication (ECOC)*, pp. 1–2, Sept. 2007.

[51] B. Zhao and X. Chen, "A 40Gbps SSB-OFDMA-PON architecture using direct-detection and source-free ONUs supporting dynamic bandwidth allocation," in *Third International Conference on Communications and Mobile Computing (CMC)*, Apr. 2011, pp. 223–225.

[52] P. Anandarajah, R. Zhou, R. Maher, D. Gutierrez-Pascual, F. Smyth, V. Vujicic, and L. Barry, "Flexible optical comb source for super channel systems," in *2013 Optical Fiber Communication Conference (OFC)*. Optical Society of America, 2013, p. OTh3I.8.

[53] K. Lee, C. Thai, and J.-K. Rhee, "All optical discrete fourier transform processor for 100Gb/s OFDM transmission," *Optics Express*, vol. 16, no. 6, pp. 4023–4028, Mar. 2008.

[54] B. Schmidt, A. Lowery, and L. Du, "Low sample rate transmitter for direct-detection optical OFDM," in *Optical Fiber Communication - incudes post deadline papers, 2009. OFC 2009. Conference on*, 2009, pp. 1–3.

[55] T. Schmidl and D. Cox, "Robust frequency and timing synchronization for OFDM," *IEEE Transactions on Communications*, vol. 45, no. 12, pp. 1613–1621, 1997.

[56] C. Chow, C. Yeh, C. Wang, F. Shih, and S. Chi, "Rayleigh backscattering performance of OFDM-QAM in carrier distributed passive optical networks," *Photonics Technology Letters, IEEE*, vol. 20, no. 22, pp. 1848–1850, 2008.

[57] C.-H. Yeh, C.-W. Chow, and H.-Y. Chen, "Adaptive 6.25-40Gb/s downstream rate using four-band OFDM channels within 10GHz bandwidth for long-reach PON," in

2012 Optical Fiber Communication Conference (OFC). Optical Society of America, 2012, p. JTh2A.51.

[58] J. Zhao and A. Ellis, "A novel optical fast OFDM with reduced channel spacing equal to half of the symbol rate per carrier," in *Optical Fiber Communication (OFC), collocated National Fiber Optic Engineers Conference, 2010 Conference on (OFC/NFOEC)*, 2010, pp. 1–3.

Chapter 3

Optical Injection with OFDM

3.1 Introduction

As discussed in Chapter 2, in any OFDM system information about the transmission channel is ascertained by means of a known transmitted training sequence which contains all subcarrier frequencies. The training sequence along with the cyclic prefix (CP), which ensures a full copy of each subcarrier is obtained at the receiver (thereby maintaining orthogonality), allows channel estimation and equalization at the receiver. This is because the effect of any linear impairments introduced by the channel (most importantly dispersion) on any subcarrier frequency can be estimated by analysing the received training sequence. The subsequent data carrying portion of each subcarrier is adjusted accordingly by applying the resultant equaliser as described in section 2.2.4. However, this equalization method cannot be applied to compensate for nonlinear distortions as the loss of subcarrier orthogonality due to the nonlinear nature of the channel occurs before the signal is downconverted to the electrical domain by photodetection, resulting in Inter Symbol (i.e. subcarrier) Interference [1].

In many aspects OFDM lends itself well to adaptation in optical communications, but this susceptibility to nonlinear distortion can be problematic as many optical components may

introduce nonlinear distortion depending on their operating conditions. In this chapter OFDM PONs employing direct modulation are proposed. The limitations posed by the nonlinearity of the directly modulated laser, as well as its reduction by optical injection are investigated both by simulation and experimental work.

3.2 Laser Diode Nonlinearity

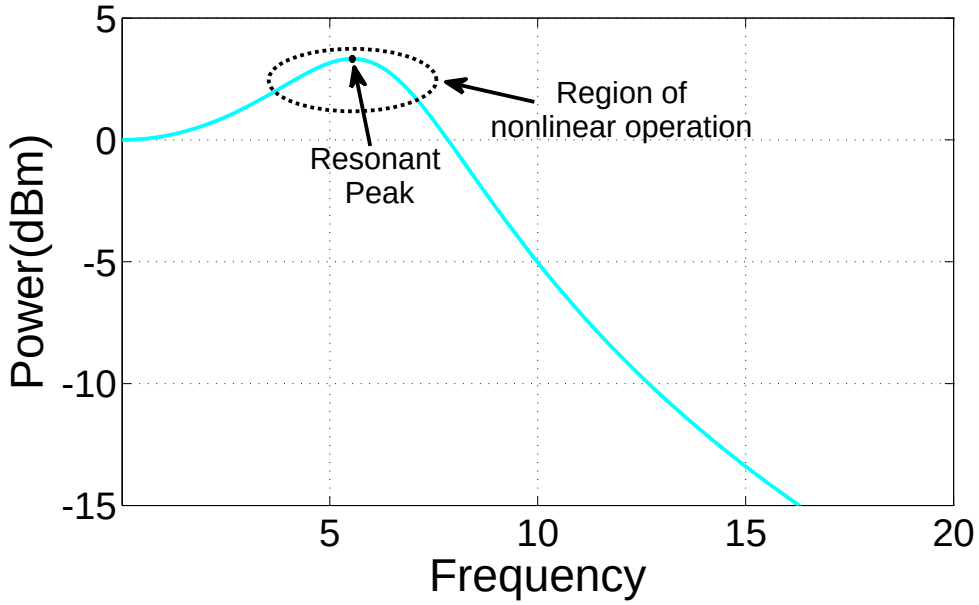

Figure 3.1: Typical modulation response of a laser diode.

Direct modulation of a laser diode can be employed to construct a cost effective optical transmitter suitable for optical access networks such as PONs as discussed in section 1.5.1. Although this technique offers many advantages over external modulation, a major drawback is the presence of nonlinearities which are introduced when direct modulation of the diode by the driving data signal is employed [2]. For OFDM systems in particular this nonlinearity can introduce a performance limitation and limit useable bandwidth.

When directly modulating a laser, nonlinear interactions between the carriers and the photons in the laser cavity occur [3]. This gives rise to nonlinear operation at certain frequencies. This nonlinear range of operation is indicated by a resonant peak, or relaxation oscillation,

in the laser's modulation response [4]. Figure 3.1 shows the resonant peak of a typical modulation response indicating a region of nonlinear operation at frequencies around the peak. It is important to note that this resonant peak merely provides an indication as to what frequencies the nonlinear interaction of the photons and carriers in the cavity is affecting. That is to say that, the nonlinear process is the interaction between the photons and the carriers within the cavity and *not* the shaping of the OFDM signal by the modulation response (this is a linear process affecting signal amplitudes at various frequencies and can be corrected by channel estimation/EQ).

3.2.1 Intermodulation Distortion

Distortion can be linear or nonlinear. As discussed in chapter 2, OFDM's use of Training sequences and channel EQ (facilitated by the inclusion of a CP) can be used to overcome linear distortions such as chromatic dispersion, which alter the amplitude and/or the phase of the transmitted signal. Nonlinear distortion generates new unwanted frequency components leading to ISI and loss of orthogonality of OFDM subcarriers [5]. Nonlinear distortion can be further broken down into Harmonic distortion and Intermodulation Distortion (IMD). Harmonic distortion refers to the case where new frequency components are generated at integer multiples of the original frequencies caused by the self mixing of those frequencies due to nonlinearity. For higher frequency OFDM subcarriers, Harmonic distortion usually occurs out of band and so can be easily dealt with by low pass filtering. However the harmonics generated by the Harmonic Distortion of lower frequency OFDM subcarriers can occur in band, degrading performance. A simple case of two sinusoids with frequencies f_1 and f_2 is shown in figure 3.2.

IMD refers to new components generated at the sum and difference of integer multiples of the transmitted frequencies and so do not occur at harmonic frequencies i.e. $|nf_1 \pm mf_2|$ where $n, m \, \epsilon \, \mathbb{Z}$ and $n, m > 0$. The Intermodulation order is given by the sum of the coefficients n and m. For example, for the IMD shown in figure 3.2, $n = 1$ and $m = 2$ so this is referred to as third order intermodulation distortion (IMD3). Generally, only

odd–ordered IMD is considered as these components lie close to the original frequencies. Even–ordered IMD products, like harmonic distortion, mostly lie out of band and can be dealt with by filtering.

As OFDM signals have many closely spaced subcarriers, generally of equal powers, IMD caused by directly modulating in the region of nonlinear operation of a laser diode results in the generation of large amounts of unwanted frequency components within the OFDM frequency band. A solution to this problem is to employ optical injection to extend the range of linear operation.

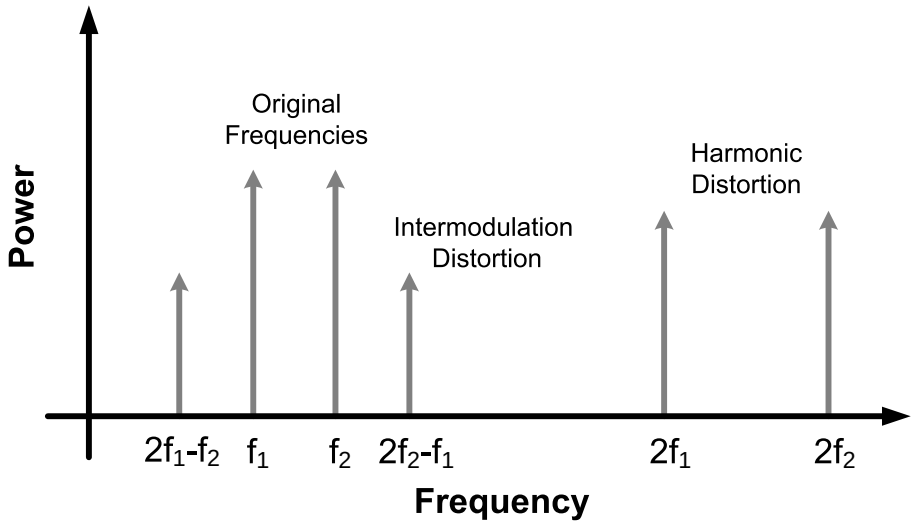

Figure 3.2: Intermodulation and harmonic distortion.

3.2.2 Optical Injection

Optical Injection is the coupling of light from a laser diode back into its own cavity or into the cavity of another laser. As early as 1980 it was shown in [6] that by coupling a portion of the output light from a semiconductor laser diode back into the laser's cavity using an external reflector, several device characteristics can be altered. These included an increase in modulation response bandwidth and the 'enhancement' of the resonant peak. It has also been shown that these effects can be achieved by coupling light from an external laser into the cavity of the another laser (master–slave configuration) [7]. External optical injection

allows for the master and slave lasers to have different characteristics and much work has focused on improving laser characteristics and system performance by choosing optimum operating conditions of both the master and slave lasers. Meng *et, al.* [8] first investigated how the frequency separation between the master and slave lasers' output (known as the detuning) impacts the stability of the output wavelength. This work also shows the extension of the modulation response and resonant peak by up to 3.7 times more than the free running case. Light injection has also been shown to improve the linewidth of the slave laser [9]. More recently, external injection has been employed as a means of attaining single mode operation from multimode Fabry–Pérot lasers by using them as the slave device [10, 11]

For direct modulation OFDM systems, which are highly intolerant to nonlinearities, optical injection can be of great benefit because it extends the system bandwidth limitation imposed by nonlinearity due to direct modulation. This is achieved by shifting the range of nonlinear operation to higher frequencies.

3.3 System Simulation

A complete optical OFDM system was simulated in Matlab (see Appendix C). A flow chart of the system simulation is shown in figure 3.3. Direct modulation of the laser and external injection were modelled using the laser rate equations, including the injection terms, derived in [12]. The rate of spontaneous emission, R_{sp} was not included in the rate equations used as it is expected that noise in the laser structure will not be responsible for a performance limitation in this system. Rather non-linearity and receiver shot/thermal noise will dominate the noise characteristics of the system. Additionally, as direct detection is being employed, laser phase noise is not expected to exert a major impact on system performance. Sample simulated laser device parameters [13] are presented in table 3.1 and were used in initial simulations, along with the driving electrical OFDM signal, to solve the extended laser rate equations with injection terms. As shown in the table, the injected photon density is

$5 \times 10^{21}\text{cm}^{-3}$ which corresponds to an optical injection power of 1.5dBm.

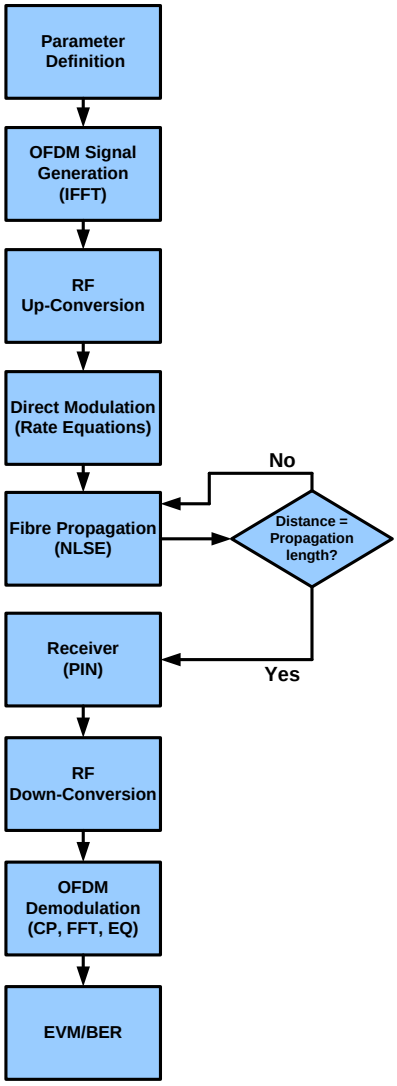

Figure 3.3: Direct modulation simulation flow chart.

The parameters in table 3.1 may be altered so as to model optical transmitters employing different lasers. Simulation results presented alongside experimental results in the following sections were all attained using the model described in this section. Although characterisation of some of the devices used in this chapter are available, some important parameters (such as the coupling coefficient κ, optical confinement factor Γ and linewidth enhancement factor α) are not available at the time of writing. In such cases, the unknown parameters were altered so as to provide a similar modulation response and relaxation oscillation

frequency to that obtained from the physical device. For this reason, simulation results shown were used to indicate the underlying trend (of improvement due to reduction in non-linearity) rather than to give a precise result given the laser structure being employed.

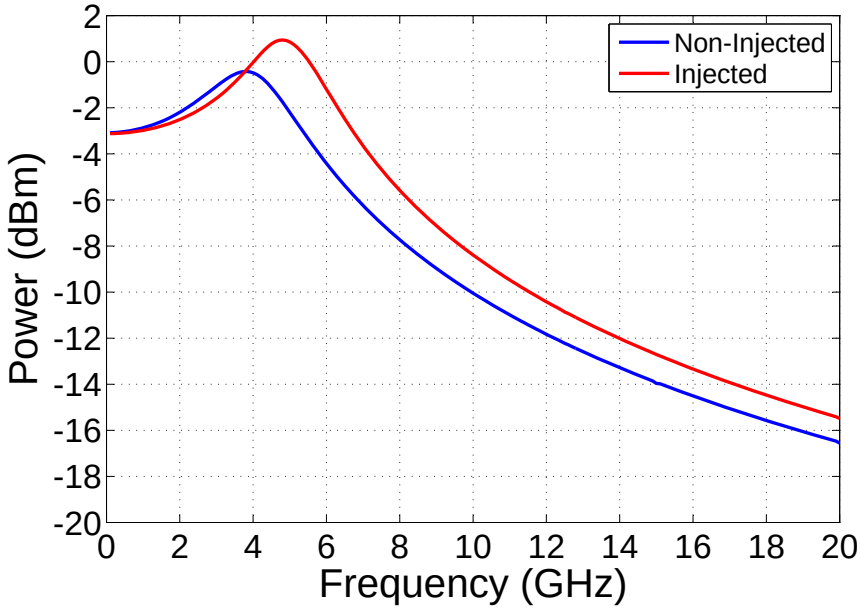

Figure 3.4: Simulated modulation response under non-injected and injected conditions.

The effects introduced by propagating over standard single mode fibre (SMF-28), namely nonlinearity, dispersion and loss, were simulated by modelling the propagation of the electric field through the fibre using the nonlinear Schrödinger equation (NLSE). The equation was solved using the split step Fourier method for a number of steps over a given transmission distance. First and second order terms only were included in the calculation of dispersion.

The modelled receiver comprised of a 10GHz bandwidth PIN photodetector with an integrated trans-impedance amplifier (TIA), including shot noise and thermal noise associated with such receivers, a digital RF mixer, low pass filtering and digital signal processing (DSP) normally associated with OFDM systems. This includes serial to parallel conversion, FFT, channel estimation and equalisation, and EVM measurement. Results were taken for both the injected and non–injected cases. In the latter case the injection level was set to zero. The modulation responses of the modelled laser under non–injected and injected conditions

Table 3.1: Sample simulated laser parameters.

Parameter	***Value***
Wavelength, λ	1540nm
Group Refractive Index, η	3.63
Optical Confinement Factor, Γ	0.35
Differential Gain Coefficient, g_0	$1 \times 10^{-12}\text{cm}^2$
Transparency Density, n_0	$1 \times 10^{18}\text{cm}^{-3}$
Facet Reflectivity Coefficient, R	0.32
Linewidth Enhancement Factor, α	6.8
Area of Active Region, A	$0.03 \times 10^{-12}\text{m}^2$
Photon Lifetime, τ_p	2ps
Carrier Lifetime, τ_n	0.3ns
Injected Photon Density, P_0	$5 \times 10^{21}\text{cm}^{-3}$
Coupling Coefficient, κ	$2.5 \times 10^{11}\text{s}^{-1}$
Detuning, Δ_f	5GHz

are shown in figure 3.4.

3.4 External Optical Injection

3.4.1 Experimental Setup

Two 10Gb/s OFDM signals were generated in order to compare performance in the system under test – (i) a more spectrally efficient signal with 64–QAM on each subcarrier and (ii) a broader bandwidth signal with 32–QAM on each subcarrier. Although the 10Gb/s 32–QAM signal requires more bandwidth, its SNR requirement for acceptable performance is reduced due to its reduced modulation order.

The real and imaginary components of these complex baseband signals were then digitally mixed with the In-Phase (I) and Quadrature (Q) components of an RF carrier to give 'real' valued OFDM signals centred on a given RF frequency above DC. A CP of 6.25% and OFDM symbol rate of 39.06MHz were used. The bandwidths of the 32 and 64–QAM signals were 2.265GHz and 1.916GHz respectively. One OFDM symbol (0.7% of the entire OFDM signal) was set to be the training sequence so as to facilitate channel estimation and equalization at the receiver. These overheads along with 0.7Gb/s, reserved for Forward

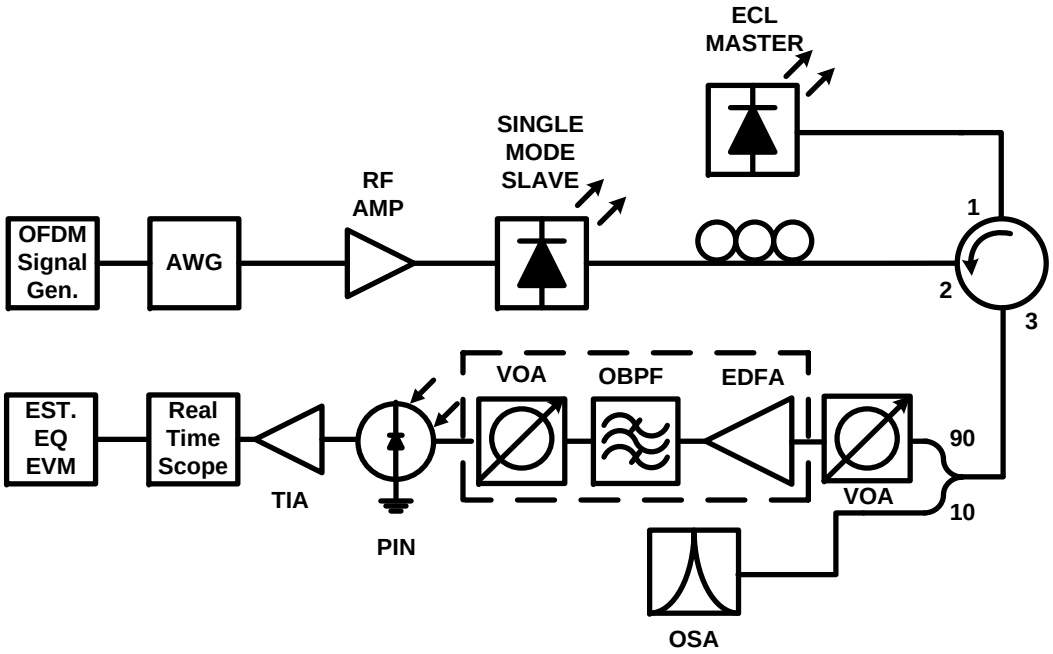

Figure 3.5: The direct modulation optical OFDM experimental setup.

Error Correction (FEC), meant that the raw data rate was 11.395Gb/s. The experiment was performed for the back to back case and also over 12km of SSMF, with and without optical injection of a single mode laser.

As figure 3.5 shows, the OFDM signals were output from a 10GSa/s Arbitrary Waveform Generator (AWG). The slave laser's threshold current was 10mA and for this experiment was biased at 21mA, giving a 3dB bandwidth of about 5GHz and optical output power of 0dBm. The slave emitted light at 1540nm. By mixing the 32 and 64–QAM OFDM signals with intermediate RF frequencies of 2.867GHz and 3.043GHz respectively, the highest frequency subcarrier in each case was placed at 4GHz, which was inside the slave laser's region of nonlinear operation under non–injected conditions. Using an optical circulator and polarization controller, light from the master laser – a tunable External Cavity Laser (ECL) – was coupled into the cavity of the slave laser. The injected optical power was kept constant at 2.8dBm throughout (measured at circulator port 2). The master was tuned to 1540.05nm and this corresponds to a detuning of roughly 5GHz, which is well within the locking range for this injection power.

The signals were detected using a 10GHz bandwidth PIN photodetector with an integrated TIA and captured with a Real Time Oscilloscope (RTS). The addition of the EDFA and optical bandpass filter at the receiver provided the necessary sensitivity to allow BER versus received power curves to be measured. All processing, including BER measurement, was completed offline using Matlab. Measurements of EVM from the received constellations were taken for both the injected and non–injected cases.

Table 3.2: Average EVM for received constellations and the improvements due to injection.

Sim./Exp.	Order	Non-Injected	Injected	Improvement
(Simulated - 0km)	32-QAM	6.96%	5.15%	1.81%
	64-QAM	7.56%	5.02%	2.54%
(Simulated - 12km)	32-QAM	7.9%	6.%	1.9%
	64-QAM	7.89%	5.09%	2.8%
(Experimental - 0km)	32-QAM	7.62%	6.07%	1.55%
	64-QAM	7.95%	6.3%	1.65%
(Experimental - 12km)	32-QAM	8.32%	7.28%	1.04%
	64-QAM	8.77%	6.9%	1.87%

3.4.2 Results and Discussion

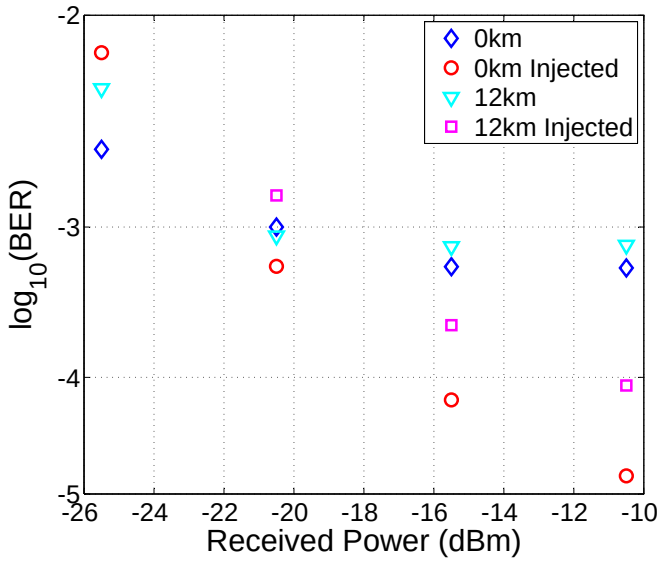

Figure 3.6: Experimental $\log_{10}$(BER) vs. Received optical power, under non-injection and injection conditions.

Table 3.2 summarises the simulated and experimental results. Strong agreement exists between the simulated and experimental improvement in EVM. Figure 3.6 shows the experimental BER versus received optical power for the back to back and 12km cases, injected and non–injected. It can be seen in figure 3.6, for both back to back and 12km scenarios, that the injection enhances the system performance by eliminating the BER floor which appears in the non–injected cases at values close to 10^{-3}. The fact that there appears to be less of an improvement due to injection after transmission over 12km is attributed to the performance being limited by dispersive fading introduced by the fibre. Figure 3.7 shows the average value of EVM per subcarrier number for the 32–QAM OFDM signal for both regimes; experimental (a) and simulated (b). The effect incurred by modulating close to the resonant peak of the laser and the subsequent improvement on each subcarrier due to injection can clearly be seen in the figure. Average EVM increases with subcarrier number as the subcarrier frequencies increase to within the laser's region of nonlinear operation, but this effect is greatly reduced by the injection; in this case only a small rise in average EVM is observed due to the extension of the laser's linear range.

The relationship between BER and EVM depends upon constellation size. This is intuitive when one considers the improvement in SNR required when moving to higher order QAM.

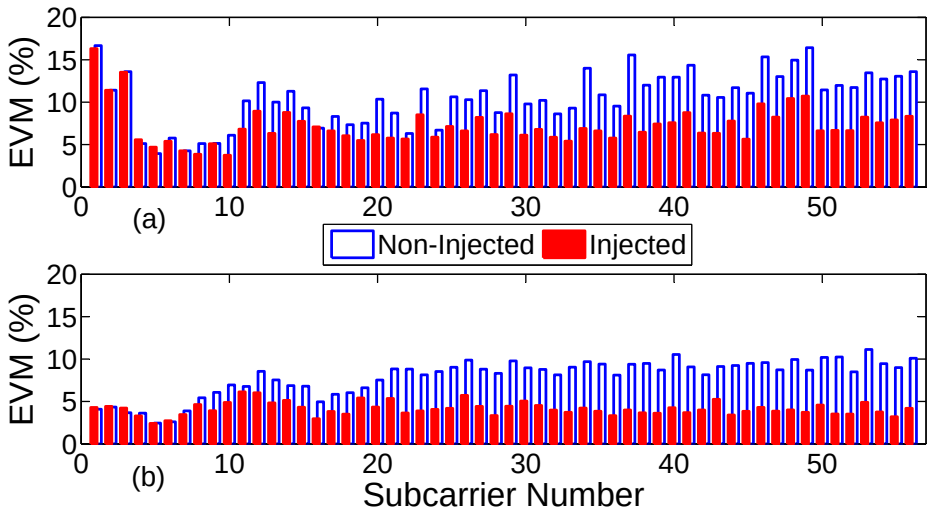

Figure 3.7: Experimental (a) and simulated (b) EVM per subcarrier under both conditions.

Table 3.3 tabulates the experimentally measured BER of the signals under both conditions. These performances were achieved at a received optical power of -3.5dBm (back to back) and -5.5dBm (12km). The results indicate that external optical injection can improve the

Table 3.3: BER for all cases (experimental).

Order	Non-Injected	Injected
(back to back)		
32-QAM	2.85×10^{-4}	1.91×10^{-5}
64-QAM	4×10^{-3}	7.2×10^{-4}
(12km)		
32-QAM	7.9×10^{-4}	8.5×10^{-5}
64-QAM	8.4×10^{-3}	1.7×10^{-3}

performance of a direct modulation OFDM system and extend the usable bandwidth for the modulating OFDM signals. This is particularly important in the case of cost effective direct modulation systems where moderate bandwidth lasers are employed. It can also potentially enhance system performance in directly modulated OFDM systems operating well beyond 10Gb/s by reducing nonlinearities.

3.5 Optical Injection with Monolithically Integrated Lasers

3.5.1 Monolithically Integrated Device

The experiment and results described in sections 3.4.1 and 3.4.2 give an indication as to the level of performance enhancement that can be attained by employing external optical injection. However, the components that were used to carry out this technique are expensive; in particular the ECL and polarization controller. Since this technique is being discussed in the context of cost efficient optical access networks, it is imperative that cost is kept to a minimum. The work described in this section was carried out using two low cost Discrete Mode (DM) lasers which are monolithically integrated (figure 3.8). The lasers are manufactured using slotted ridge waveguide technology which uses the arrangement of etched slots on a FP laser ridge waveguide to suppress all but one of its many modes, thus achiev-

ing a single mode output [14]. The laser has a ridge width of 2.5μm. Its cavity is 700μm long and is divided into two sections (400μm and 300μm). The etched trench separating the two sections was 2μm wide. The integration of these devices makes the injection technique feasible for cost efficient optical communications systems by reducing cost and footprint over transmitters which employ external modulators and also renders the system polarization independent.

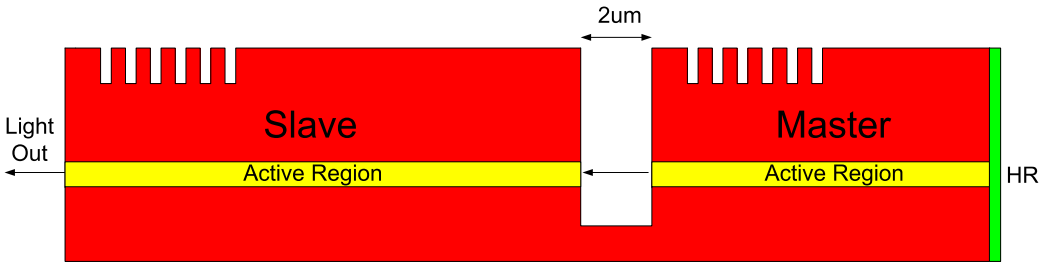

Figure 3.8: Integrated laser device.

The modulation response of the integrated device under both non-injected and injected conditions (shown later in this chapter), as well as the non-linearity introduced by direct modulation will clearly be the limiting factors for a direct detection OFDM system. However many other aspects of this device have been characterised in [15] and some of these results are presented in appendix D. Linewidth measurements for the device are not included as it is not expected that this parameter will impact on the performance of the direct detection scheme proposed.

3.5.2 Experimental Setup

The revised experimental setup is shown in figure 3.9. The threshold current of the slave laser is 20mA while the threshold of the master is 12mA and biasing was set to 1.5 times and twice the threshold of the master and slave respectively. Detuning was +10GHz when the master section of the device was biased at 24mA. The optical launch power increased from 3.7dBm to -1dBm when both master and slave are biased.

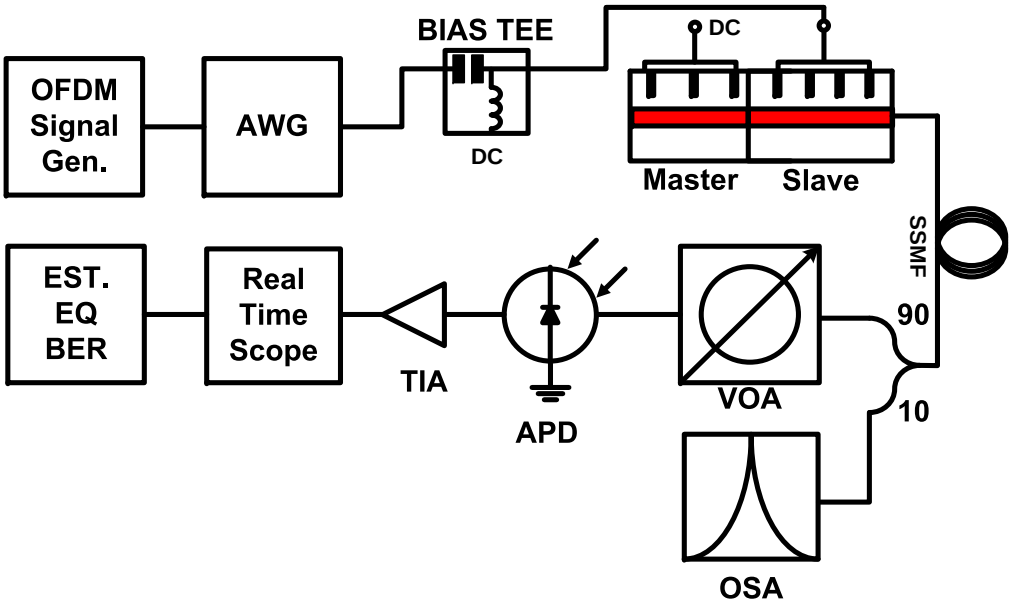

Figure 3.9: OFDM with integrated optical injection system setup.

Both regular OFDM signals (with the same level of modulation on each carrier) as well as adaptive OFDM signals were output from a 10GSa/s Tektronix AWG giving an available bandwidth of 5GHz due to the Nyquist criterion. The signals were used to drive the slave section of the device after a bias of 30mA had been added. The optical signal was then transmitted over different lengths of SSMF before being attenuated to an appropriate level for detection by a VOA. An Avalanche Photodetector (APD) with an integrated TIA was used for signal detection. The electrical signal was captured using an Agilent RTS also operating at 10GSa/s. Signal processing, such as channel estimation, EQ, EVM and BER measurement was completed offline.

Regular 10Gb/s OFDM signals were generated with 16–QAM on all subcarriers. From a 256 input IFFT, 74 subcarriers were used to carry data, with a spacing of 39.06MHz, giving a signal bandwidth of about 3GHz. In this case the real and imaginary components of the complex OFDM signal were mixed with a 1.7GHz cosine and sine wave respectively in order to generate a 'real' signal for direct modulation. Again, 7% data overhead was reserved for FEC and 6.25% for CP, giving a raw data rate of 11.56Gb/s. The OFDM spectrum is shown in figure 3.10a.

The LC algorithm described in section 2.5 was used to generate the AM–OFDM signals. A 256 IFFT was used with a subcarrier spacing of 39.06MHz. The number of subcarries used, their respective power levels, and the constellation sizes are determined for each system configuration by use of the LC algorithm. Individual subcarrier SNRs were determined by the use of an OFDM pilot signal with 16–QAM on each subcarrier. Typically, 100 subcarriers were used, yielding a signal bandwidth of 3.9GHz and a PAPR of 12dB; however, this varied slightly depending on the specifics of the system under test. A CP of 6.25% and FEC of 7% were used for all signals. A typical bit/power loaded AM–OFDM spectrum is shown in figure 3.10b.

3.5.3 Results and Discussion

3.5.3.1 Reduction of Non–linearity

Figure 3.11 shows the modulation responses of the integrated laser device under non–injected and injected conditions. With injection, the resonant peak value moves from 2.58GHz to 4.27GHz, indicating the expansion of the linear range of operation. This expansion of the linear region of operation by injection can be attained for high and low

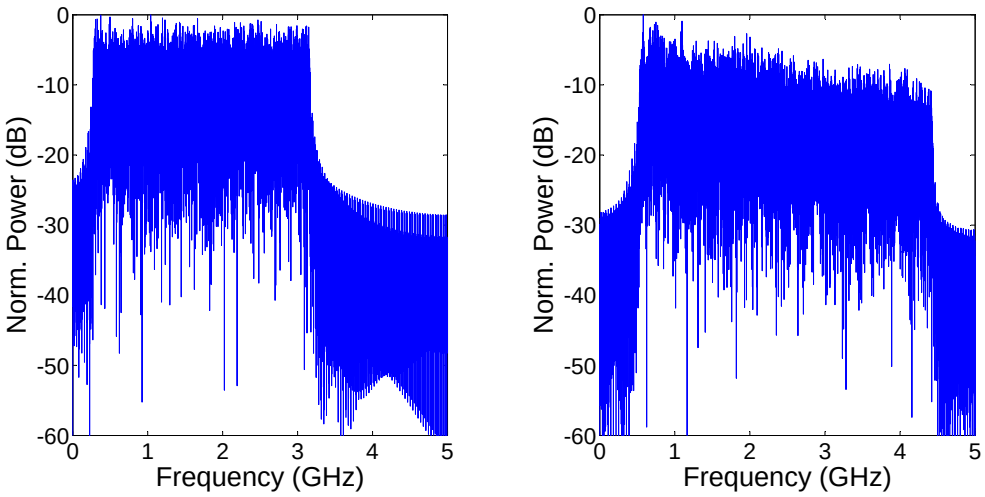

(a) (b)

Figure 3.10: 10Gb/s (a) and Adaptive (b) OFDM spectra.

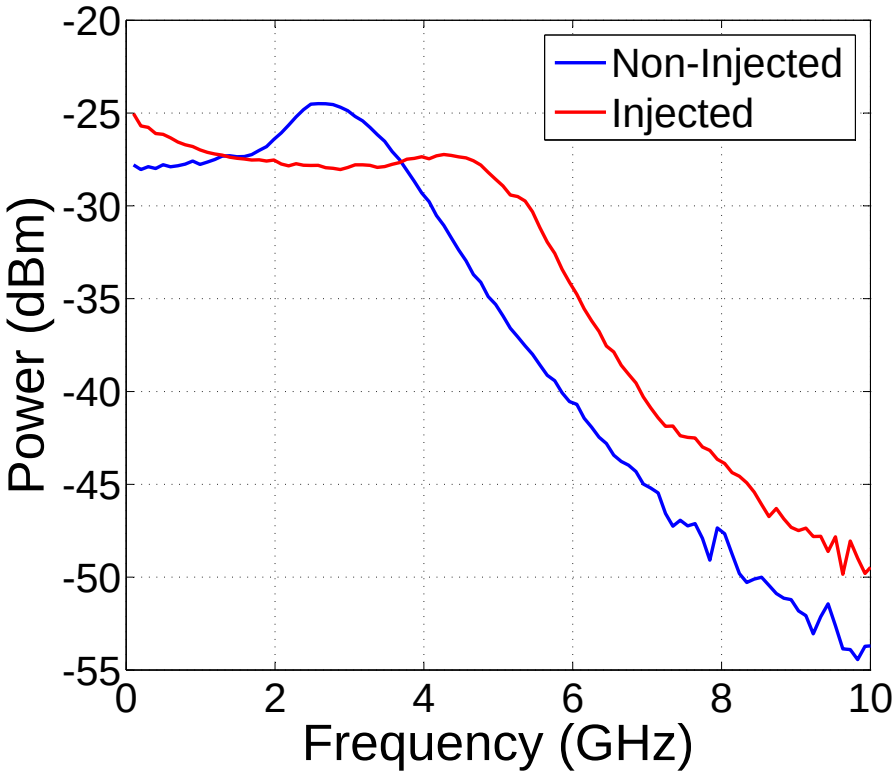

Figure 3.11: The modulation responses of the integrated device with and without optical injection.

bandwidth lasers and is not limited to integrated devices. However, the use of low cost, moderate bandwidth DM lasers with integration improves cost effectiveness and makes this approach especially attractive for low cost optical communication systems.

Figure 3.12 shows the superimposed results of two tone tests performed on the device for injection and non–injection conditions. The test was performed at a centre frequency of 3GHz and the Optical Modulation Index (OMI) was 75%. The slave section is directly modulated with two tones and the output optical signal is detected and then recorded while the slave alone is lasing, and also while both the master and slave are biased to achieve optical injection. By showing the level of the IMD3 in the received signal, the test provides an indication of the level of nonlinearity introduced to the system by direct modulation. By performing this test for both operating conditions, the reduction in nonlinearity due to optical injection can be estimated. Shown in Fig. 3.12 is a decrease of 10dB, from -15dB to

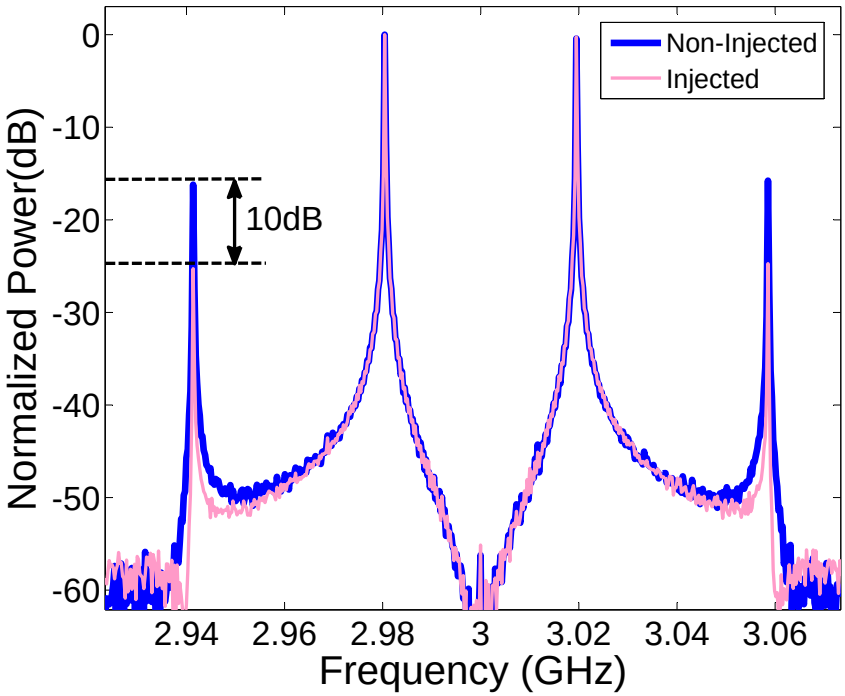

Figure 3.12: Two tone test at 3GHz for the integrated discrete mode device.

-25dB, in IMD3 when optical injection is employed. The tone spacing is set to the OFDM subcarrier spacing used for transmission: 39.06MHz.

3.5.3.2 10Gb/s OFDM

Table 3.4 summarises the performance in terms of BER of the system, as well as showing the system improvement attained by employing injection. All measurements were taken at a received optical power of -17dBm. Higher optical powers resulted in saturation of the APD receiver. Improvements due to optical injection are reduced as dispersive effects begin to dominate system performance with increased length. Dispersive fading in the fibre due to the double side band nature of the signal becomes evident after 50km transmission and this can degrade performance [16]. This effect is discussed later in the section.

Figure 3.13 shows the improvement in performance in the back to back and 50km cases gained by employing optical injection. The difference in receiver sensitivity between the two injected cases can be attributed to the dispersive fading of the received RF signal which

Table 3.4: BER of received 10Gb/s OFDM signals.

Distance	Non-Injected	Injected
0km	1×10^{-3}	2.1×10^{-6}
25km	1.3×10^{-3}	3.76×10^{-6}
50km	2.4×10^{-3}	3.25×10^{-5}

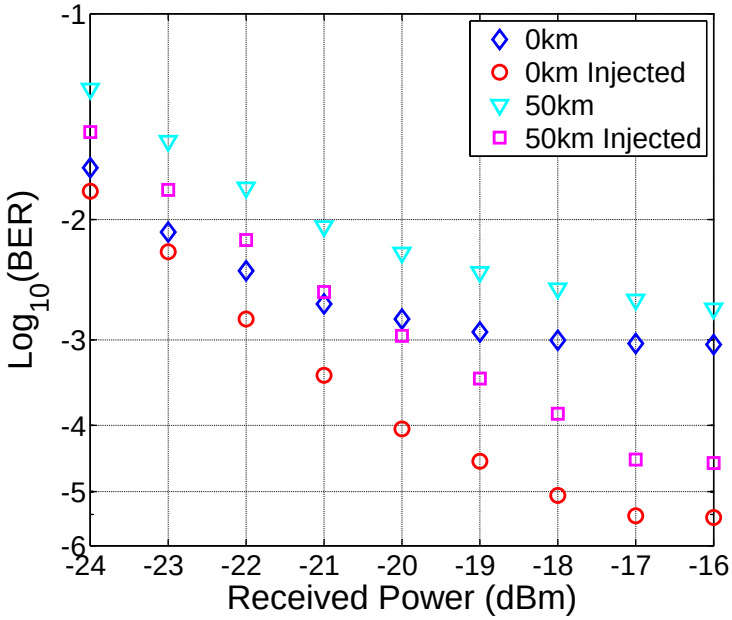

Figure 3.13: Received optical power vs. $\log_{10}$(BER) for back-to-back and 50km of SSMF.

is evident over 50km of fibre, but not in the back to back scenario. The non–injected cases display an error floor close to a BER of 1×10^{-3}, caused by the non–linear nature of the channel when injection is not used. By injection, this non-linearity is reduced and the error floor is improved with the system no longer being limited by non–linearity, but rather by receiver saturation.

3.5.3.3 AM–OFDM

Table 3.5 presents experimental and simulated raw data rates that can be achieved while maintaining a BER of 1×10^{-3}. Simulations were undertaken using the model described in 3.3. The actual data rates, taking into account the CP (6.25%) and forward error correction (FEC) (7%) overheads, are given in brackets. Also shown is the percentage improvement

in terms of data rate. The experimental rates were achieved for a received optical power of -17dBm giving an optical power budget of 13.3dB and 16dB in the non–injected and injected cases respectively. Again, higher optical power resulted in the saturation of the receiver.

In all cases a significant improvement in achievable data rate is evident after optical injection and this is matched in the simulated results. As transmission distances are increased the improvements are lessened due to the double sideband nature of the signal which results in dispersive fading over longer lengths of fibre [17]. As dispersive fading begins to dominate system performance, the relative improvement gained by injection becomes less evident.

Table 3.5: Increase in bit rate gained by optical injection.

Distance (km)	Non-Injected(Gb/s)	Injected(Gb/s)	Improvement
(Simulated)			
0	14.1 (12.45)	17.578 (15.52)	25%
25	12.227 (10.8)	16 (14.13)	31%
50	11.6 (10.24)	14.12 (12.47)	22%
(Experimental)			
0	13.359 (11.8)	17.54 (15.49)	31%
25	12.109 (10.69)	15.76 (13.86)	30%
50	11.914 (10.52)	13.9 (12.27)	17%

Figure 3.14a and 3.14b show the experimental and simulated EVM per subcarrier over 25km of SSMF for both operating conditions respectively. When the slave section alone is lasing the EVM increases rapidly up to as high as 24% as the subcarrier frequencies rise to within the nonliner region of operation of the device. This rise in EVM with frequency is stemmed when optical injection is employed. As the linear region of operation is expanded, the rise in EVM is greatly reduced; this is clear from both the experimental and simulated measurements.

Figure 3.15 shows the experimental bit/power distribution assigned by the LC algorithm, again for both operating conditions, when the transmission distance is 25km. The effect of directly modulating data within the nonlinear region of the device is evident as the num-

ber of bits per QAM symbol (effective bit/power loading) reduces to QPSK at the upper subcarriers in the non–injected case. A decrease is also evident in the injected case, but it is not as drastic, eventually reducing from six bits per QAM symbol (64–QAM) to four (16–QAM).

When assigning a bit distribution, the LC algorithm calculates incremental energies required on each subcarrier to move to different QAM orders based on information about the channel (measured SNR on each subcarrier) as described in section 2.5. A problem arises when subcarriers interact, as is the case in a nonlinear channel. Initially, a pilot signal with 16–QAM is propagated and the SNR measured for each subcarrier includes the noise contribution due to subcarrier mixing caused by nonlinearity (IMD). However, when the bit distribution is updated by the LC algorithm the effect is to power load different subcarriers, or in some cases to drop subcarriers completely, according to their individual SNRs. Thus in the presence of nonlinearity these power/bit loaded subcarriers will not interact in exactly the same way as indicated by the pilot signal. If follows that the bit distribution given by the LC algorithm may not be the optimum one for multicarrier signals in a nonlinear channel. However, it provides a good approximation and facilitates a large increase in throughout compared to regular non–adaptive OFDM.

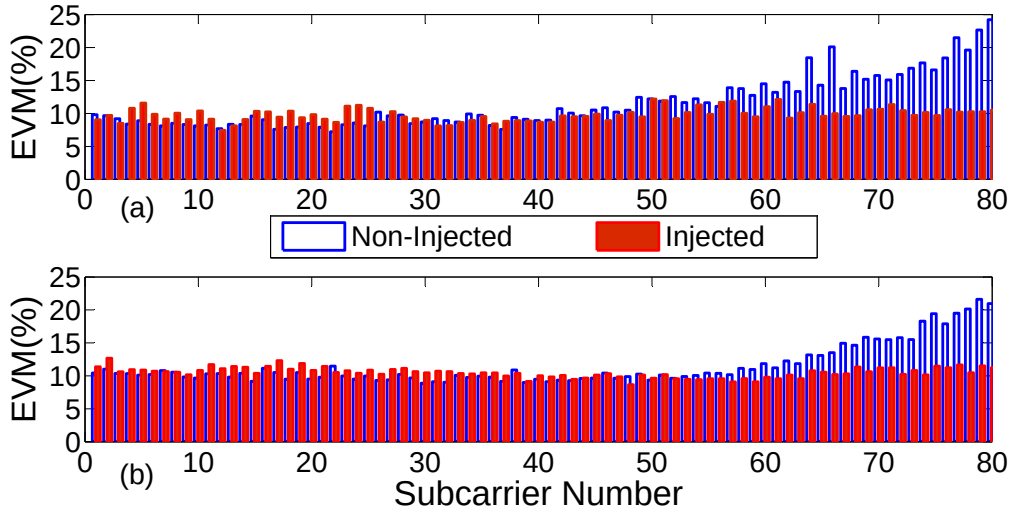

Figure 3.14: Experimental (a) and simulated (b) EVM per subcarrier under both conditions.

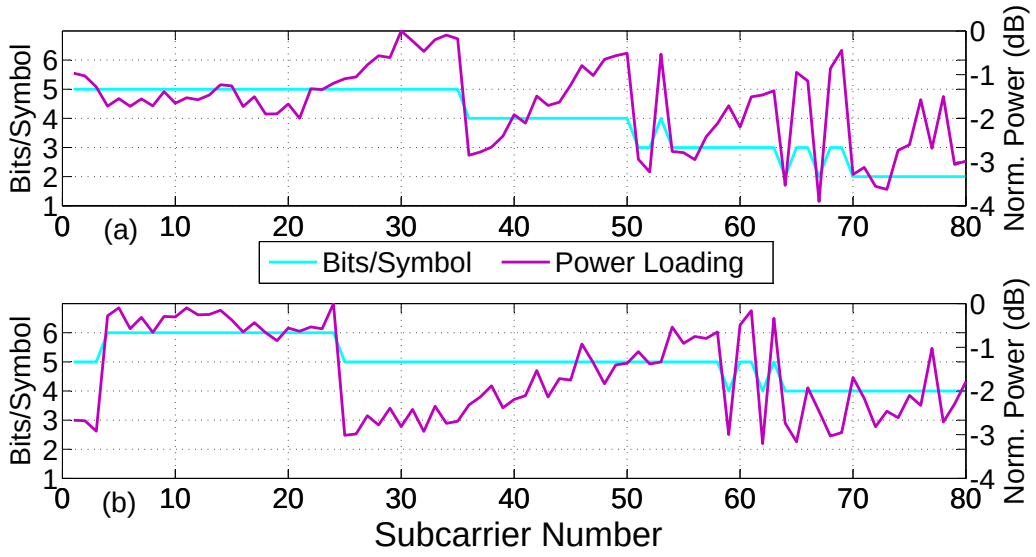

Figure 3.15: Adaptive modulation bit and power loading for non-injected (a) and injected (b) cases.

3.5.3.4 Dispersive Fading

Dispersive fading occurs due to the double side band nature of the signal and can degrade performance [16]. For double sideband optical OFDM each subcarrier is represented by two optical frequencies which are subjected to different amounts of dispersion as a result of being transmitted through the optical channel. The subsequent phase difference between the two sets of equal amplitude subcarriers means that destructive interference can occur at certain subcarrier frequencies, giving rise to deep fades within the OFDM signal spectrum [18]. Figures 3.16a and 3.16b show the received OFDM spectra, under injection conditions, over 25km and 50km respectively. The effect of dispersive fading is more evident over 50km as higher frequency powers are reduced to close to 10dB below the maximum at higher frequencies.

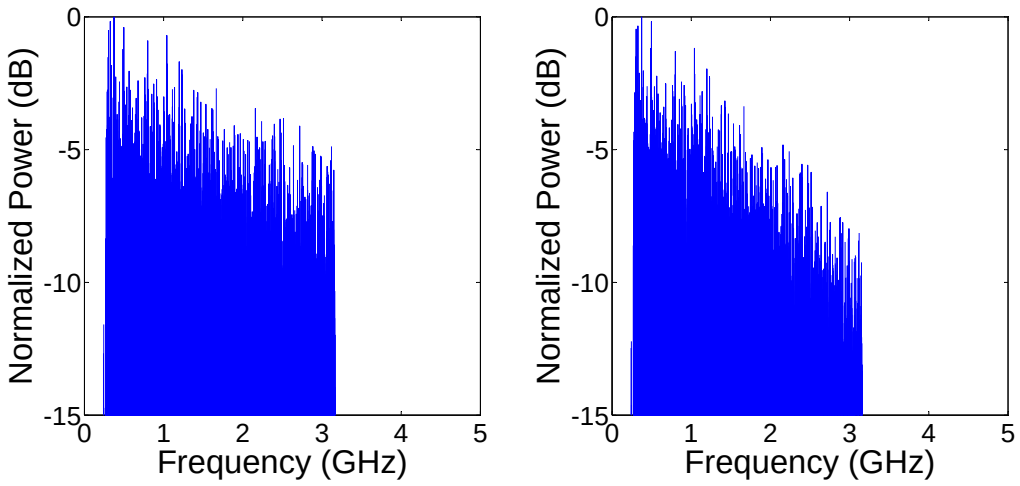

(a) (b)

Figure 3.16: Received OFDM spectra after 25km (a) and 50km (b) transmission.

3.6 Conclusion

Due to its cost effectiveness, and high spectral efficiency, direct modulation optical OFDM is a promising technology for use in next generation optical access networks. It has been shown experimentally, and by simulation, that the use of external optical injection can improve the performance of these systems by reducing non–linearity. Furthermore, it has been demonstrated that the use of optical injection with integrated DM lasers, which is shown to reduce IMD3 by up to 10dB, can also be used to overcome non–linear limitations imposed by the properties of the modulating laser. Results presented in this chapter show how adaptive power/bit loading of OFDM subcarriers by the Levin–Campello algorithm can be used to maximise throughput within the moderate bandwidths afforded in direct modulation systems, with up to 17.54Gb/s raw data rate being achieved when injection is used. Moreover, it is shown that AM–OFDM signals can be easily re–adjusted to further increase throughput given the bandwidth expansion and reduction in non–linearity which is achieved through the use of optical injection.

Expanding the linear range of operation of a directly modulated laser by optical injection is a technique which can improve the performance of direct modulation OFDM systems em-

ploying all laser transmitters. The integration of two DM lasers operating in master–slave configuration makes this technique feasible for use in low cost optical OFDM communication systems because of its small size and cost.

The direct modulation OFDM systems discussed in this chapter include the use of fixed wavelength lasers as transmitters in access configurations. Wavelength tuneable lasers will be a key feature of transmitters in future reconfigurable optical networks. Until recently, their use has been restricted to long haul applications due to their cost. The next chapter will explore the use of direct modulation OFDM with tuneable lasers which are suitable for implementation in future optical access networks.

References

[1] J. Armstrong, "OFDM for Optical Communications," *Journal of Lightwave Technology*, vol. 27, no. 3, pp. 189–204, 2009.

[2] L. Chrostowski, C.-H. Chang, and C. Chang-Hasnain, "Enhancement of dynamic range in 1.55nm VCSELs using injection locking," *IEEE Photonics Technology Letters*, vol. 15, no. 4, pp. 498–500, 2003.

[3] J. Chen, R. Ram, and R. Helkey, "Linearity and Third-Order Intermodulation Distortion in DFB semiconductor lasers," *IEEE Journal of Quantum Electronics*, vol. 35, no. 8, pp. 1231–1237, 1999.

[4] G. H. M. van Tartwijk and D. Lenstra, "Semiconductor lasers with optical injection and feedback," *Journal of Optics: Quantum Semiclassical Optics*, vol. 33, p. 90, 1995.

[5] C. van den Bos, M. Ksuwenhoven, and W. Serdijn, "Effect of smooth nonlinear distortion on OFDM Symbol Error Rate," *IEEE Transactions on Communications*, vol. 49, no. 9, pp. 1510–1514, 2001.

[6] R. Lang and K. Kobayashi, "External optical feedback effects on semiconductor injection laser properties," *IEEE Journal of Quantum Electronics*, vol. 16, no. 3, pp. 347–355, 1980.

[7] G. Yabre and J. L. Bihan, "Reduction of nonlinear distortion in directly modulated semiconductor lasers by coherent light injection," *Journal of Quantum Electronics*, vol. 33, no. 7, p. 1132, 1997.

[8] X. Meng, T. Chau, and M. Wu, "Experimental demonstration of modulation bandwidth enhancement in distributed feedback lasers with external light injection," *Electronics Letters*, vol. 34, no. 21, pp. 2031–2032, 1998.

[9] G. Agrawal, "Line narrowing in a single-mode injection laser due to external optical feedback," *IEEE Journal of Quantum Electronics*, vol. 20, no. 5, pp. 468–471, 1984.

[10] L. Barry, R. O'Dowd, J. Debau, and R. Boittin, "Tunable transform-limited pulse generation using self-injection locking of an FP laser," *IEEE Photonics Technology Letters*, vol. 5, no. 10, pp. 1132–1134, 1993.

[11] W. Hung, C. Chan, L. Chen, and F. Tong, "An Optical Network Unit for WDM access networks with downstream DPSK and upstream re-modulated OOK data using injection-locked FP laser," in *2003 Optical Fiber Communications Conference (OFC)*, vol. 1, 2003, pp. 281–282.

[12] G. Agrawal and N. K. Dutta, *Long-Wavelength Semiconductor Lasers*. Van Nostrand Reinhold Company, New York, 1986.

[13] J. Helms, "Intermodulation and harmonic distortions of laser diodes with optical feedback," *Journal of Lightwave Technology*, vol. 9, no. 11, pp. 1567–1575, Nov. 1991.

[14] C. Herbert, D. Jones, A. Kaszubowska-Anandarajah, B. Kelly, M. Rensing, J. O'Carroll, R. Phelan, P. Anandarajah, P. Perry, L. Barry, and J. O'Gorman, "Discrete mode lasers for communication applications," *IET Optoelectronics*, vol. 3, no. 1, pp. 1–17, Feb. 2009.

[15] P. Anandarajah, S. Latkowski, C. Browning, R. Zhou, J. O'Carroll, R. Phelan, B. Kelly, J. O'Gorman, and L. P. Barry, "Integrated two-section discrete mode laser," *Photonics Journal, IEEE*, vol. 4, no. 6, pp. 2085–2094, 2012.

[16] J. Han, B. Seo, Y. Han, B. Jalali, and H. Fetterman, "Reduction of fiber chromatic dispersion effects in fiber-wireless and photonic time-stretching system using polymer modulators," *Journal of Lightwave Technology*, vol. 21, no. 6, p. 1504, Jun. 2003.

[17] G. Meslener, "Chromatic dispersion induced distortion of modulated monochromatic light employing direct detection," *IEEE Journal of Quantum Electronics*, vol. 20, no. 10, pp. 1208–1216, Oct. 1984.

[18] U. Gliese, S. Norskov, and T. Nielsen, "Chromatic dispersion in fiber-optic microwave and millimeter-wave links," *IEEE Transactions on Microwave Theory and Techniques*, vol. 44, no. 10, pp. 1716–1724, 1996.

Chapter 4

Tuneable Lasers with OFDM

4.1 Introduction

Wavelength Division Multiplexing (WDM) can be used to increase system capacity and is currently deployed in core and metro networks as outlined in section 1.2. State-of-the-art access network protocols such as EPON (IEEE 802.3ah) and GPON(ITU-T G.984) are based on Time Division Multiplexing (TDM) and use two wavelengths, each designated for either upstream or downstream transmission. The downstream optical carrier is shared among all of the subscribers by means of a passive splitter. Although these types of networks make use of the large bandwidths available in optical fibres, they are limited in terms of scalability due to their single channel downstream operation. The number of ONUs in the network is limited due to signal attenuation introduced by the passive splitter, and data rates are limited to that which can be provided on a single channel.

WDM overcomes these limitations as it supports both the upstream and downstream transmission of multiple wavelengths over the same fibre infrastructure. As all wavelengths are routed to individual ONUs by a passive Arrayed Waveguide Grating (AWG), no power splitting of the individual optical carriers takes place and each ONU may operate up to the data rate which can be provided on a single channel.

To date, a lack of demand for such high data rates, coupled with immature and expensive optical components, have meant that WDM access networks have not been commercialised [1]. The growing demand for new services such as IPTV and online gaming means that WDM–PONs will need to be implemented; this will be facilitated by the development of cost effective tuneable laser transmitters which can be employed both at the OLT and ONU to provide network flexibility.

This chapter will examine the direct modulation of tuneable lasers with OFDM. This combination of wavelength agile transmitters with the high spectral efficiency provided by OFDM can facilitate both the flexibility and data rate required for next generation PONs.

4.2 Tuneable Lasers with PONs

4.2.1 Colourless Operation

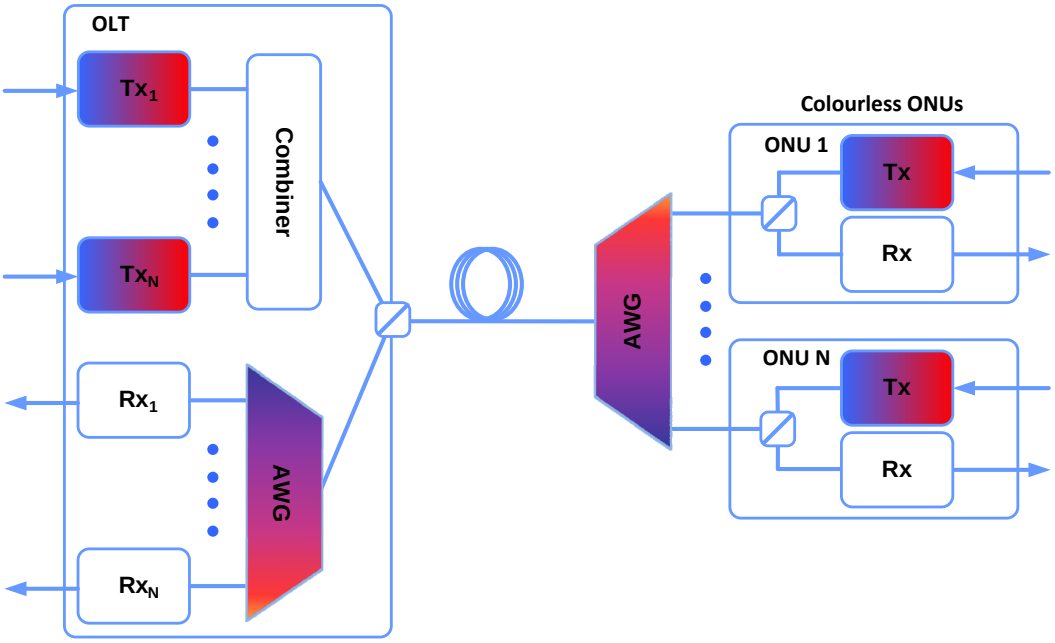

Figure 4.1: Colourless WDM–PON structure.

Figure 4.1 shows a WDM–PON architecture where each ONU has a unique wavelength designated to it. This type of architecture can also be referred to as Wavelength Division

Multiple Access (WDMA) [2]. If laser transmitters with a fixed wavelength are employed throughout the network, each ONU must be wavelength specific (i.e. capable of receiving or transmitting on one wavelength only). This increases cost as each ONU must be designed independently. Furthermore, flexibility is compromised as upstream transmission can only ever take place on the same wavelength. Ideally, all ONUs should be identical and capable of operation on all channels utilised in the network. This reduces manufacturing costs (provided cost effective tuneable laser diodes can be deployed) and increases the potential for network reconfigurability. This type of operation is known as 'colourless' as each ONU is agnostic to its operating wavelength. For colourless operation, it is not essential to have tuneable lasers at the OLT as shown in figure 4.1. However, doing so allows for any transceiver module within the OLT (each emitting a different wavelength to one another) to transmit data to any ONU in the network without the requirement for re–routing at the RN, thereby introducing another degree of network flexibility.

4.2.2 Architectures

Colourless WDM–PONs can be categorised into two types [3]: (i) self emission and (ii) wavelength supply.

- ❏ A self emission type WDM–PON architecture is show in figure 4.1. Here, each ONU is equipped with a tuneable laser which is capable of transmitting on several wavelengths on the grid (typically a CWDM grid [1]). Downstream transmission is carried out by modulating the light from an array of fixed or tuneable lasers. These wavelengths are multiplexed for transmission to the RN, where they are then routed to the corresponding ONUs. In this type of WDM–PON ONUs can transmit and receive on different wavelengths.

- ❏ Wavelength supply type WDM–PONs do not employ independently tuneable lasers at the ONU. Instead, either the downstream optical carrier is stripped out and re–modulated using an external modulator or a Reflective SOA (RSOA) [4], or the

downstream carrier is used as a seed in order to lock a laser diode at the ONU to the supplied wavelength [5]. Downstream transmission is carried out as in the self emission case. The nature of this type of architecture requires that all ONUs transmit and receive on the same wavelength.

4.2.3 Direct Modulation of Tuneable Lasers

Direct modulation of a laser diode is desirable in access networks for the reasons outlined in section 1.5.1; namely, cost and footprint compared to transmitters employing external modulators. For these reasons, when proposing the use of tuneable lasers in a WDM–PON it is important to investigate their suitability for direct modulation. Some tunable lasers such as External Cavity Lasers (ECLs) provide excellent tunability but are unsuitable for direct modulation due to their long cavity length. Other devices such as DFB and DM lasers may be tuned using a combination of temperature and biasing current; however as the biasing current is varied when direct modulation is employed, the tuning may not remain stable. The work presented in the following sections shows how direct modulation of a tuneable laser suitable for use in WDM–PONs may be carried out.

4.3 Discrete Mode Tuneable Laser

The laser device used in the work presented in this chapter was a dual section slotted FP laser diode. Device details and in depth characterisation can be found in [6]and [7]. The slots are etched into the top of an otherwise conventional laser ridge waveguide, transforming the multimode spectrum of the FP laser into a very high quality single mode device [8]. Increased tuning range operation of the laser is achieved by optimising the laser's mirror reflectivities in each section by employing the Vernier effect to extend the tuning range associated with the limited refractive index change with current [7]. This device requires no additional re–growth or processing steps when compared with other tuneable devices, which minimises the fabrication complexity, thereby increasing wafer yield while reducing

cost. The device is temperature controlled by a Thermo-Electric Cooler (TEC) and both of its sections may be biased independently. Wavelength tuning is achieved as single mode operation (defined as Side Mode Suppression Ratio (SMSR) $\geq$ 30dB [9]), can be attained at various wavelengths depending upon the biasing of both sections and temperature conditions. Although the device is not switched quickly in this work, it is capable of a switching time within the ns range [7]. This could be important parameter in the context of OFDM systems employing dynamic bandwidth assignment and Medium Access Control (MAC) protocols. The laser linewidth was not characterised for this device as it is not a critical parameter for the proposed direct detection scheme.

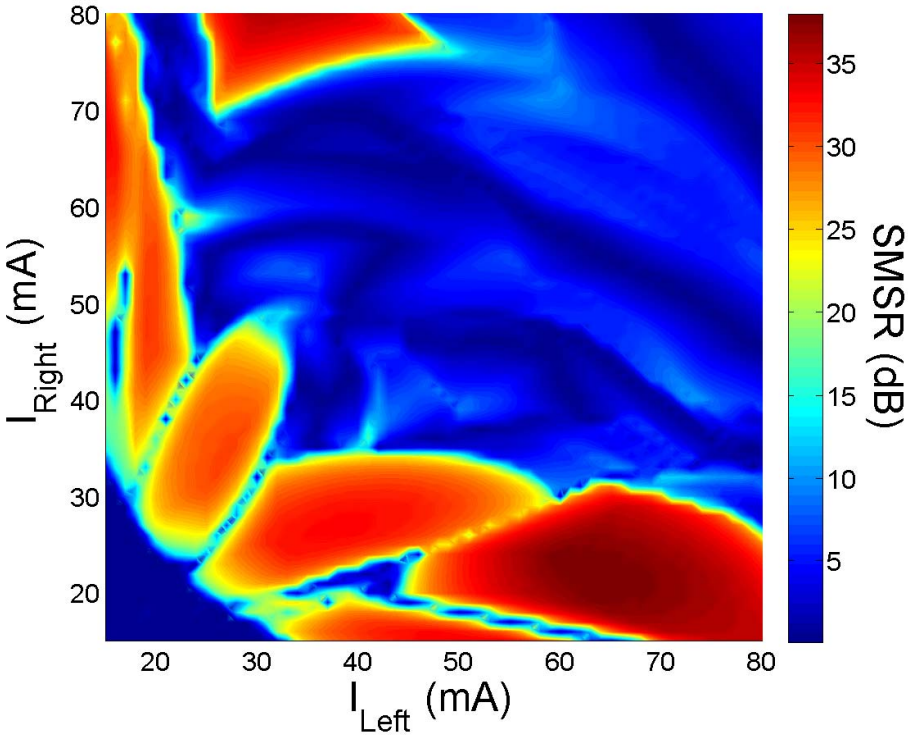

Figure 4.2: SMSR for all biasing conditions.

4.3.1 Device Characterisation

To ascertain bias conditions for which single mode lasing is achieved, both SMSR and output wavelength were measured (using an OSA) for a set of bias currents to each section

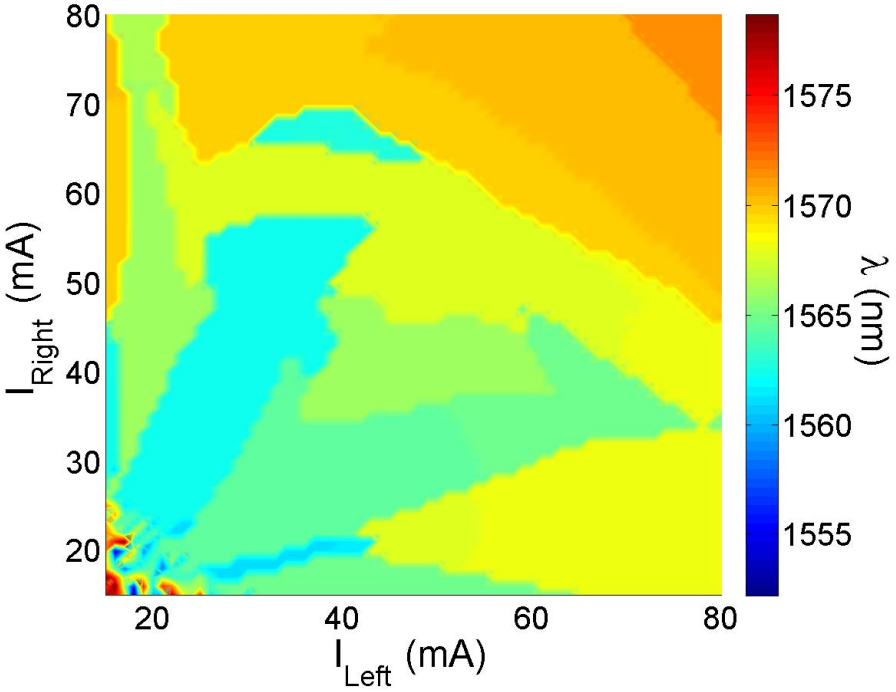

Figure 4.3: Output wavelength for all biasing conditions.

ranging from 0 to 80mA in 1mA steps. This process was repeated for various temperatures ranging from 2.5°C to 17°C. Figure 4.2 shows such an SMSR map obtained at a temperature of 17°C. It is clear from the map that the number of operating points is limited and many biasing conditions do not result in single mode operation. This is a feature of this prototype device. It is hoped that future iterations will increase the number of available modes, while minimising cost so as to maintain its suitability for optical access networks.

To compute the number of available modes, figure 4.2 must be viewed in tandem with figure 4.3, which is the associated wavelength map for all tested biasing conditions. From figure

Table 4.1: Single mode lasing at 17°C.

I_{left}(mA)	I_{right}(mA)	SMSR (dB)	λ(nm)
66	23	37.6	1568
40	32	30.0	1564.5
26	34	30.4	1562.3
15	68	33.7	1569.9
33	80	35.5	1569.9

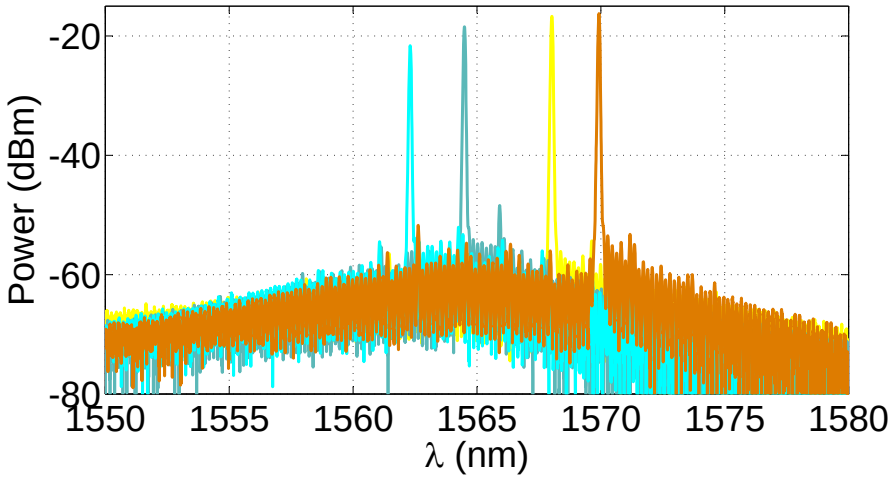

Figure 4.4: Available modes at 17°C. Colours correspond to figure 4.3.

4.2 it can be seen that five areas of high SMSR ($\geq$ 30dB) exist. Observing the corresponding current conditions on the wavelength map in figure 4.3 shows that two of these current combinations result in the same output wavelength. Table 4.1 gives the current conditions which result in high SMSR and corresponding output wavelength. At this temperature four modes are available for use and the bias setting of [I_{left}, I_{right}] = [15,68]mA is omitted as it results in a lower SMSR of the output wavelength 1569.9nm compared to the alternative setting. This process was repeated for various temperatures and the resulting SMSR and wavelength tuning maps can be found in Appendix E.

For each set of current and temperature conditions which ensured single mode lasing, there was an associated modulation response for each section. Figure 4.5 shows modulation responses for three sets of these conditions and the modulation bandwidths achieved are around 4GHz. In the figure, solid lines represent the modulation responses measured when the 'Left' section was directly modulated and dashed lines giving the associated response for the 'Right' section. The output power of the device varied between -3dBm and -7dBm depending on biasing and temperature. Poor fibre coupling in the package contributed to the low output power, with an approximate coupling loss of 6dB. This value is higher than the typical coupling loss which can be achieved (3dB) and was ascertained by measuring the output power of the device before and after packaging.

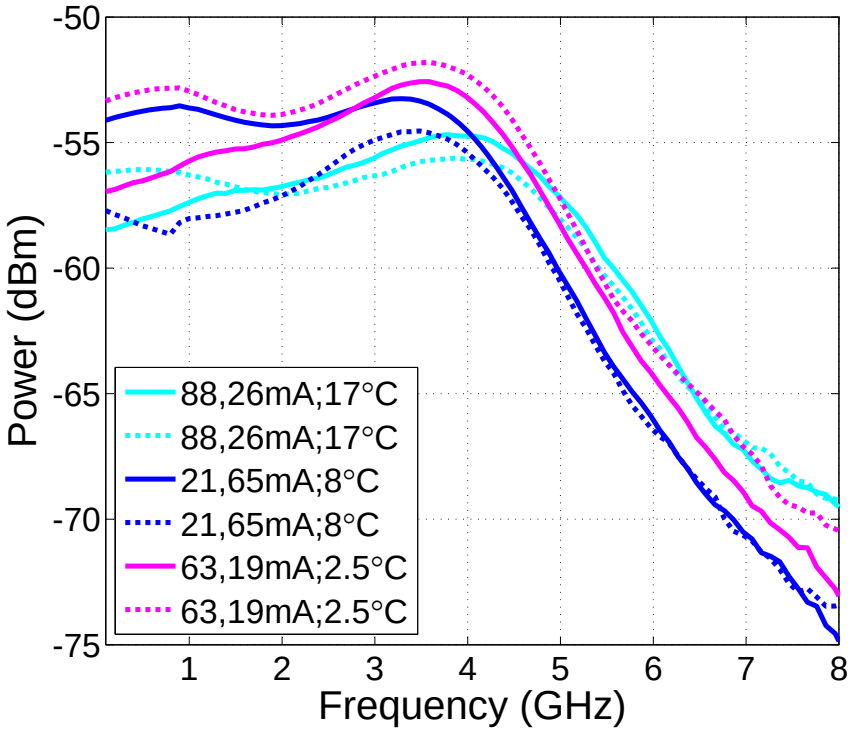

Figure 4.5: Modulation responses at various bias/temperature settings.

4.4 Direct Modulation OFDM with a Tuneable Laser

4.4.1 Experimental Setup

Figure 4.6 shows the experimental set up with the two sections of the device labelled 'Left' and 'Right'. Firstly, the device under test was characterized by varying the bias current to both sections as well as the operating temperature while observing the output wavelength, as described in section 4.3.1. Conditions which ensured single mode operation were noted and several of these were used for data transmission.

OFDM pilots and transmission signals were created offline using Matlab. The SNR of each subcarrier was estimated by propagating OFDM pilot signals with 16–QAM on every subcarrier. The Levin-Campello (LC) bit/power loading algorithm [10] was then used to calculate the optimal bit distribution across those subcarriers; assigning different constellation sizes to each subcarrier. A 256 input Inverse Fast Fourier Transform (IFFT) was used

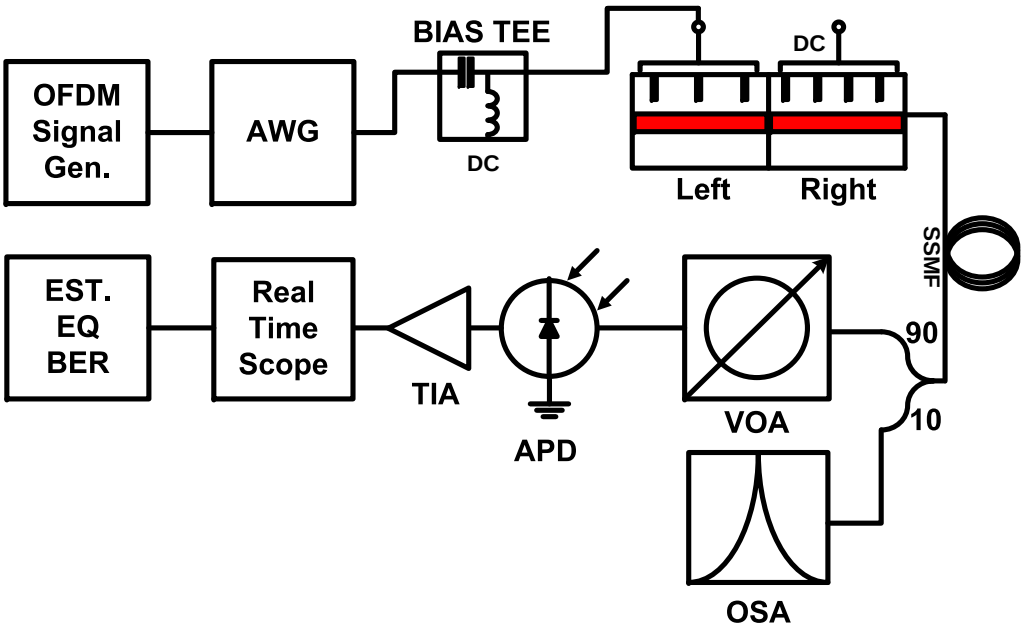

Figure 4.6: Experimental setup for direct modulation of the DM laser with AM–OFDM.

and the subcarrier spacing was set to 39.06MHz. The number of subcarriers, and hence signal bandwidth, used for each system configuration was determined by the LC algorithm. Typically, bandwidths were between 3GHz and 4GHz. A CP of 6.25% (this value resulted in a whole number of transmit samples as well as being sufficiently long to handle any dispersion time encountered in the experimental work) was added and 7% of the AM–OFDM signal was reserved for FEC (allowing BERs of $\leq 1 \times 10^{-3}$ to result in error free transmission). A real signal was created by modulating the real and imaginary components of the complex baseband AM–OFDM signal with the In-phase (I) and Quadrature (Q) components of an RF carrier respectively. The resultant signal was output from the Digital to Analogue Converter (DAC) of an AWG sampling at 10GSa/s. Typical PAPR of the AM-OFDM signals was 12dB.

The AM–OFDM signal was then used to directly modulate one section of the device in conjunction with a DC bias. The decision to modulate either the left or right side section depended on which section could be modulated with the largest RF signal before the SMSR of the optical output was reduced below 30dB. As stated above, optical launch power varied

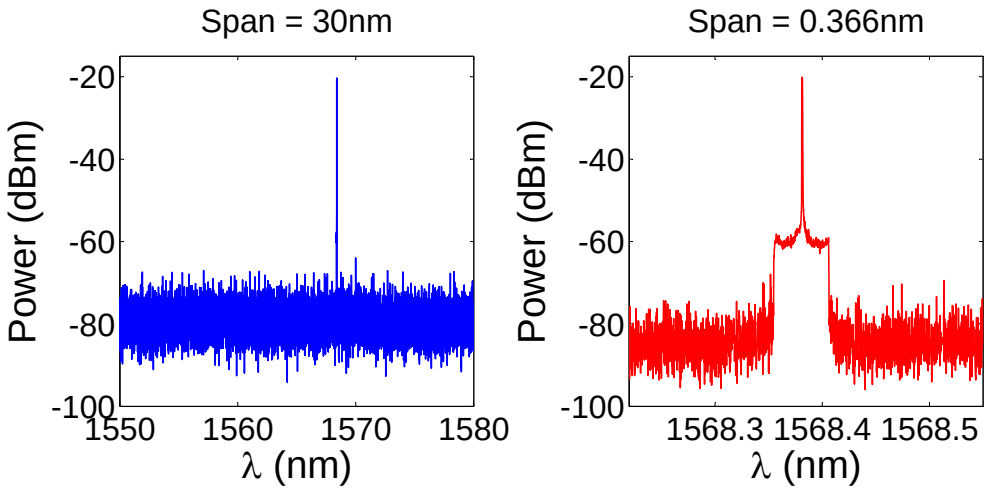

Figure 4.7: Modulated/Unmodulated optical spectra at the DM laser output.

depending on the operating conditions. Transmission was carried out over 0km, 25km and 50km of SSMF. Figure 4.7 shows an example mode both unmodulated and modulated with an OFDM signal. Where necessary, the received optical signal was attenuated by a VOA to an appropriate level so as to avoid saturation of the APD with an integrated TIA; this occurred at approximately -12dBm. The received RF signal was captured using a RTS also sampling at 10GSa/s. Required DSP including channel estimation and equalization as well as EVM and BER calculation was completed offline.

4.4.2 Results and Discussion

4.4.2.1 Single Mode Operation

Figure 4.8 shows superimposed optical spectra of some of the available modes attained using a combination of temperature tuning and various biasing settings for each section. The insets show received 16, 32 and 64-QAM constellation diagrams on selected AM-OFDM subcarriers after transmission over 25km on the 1560.02nm, 1564.46nm and 1571.72nm channels respectively. The device is shown to be tuneable from 1557.68nm to 1571.72nm, giving a tuning range of 14.04nm.

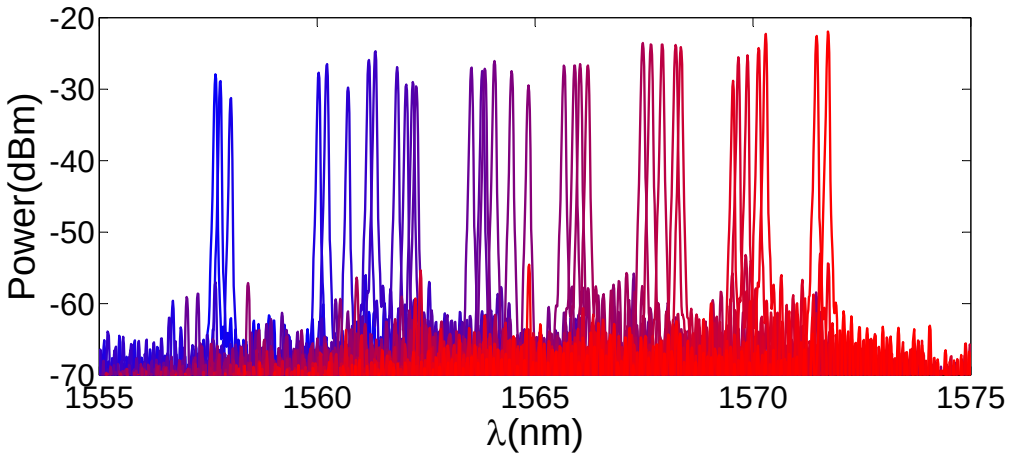

Figure 4.8: Superimposed available modes spanning the range 1558nm to 1572nm.

4.4.2.2 AM–OFDM

Table 4.2: Received raw data rates for all channels.

λ(nm)	0km(Gb/s)	25km(Gb/s)	50km(Gb/s)
1560.02	21.13	15.80	11.10*
1562.30	15.00	14.68	11.05*
1564.46	17.89	17.40	14.30
1566.66	20.12	16.60	9.26*
1568.00	19.26	17.73	12.30
1569.92	21.52	16.64	11.30
1571.72	18.20	17.18	12.15

Seven modes were selected from across the range of available wavelengths for AM-OFDM transmission to be performed. Table 4.2 shows the raw data rates achieved for each mode over all transmission distances while maintaining a BER of 1×10^{-3}. Given that the optical launch power varied due to differing biasing conditions, that no optical amplification was used, and that transmission distance varied, the received optical power did not remain constant. This contributes to a decrease in data rates over 25km and 50km compared to the 0km case as shot and thermal noise at the receiver make a greater contribution to the Signal to Noise Ratio (SNR) of the lower received power AM-OFDM signals. Nevertheless, greater than 10Gb/s data rates are displayed on all modes over 0km and 25km and on most modes over 50km. Data rates marked with an asterix in the 50km column fall short of the required

raw data rate for 10Gb/s transmission given the CP and FEC overheads needed.

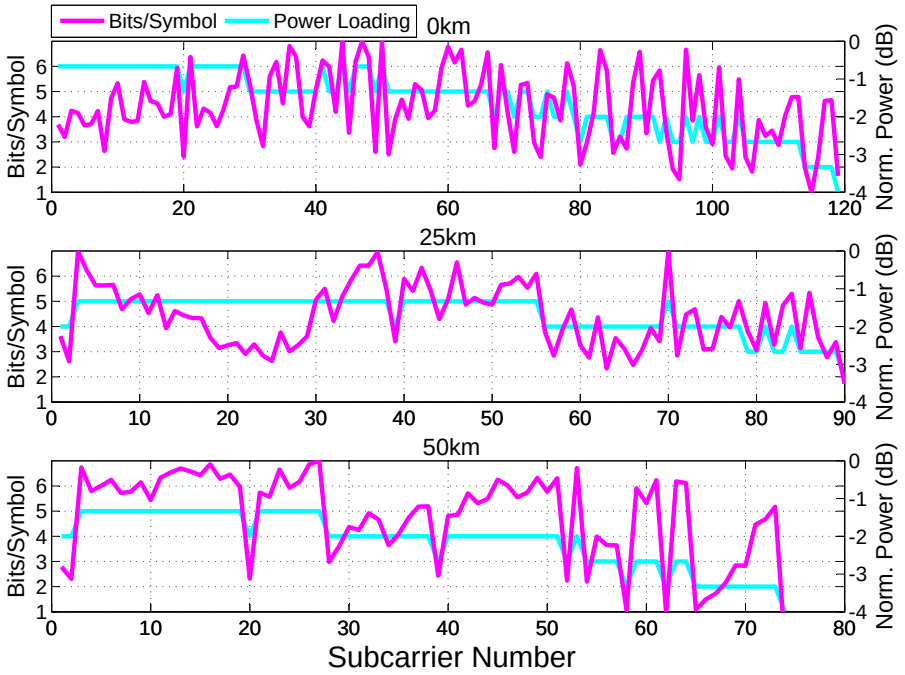

Figure 4.9: Bits/Symbol and power assigned to each OFDM subcarrier.

Figure 4.9 shows the bit and power loading distributions calculated using the rate adaptive form of the LC algorithm for the 1569.92nm channel in the back-to-back case and over 25 and 50km. The figure shows that the order of modulation decreases as subcarrier frequencies enter the lasers' frequency range of non-linear operation. This occurs at frequencies close to the resonance peak (or relaxation oscillation) of the modulation response and is due to the non-linear interaction between carriers and photons in the laser cavity [11]. The number of subcarriers used decreases as transmission distance increases. As stated, in the case of transmission over 25km the lower received optical power leads to a dis-improvement of SNR at the receiver. Subsequently, the LC algorithm updates the bit distribution and some higher frequency subcarriers are dropped due to the new level of power required on those subcarriers to successfully transmit lower order formats. The power saved by not transmitting these subcarriers is redistributed to maintain successful transmission on other subcarriers and maximise throughput. The net effect is a decrease in throughput from 21.52Gb/s to 16.64Gb/s. This effect is also evident over 50km where a further dis-improvement in SNR,

coupled with the dispersive fading experienced over this transmission distance, results in the number of subcarriers dropping to 74 and overall throughput dropping to 11.3Gb/s.

4.4.2.3 Dispersive Fading

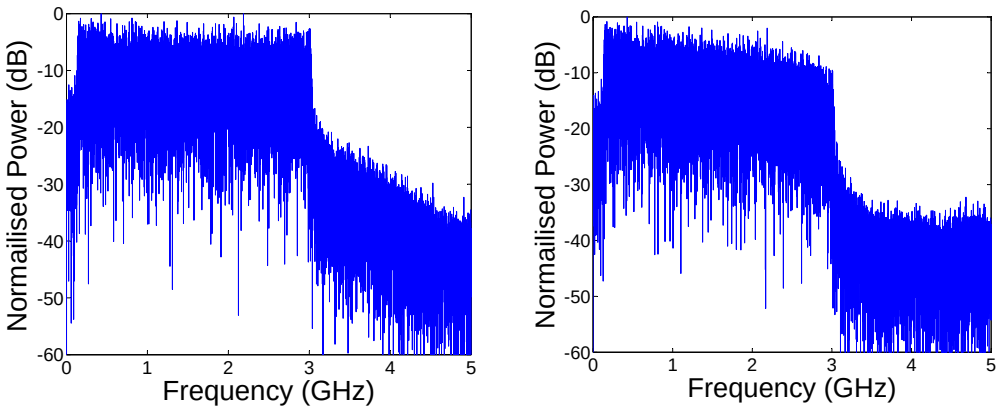

(a) (b)

Figure 4.10: Received OFDM spectra after 25km (a) and 50km (b) transmission.

In addition to loss, the transmitted signals also experience dispersive fading over 50km. This is due to the double sideband nature of the transmitted signals and its effect is to introduce nulls at frequencies which vary with transmission distance [12]. Subsequently, the SNRs of the affected subcarriers are decreased, the bit distribution given by the LC algorithm is updated to take this into account and data throughput is decreased; this is shown in Table 4.2. Figures 4.10a and 4.10b show the received electrical spectra of the same 16-QAM pilot signal (no power/bit loading) with 74 subcarriers and centred at 1.6GHz over 25km (4.10a) and 50km (4.10b) on the 1564.46nm channel with identical optical launch power. The effects of dispersive fading can clearly be seen as the received signal power decreases by up to 10dB at higher frequencies in the 50km case.

Figure 4.11 shows received optical power vs. $\log_{10}$(SER) on the 1560.02nm channel. SER was estimated from the calculated EVM as described in section 2.3.2. System performance in the back–to–back case and over 25km of SSMF is almost identical for the same received powers as, dispersion over 25km is dealt with by equalisation and the launch power was not

high enough to incur fibre non-linearities. A 4dB penalty in receiver sensitivity is observed over 50km compared to the other cases, indicating the impact of dispersive fading on system performance.

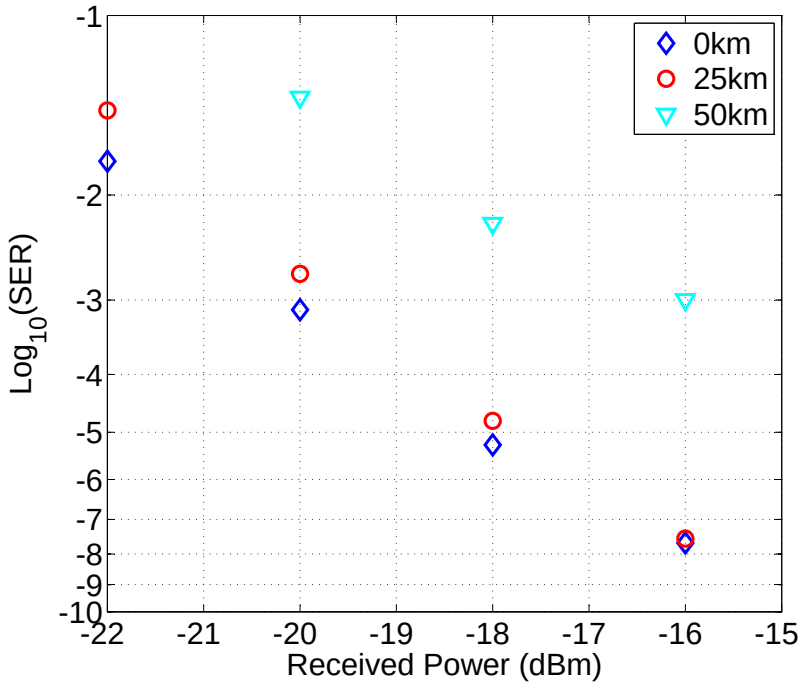

Figure 4.11: Received Power vs. $\log_{10}$(SER) for all distances.

4.5 Conclusion

The work presented in this chapter shows, for the first time, the direct modulation of a tuneable laser by an AM-OFDM signal. The tuneable dual section slotted FP laser under test has been characterised in terms of SMSR and output wavelength for varying bias and temperature conditions. It has been found that single mode operation can be achieved on over thirty modes across a spectral range of 14nm when using a combination of current and temperature tuning. Improvements in this prototype device will increase both the number of available channels and the output power thereby making it more suitable for WDM–PON applications in terms of both cost and operating wavelengths.

Furthermore, AM-OFDM transmission is performed on seven selected modes and perform-

ance on each is measured in terms of the maximum achievable data throughput. Data rates of greater than 10Gb/s are displayed for all of these modes over 25km of SSMF and on the majority of modes over 50km where dispersive fading is the limiting factor on performance.

The application of direct modulation in conjunction with the highly spectrally efficient AM-OFDM signal and a tuneable slotted Fabry-Pérot laser offers a cost effective solution for transmitters in PONs where low cost is of primary importance due to their potentially high market volume. Moreover, the problems of insertion loss, polarisation dependence and footprint associated with systems employing external modulators are overcome, adding to the suitability of this system design for deployment in future WDM–PONs.

References

[1] A. Banerjee, Y. Park, F. Clarke, H. Song, S. Yang, G. Kramer, K. Kim, and B. Mukherjee, "Wavelength-Division-Multiplexed Passive Optical Network (WDM-PON) technologies for broadband access: A review [invited]," *Journal of Optical Networking*, vol. 4, no. 11, pp. 737–758, Nov. 2005.

[2] C.-H. Lee, W. V. Sorin, and B. Y. Kim, "Fiber to the Home using a PON infrastructure," *Journal of Lightwave Technology*, vol. 24, no. 12, pp. 4568–4583, Dec. 2006.

[3] R. Davey, J. Kani, F. Bourgart, and K. McCammon, "Options for future optical access networks," *IEEE Communications Magazine*, vol. 44, no. 10, pp. 50–56, Oct. 2006.

[4] J. Lazaro, B. Schrenk, A. Maziotis, I. Cano, P. Bakopoulos, J. Prat, and H. Avramopoulos, "Full-duplex 20/10Gb/s WDM-PON with remodulation of chirped ASK and multi-level quaternary PAM and OFDM," in *2012 Optical Fiber Communication Conference (OFC)*, 2012, p. OTh1F.6.

[5] W. Hung, C. Chan, L. Chen, and F. Tong, "An Optical Network Unit for WDM access networks with downstream DPSK and upstream re-modulated OOK data using injection-locked FP laser," in *2003 Optical Fiber Communications Conference (OFC)*, vol. 1, 2003, pp. 281–282.

[6] K. Shi, F. Smyth, D. Reid, B. Roycroft, B. Corbett, J. Song, P. O'Brien, F. Peters, and L. Barry, "Characterization of a novel three-section tunable slotted Fabry-Perot

laser," in *2010 Optical Fiber Communication Conference (OFC)*. Optical Society of America, 2010, p. OWU3.

[7] R. Phelan, W.-H. Guo, Q. Lu, D. Byrne, B. Roycroft, P. Lambkin, B. Corbett, F. Smyth, L. Barry, B. Kelly, J. O'Gorman, and J. Donegan, "A novel two-section tunable Discrete Mode Fabry-Perot laser exhibiting nanosecond wavelength switching," *IEEE Journal of Quantum Electronics*, vol. 44, no. 4, pp. 331–337, 2008.

[8] C. Herbert, D. Jones, A. Kaszubowska-Anandarajah, B. Kelly, M. Rensing, J. O'Carroll, R. Phelan, P. Anandarajah, P. Perry, L. Barry, and J. O'Gorman, "Discrete mode lasers for communication applications," *IET Optoelectronics*, vol. 3, no. 1, pp. 1–17, Feb. 2009.

[9] L. Coldren, "Monolithic tunable diode lasers," *IEEE Journal of Selected Topics in Quantum Electronics*, vol. 6, no. 6, pp. 988–999, 2000.

[10] J. Campello, "Optimal discrete bit loading for multicarrier modulation systems," in *1998 IEEE International Symposium on Information Theory*, Aug. 1998, p. 193.

[11] G. H. M. van Tartwijk and D. Lenstra, "Semiconductor lasers with optical injection and feedback," *Journal of Optics: Quantum Semiclassical Optics*, vol. 33, p. 90, 1995.

[12] G. Meslener, "Chromatic dispersion induced distortion of modulated monochromatic light employing direct detection," *IEEE Journal of Quantum Electronics*, vol. 20, no. 10, pp. 1208–1216, Oct. 1984.

Chapter 5

Burst Mode OFDM

5.1 Introduction

So far, OFDM has been investigated as a modulation format for use in Passive Optical Networks. PONs, by their nature, require cost effective components and this has been the main reason behind the use of direct modulation in the previous chapters. However, the exploitation of OFDM's inherent spectral efficiency and tolerance to chromatic dispersion is not just limited to optical access networks. It is important to investigate the performance of OFDM with transmitters that are suitable for implementation with longer distance networks such as WDM Metro networks as, coupled with the higher level of hardware complexity afforded by these higher level networks, OFDM is capable of providing very high data rates and good spectral efficiency on each optical carrier.

The following sections demonstrate experimentally the use of externally modulated OFDM in a switching environment which provides the necessary reconfigurability required for next generation Metro networks. Additionally, the use of Single Sideband (SSB) OFDM as a means of increasing spectral efficiency and overcoming the effects of dispersive fading is described and demonstrated.

5.2 Burst Mode Networks

Burst switching is similar to packet switching, the difference being that data bursts may contain many packets of data. In this way, payloads used in burst switching are not restricted to be the length of one packet but can be considerably longer. Burst mode operation can be achieved in the optical domain by modulating data onto an optical carrier provided by a laser whose wavelength can be quickly switched, typically by the application of varying voltage bias conditions. Optical Burst Switching (OBS) and burst mode networks have been proposed for use in Metropolitan Area Networks which can be referred to as MANs or 'Metro networks' [1, 2]. By providing increased reconfigurability, burst mode operation can contribute to the efficient use of a shared resource which is typically the case in Metro networks, where a simple ring topology is used to connect all network nodes [3]. Indeed, the use of all optical wavelength switching for On–Off Keyed (OOK) data in such a ring topology has previously been investigated and commercialised [4]. Within MANs, which currently employ WDM, it is desirable to use higher order modulation formats as the increased spectral efficiency allows for a greater number of optical carriers to be used [5]. Previously, Optical Packet Switching (OPS) with Polarization Division Multiplexed QPSK, using a coherent receiver, and Differential QPSK, using a delay interferometer, have been demonstrated in [5] and [6] respectively.

OFDM is a modulation technique which is widely used in both wired and wireless communications and indeed has been specified for packet based radio communications standards such as WiMAX, LTE and ADSL. OFDM's compact arrangement of subcarriers, which are orthogonal to each other in the frequency domain, ensures high spectral efficiency and is the main reason behind OFDM's use in current radio standards. However, what makes OFDM particularly attractive for use in optical communications is its inherent tolerance to chromatic dispersion as discussed in chapter 2.

Using OFDM in OBS Metro networks would not only increase data throughput on each wavelength channel, but would give potential for increased network reconfigurability as,

through DSP, OFDM signals can be easily tailored to suit user/channel demands and allow for dynamic bandwidth allocation to subcarrier granularity [7]. An OBS OFDM system has previously been demonstrated in an Optical Access Network (OAN) configuration employing burst mode AM–OFDM and two un–switched lasers at the transmitter [8]. The experimental work presented in this chapter shows for the first time the application of Single Sideband OFDM (SSB–OFDM) to an OBS system using only a single fast switching laser at the transmitter. Direct detection is employed, which relaxes the constraints on the frequency and linewidth fluctuations (which occur after a switching event) compared to systems employing coherent receivers.

5.3 SSB–OFDM

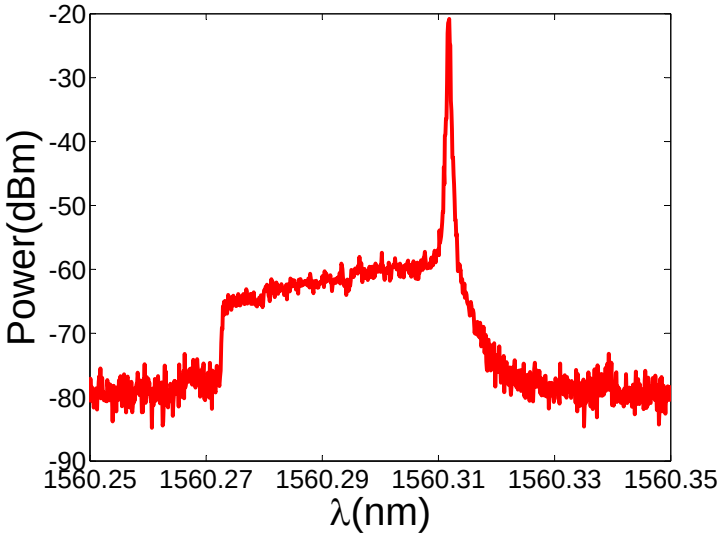

Figure 5.1: An example optical SSB-OFDM spectrum taken experimentally with an OSA.

Compatible Single Sideband (CompSSB) was first proposed in the late 1950's as a means of increasing the spectral efficiency of radio broadcast signals [9]. These CompSSB signals were designed to be detected by squaring receivers which were common at the time. The use of OFDM with this technique was first proposed for optical communications by Schuster *et al.* in 2007 [10]. In that paper, a mapping for SSB–OFDM generated with a complex (I–Q)

optical modulator is derived. This particular technique is further contrasted to Offset SSB–OFDM (a technique proposed by Lowery *et al.* as a means of increasing spectral efficiency and maximising throughput given the relatively low electrical bandwidths available from transmitter DACs [11]) in [12]. A new mapping was shown in [13] to achieve SSB–OFDM modulation with a Dual Drive Mach Zehnder Modulator (DD–MZM) which is the approach taken in the work described below.

For any 'real' baseband signal $\sigma(t)$ the Hilbert transform can be used to generate SSB modulation.

$$s(t) = \sigma(t) + jH[\sigma(t)] \tag{5.1}$$

where $s(t)$ is the SSB representation and H denotes the Hilbert transform. In CompSSB the information is applied as the exponential coefficient for the envelope of the optical field $E(t)$ [10, 13],

$$E(t) = e^{\sigma(t)+jH[\sigma(t)]} \tag{5.2}$$

$$= e^{\sigma(t)} \cdot e^{jH([\sigma(t)]} \tag{5.3}$$

$$= A(t)e^{j\Phi(t)} \tag{5.4}$$

where

$$A(t) = e^{\sigma(t)} \tag{5.5}$$

$$\Phi(t) = H(\sigma(t)) \tag{5.6}$$

Since we are using direct detection the data is recovered from the amplitude term, $A(t)$. In [13] $\sigma(t)$ is set to equal the OFDM signal, $\Omega_{ofdm}(t)$, and hence from equation 5.5 we can see that the received signal $A(t) = e^{\sigma(t)} = e^{\Omega_{ofdm}(t)}$. This means that a natural logarithm must be applied digitally after detection to retrieve $\Omega_{ofdm}(t)$. This method leads to ambiguity for AC coupled systems and can contribute to increased quantisation noise at the receiver Analogue–to–Digital Converter (ADC) due to the higher Peak–to–Average

Power Ratio (PAPR) of the received signal resulting from the exponential term.

By simply letting $\sigma(t) = \ln(\Omega_{ofdm}(t))$ at the transmitter (this requires that all signal values are positive), the OFDM signal itself can be retrieved using direct detection,

$$A(t) = e^{\sigma(t)} \tag{5.7}$$

$$= e^{\ln(\Omega_{ofdm}(t))} \tag{5.8}$$

$$= \Omega_{ofdm}(t) \tag{5.9}$$

with no need for additional processing at the receiver, provided the necessary amplitude and phase changes required for CompSSB are realised. To realise these conditions we must examine the DD–MZM transfer function. Considering the input and output optical fields,

$$E_o(t) = 2E_i(t)e^{j\omega t}e^{j\phi_0(t)}\sin(\Delta\phi(t)) \tag{5.10}$$

where $E_o(t)$ is the output optical field, $E_i(t)$ is the input optical field, $\phi_0(t) = [\phi_1(t) + \phi_2(t))]/2$ and $\Delta\phi(t) = [\phi_1(t) - \phi_2(t)]/2$ where $\phi_1(t)$ and $\phi_2(t)$ are the input electrical phases to either arm of the modulator. Now taking the small signal approximation, where $\Delta\phi(t) + \pi/2 \ll \pi$,

$$E_o(t) = 2E_i(t)e^{j\omega t}e^{j\phi_0(t)}(\Delta\phi(t)) \tag{5.11}$$

We see that the last two terms of equation 5.11 can be controlled such that conditions for CompSSB are met i.e. let

$$\Delta\phi(t) \cdot e^{j\phi_0(t)} = A(t)e^{j\Phi(t)}$$

$$\Rightarrow \Delta\phi(t) = A(t), \quad e^{j\phi_0(t)} = e^{j\Phi(t)} \tag{5.12}$$

$$\Rightarrow [\phi_1(t) - \phi_2(t)]/2 = A(t), \tag{5.13}$$

$$[\phi_1(t) + \phi_2(t))]/2 = \Phi(t) \tag{5.14}$$

Substituting values from equations 5.5 and 5.6 into the simultaneous equations 5.13 and 5.14, the phase changes required for CompSSB, $\phi_1(t)$ and $\phi_2(t)$, can be expressed in terms of $\sigma(t)$ and hence also the OFDM signal, $\Omega_{ofdm}(t)$.

$$\phi_1(t) = H[\sigma(t)] + e^{\sigma(t)}, \quad \phi_2(t) = H[\sigma(t)] - e^{\sigma(t)} \tag{5.15}$$

where $\phi_1(t)$ and $\phi_2(t)$ are the two electrical signals applied to the DD–MZM.

5.4 Optical Burst Switched SSB–OFDM

5.4.1 Experimental Setup

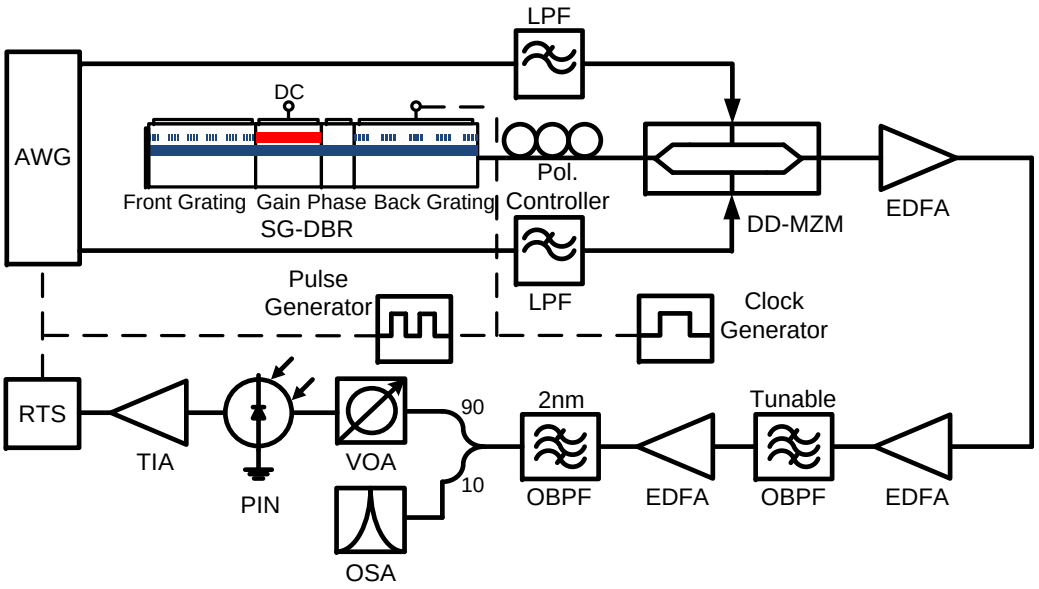

Figure 5.2: Experimental set up of the OBS system.

The experimental set up is shown in figure 5.2. SSB–OFDM data is used to modulate light from a switching Sampled Grating Distributed Bragg Reflector (SG)–DBR laser via a DD–MZM. Further details on this device, as well as linewidth measurements, are given in [14] where the laser is referred to as SG-DBR1. After transmitter and receiver amplification a bandwidth and wavelength tuneable Optical Bandpass Filter (OBPF) at the receiver, which

is tuneable across the entire C-band, is set to select only the desired wavelength channel, after which the signal is again amplified. The bandwidth of this filter can be varied to simulate the effects of different WDM grid sizes (e.g. 100GHz, 50GHz, 25GHz and 12.5GHz). The 2nm receiver filter is used to filter out Amplified Spontaneous Emission (ASE). The received optical power was set to 0dBm by a VOA before being detected using a 10GHz bandwidth PIN detector. This experiment was performed for an optical back to back case as the process of switching was expected to be the main limitation on performance rather than the effects of transmission through fibre which are easily dealt with by the CP and receiver amplification.

Table 5.1: OFDM Properties.

IFFT/FFT Size	256
IFFT Data Inputs	120
Modulation	16–QAM
OFDM Symbol Rate	39.06MHz
Bandwidth	4.74GHz
Raw Data Rate	18.74Gb/s
Net Data rate	15Gb/s
CP	6.25%
FEC	7 %

SSB–OFDM burst signals were created using the parameters given in table 5.1. The overall sampling rate was set to 10GSa/s, which was the maximum available from the AWG used. This set an upper frequency limit of 5GHz and OFDM signals were tailored to maximise the use of the available electrical bandwidth. Real SSB–OFDM signals were constructed using RF IQ modulation, as previously described in sections 3.4.1 and 4.4.1, at 2.48GHz. Two SSB–OFDM burst signals, A and B, were generated, each containing 15 OFDM symbols, and each with one Training Symbol (TS) which was used for channel estimation. The training symbol was placed at the beginning of one burst (i.e. 1^{st} OFDM symbol position), denoted 'Burst A', and in the centre of the second burst (i.e. 8^{th} OFDM symbol position), denoted 'Burst B'. Aside from the placement of the training sequence, bursts A and B were identical in all other properties.

A clock generator operating at 1MHz was used to switch the SG–DBR laser between

1547.88nm and 1560.32nm by switching the current to the back section of the device. For this device, the switching time depended upon the specific wavelengths being used, but between these specific modes (1560.32nm to 1547.88nm) was approximately 5ns [15]. A pulse generator was used to output a delayed version of this switching signal, which was used as an external trigger for the AWG, operating in burst mode. By varying this delay, the time at which the burst is modulated onto the optical carrier relative to a switching event can be varied. As a complete copy of the transmitted OFDM signal is required at the receiver in order to retrieve any data, it is not possible to observe a gradually improving performance throughout a switching event as is the case in [6]. Instead, the concept of 'delay times' is introduced where a delay of '0ns' is defined as the first available time, after a switching event, at which a complete copy of the OFDM burst can be received. All subsequent delays are relative to this value.

Data was burst onto one channel only while the other was filtered out at the receiver by the OBPF. The receiver RTS operated at 50GSa/s. Downsampling and other necessary processing was completed offline in Matlab.

5.4.2 Results and Discussion

5.4.2.1 Training Sequence Placement

Figures 5.3a and 5.3b show the Error Vector Magnitude (EVM), of a complete burst, versus subcarrier number for bursts beginning at various delays after a switching event. The first receiver filter is set to have a wide bandwidth (100GHz) and is centred on the 1560.32nm channel. For burst A, although the total BER across all subcarriers reduces to below the FEC limit of 1×10^{-3} after 4ns, we can observe that lower frequency subcarriers for bursts beginning around this time have an extremely high EVM. This effect is attributed to ringing caused by the fact that there was no impedance matching between the back section of the SG–DBR and clock source used to drive this section and hence switch the output wavelength. This effect manifests itself as a fluctuation in optical power from the laser after

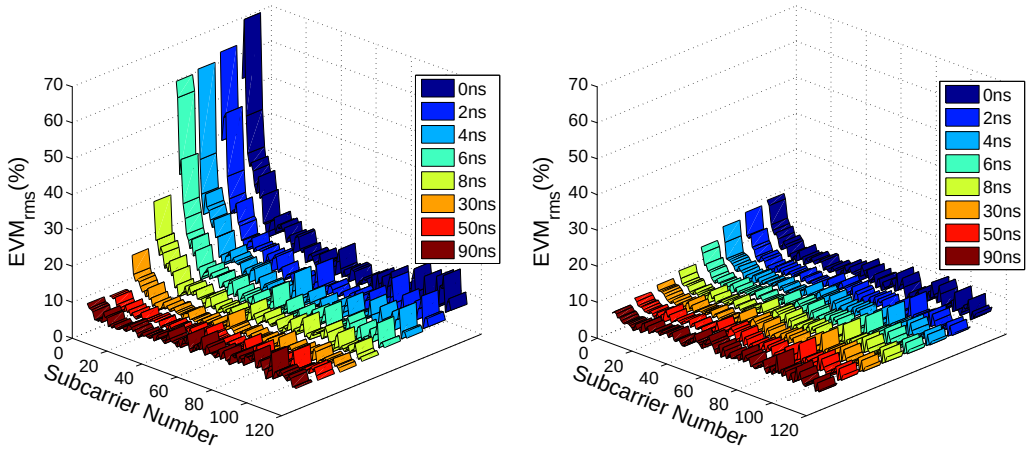

(a) (b)

Figure 5.3: EVM vs. subcarrier number for bursts beginning at various delay times after a switching event using bursts A (a) and B (b).

a switch. This electrical amplitude fluctuation was visible at the beginning of each switch. As the fluctuation is shorter than one OFDM symbol period (32ns), a problem arises when the first symbol is set to be the TS, as is the case for burst A. As the TS is used for the equalisation of all subsequent symbols, the poor performance of the TS is propagated throughout the entire burst, resulting in a large contribution to EVM by each OFDM symbol.

As stated, burst B resembles burst A, but contains the training symbol in the centre of the burst rather than at the start. This type of burst assembly ensures that errors encountered due to the poor performance of the first OFDM symbol do not propagate through the burst upon equalisation. However, provision would have to be made for the poor performance of the first OFDM symbol. Figure 5.3b shows greatly reduced EVM on lower frequency subcarriers, as only the first symbol makes a relatively large contribution to the EVM values and not all symbols, as is the case in Figure 5.3b. In this case the BER (for the complete burst) for a delay of 0ns was 3×10^{-4}.

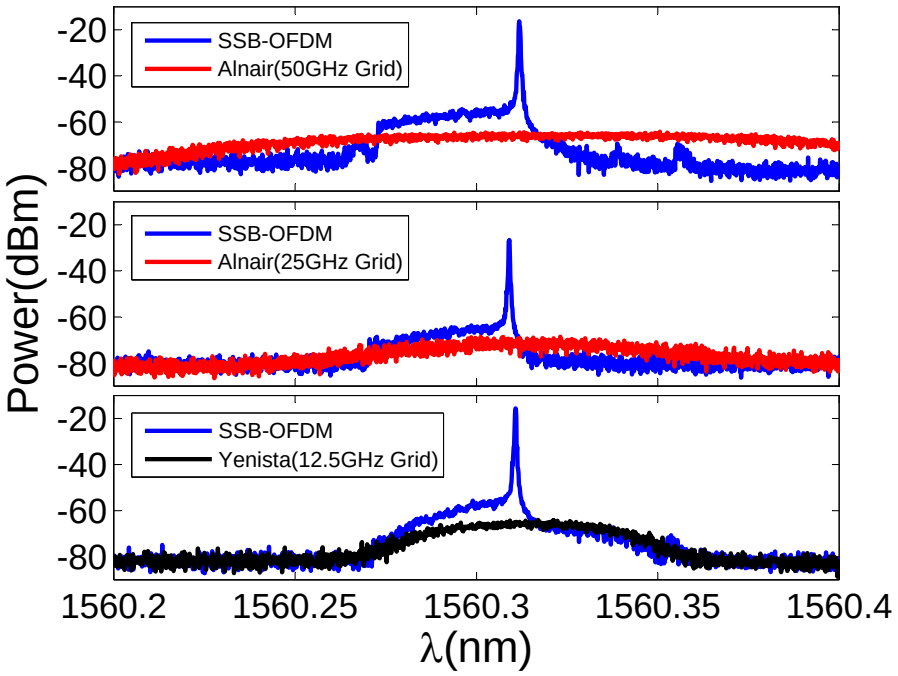

Figure 5.4: Optical spectra of the SSB–OFDM signal with the 50GHz, 25GHz (Alnair filter) and 12.5GHz (Yenista filter) grid filter profiles superimposed.

5.4.2.2 Impact Of WDM Filtering

The more conventional Burst A was chosen for further system performance investigation with various filter profiles. Filter profiles compatible with 50GHz, 25GHz, and 12.5GHz WDM grids were chosen. These profiles, set using the first OBPF, can be seen in figure 5.4, along with the SSB–OFDM data signal (carrier centred). The 3dB bandwidth of each profile was set to one third of the respective WDM grid.

This system configuration introduces two additional impairments compared to a wide filtering case. Firstly, higher frequency subcarriers may be attenuated by the narrow filtering. Secondly, the Gaussian shape of the filter at lower bandwidth settings can convert a frequency fluctuation in the output wavelength (after a switching event) to an amplitude fluctuation which can be detrimental to the performance of a direct detection system [16]. The latter impairment is minimised by centring the filter profile at the carrier frequency as shown in figure 5.4, so that any frequency fluctuation of the carrier takes place around

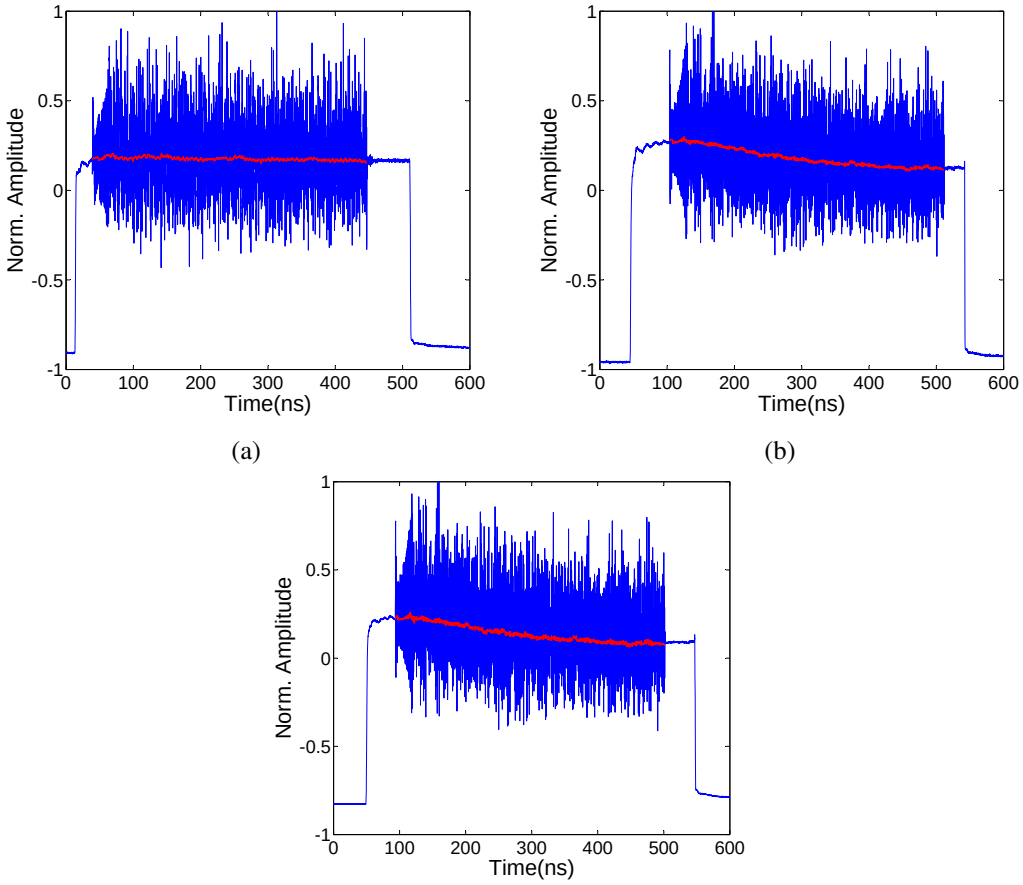

Figure 5.5: Switches from channel 1547.88nm to 1560.32nm using 50GHz (a) 25GHz (b) and 12.5GHz (c) grid filtering. Average optical power throughout the bursts are shown in red.

the top of the Gaussian shaped filter profile. For the 12.5GHz and 25GHz grid cases this amplitude fluctuation was unavoidable due to the narrow bandwidths employed. The more Gaussian shape at the centre of the Alnair filter (25GHz grid) compared to the Yenista filter (12.5GHz grid), which can also be seen in figure 5.4, caused this frequency–to–amplitude fluctuation to be more exacerbated in the 25GHz grid case. Figure 5.5 shows, in the time domain, the received switched signal containing the OFDM burst for the same switching event (1547.88nm to 1560.32nm) for 50GHz (a) 25GHz (b) and 12.5GHz (c) filtering. In all cases, the OFDM burst delay is set to >50ns where the effects of ringing are minimal. The frequency–to–amplitude fluctuation effect can be seen clearly in figure 5.5b and c as

the received optical power varies throughout the switching period.

Figures 5.6a and 5.6b show results obtained for the 12.5GHz and 50GHz WDM grid scenarios, where the first receiver OBPF bandwidth was set to 4.2GHz and 16.6GHz between 3dB points respectively. Figure 5.7 shows results obtained for the 25GHz grid case (8.3GHz between 3dB points) with inset constellations of all OFDM subcarriers received in bursts beginning 2ns and 30ns after a switching event.

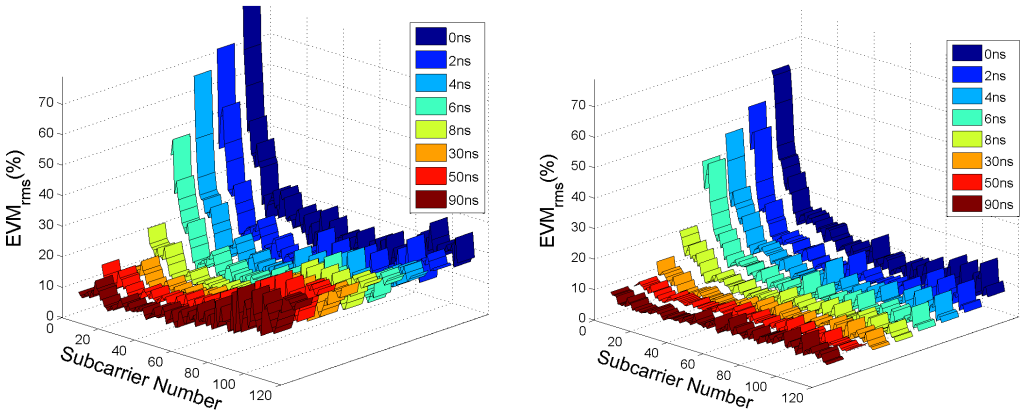

(a) (b)

Figure 5.6: EVM vs. subcarrier number for bursts beginning at various delay times after a switching event using 12.5GHz (a) and 50GHz (b) grid filtering.

The effects of 12.5GHz grid can be seen in figure 5.6a where a Yenista OBPF was employed due to its narrower filtering capabilities. The effects of attenuation are clear here as higher frequency OFDM subcarriers are much more attenuated than in the other cases and this is to be expected, given the signal bandwidth and filter profile used which can be seen in figure 5.4. In this case, burst BER reduces to below the FEC limit (1×10^{-3}), after 8ns, to 4.5×10^{-4} with a corresponding average EVM of 13.02%. These values are roughly maintained for subsequent delays as the EVM Vs. subcarrier number curves exhibit the same trend at low and high frequencies, indicating a performance limitation introduced by narrow filtering.

Figure 5.6b shows that the performance of the system with 50GHz grid filtering is very similar to the wide filtering case discussed in section 5.4.2.1. Given the relatively small signal

bandwidth and the flat shape of the OBPF at this setting, this result is to be expected. The same trend of poor performance on lower frequency subcarriers at burst times close to the switching event (due to the short amplitude fluctuation introduced by the lack of impedance matching – see section 5.4.2.1) is still evident. In this case, 4ns is required for the overall BER and the corresponding EVM reduce to 8.9×10^{-4} and 11.8% respectively.

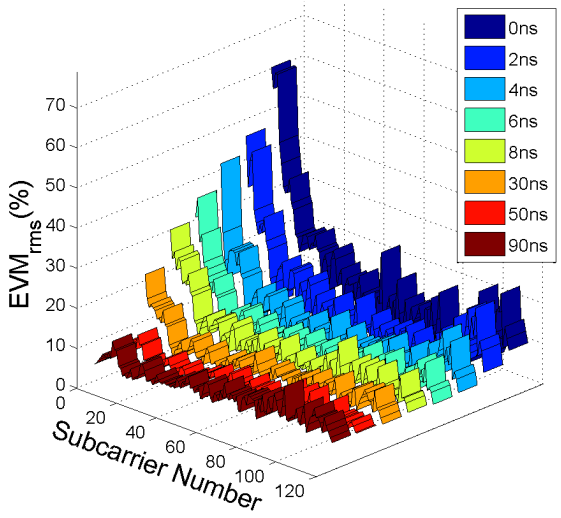

Figure 5.7: EVM vs. subcarrier number for bursts beginning at various delay times after a switching event using 25GHz grid filtering.

Results for 25GHz grid filtering in figure 5.7 show a degradation in performance compared to 50GHz grid filtering. Here, attenuation at higher subcarrier frequencies begins to degrade system performance with a 1dB penalty compared to the 50GHz grid case in terms of EVM across all subcarriers at '0ns' delay shown. Furthermore, the influence of the frequency–to–amplitude fluctuation, due to the narrower filter profile employed, can be seen as EVM increases across all subcarriers for every delay. Again, burst BER is reduced below the FEC limit to 7.5×10^{-5} after 8ns with a corresponding average EVM of 9.05%, although it would take up to 50ns to support 16–QAM on every subcarrier if each OFDM subcarrier was considered individually. Shown in figure 5.8a and 5.8b are received constellations from a single burst for delays of 2ns and 30ns respectively where 25GHz grid filtering is employed. The fact that there is an asymmetric distribution of errors between the constellations points is attributed to the degradation of the training sequence due to ringing, a non–Gaussian

process. This effect is lessened as delay times are increased, as shown in 5.8b.

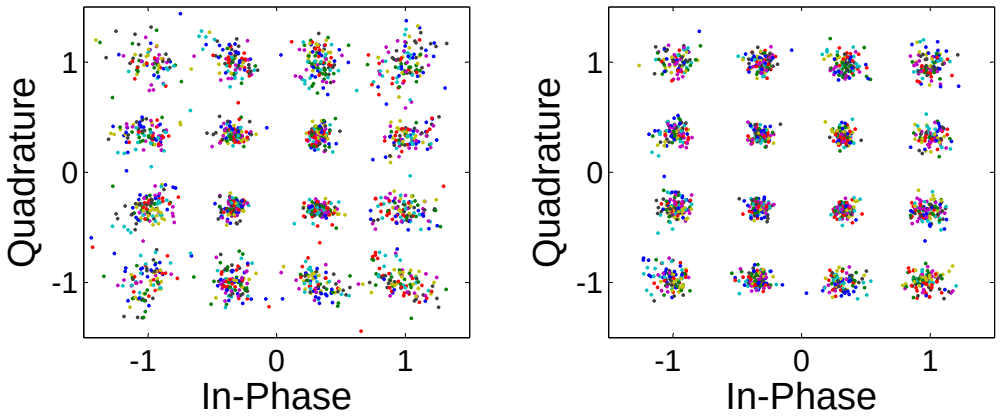

(a) (b)

Figure 5.8: Received constellations at 2ns delay (a) and 30ns delay(b) for 25GHz grid filtering.

It is clear that for OBS systems employing very narrow filtering such as a 12.5GHz WDM grid, there is a trade off between incurring frequency–to–amplitude fluctuations and the attenuation of higher frequency OFDM subcarriers. Centring the OBPF profile over the optical carrier reduces the risk of frequency–to–amplitude fluctuations as discussed above, but also ensures the attenuation of higher frequency OFDM subcarriers (for larger bandwidth OFDM signals). Depending on the profile employed, it may be advantageous to centre the profile closer to the centre of the SSB–OFDM data, rather than the optical carrier. This not only reduces the attenuation on upper subcarriers, but could help to equalise signal to carrier power ratio if necessary. To help to optimise this trade off, ways in which the receiver filter profile may be centred over the optical carrier for a duration equal to the settling time of the laser's output frequency before shifting the profile to a position closer to the centre of the data sideband could be investigated.

5.5 SSB–OFDM for overcoming Dispersive Fading

Aside from providing the potential for increased spectral efficiency, employing SSB modulation formats allows the effects of dispersive fading to be mitigated. Dispersive fading is

particularly undesirable in OFDM systems as it generates spectral nulls in the signal band, leading to the loss of subcarrier orthogonality. The effect of dispersive fading has already been shown in sections 3.5.3.4 and 4.4.2.3 to affect the performance of DSB direct modulation OFDM systems. As dispersive fading occurs due to a phase difference between two sidebands after transmission through a certain amount of fibre (as described in section 3.5.3.4), by simply transmitting only one sideband its effects can be mitigated.

5.5.1 Experimental Setup

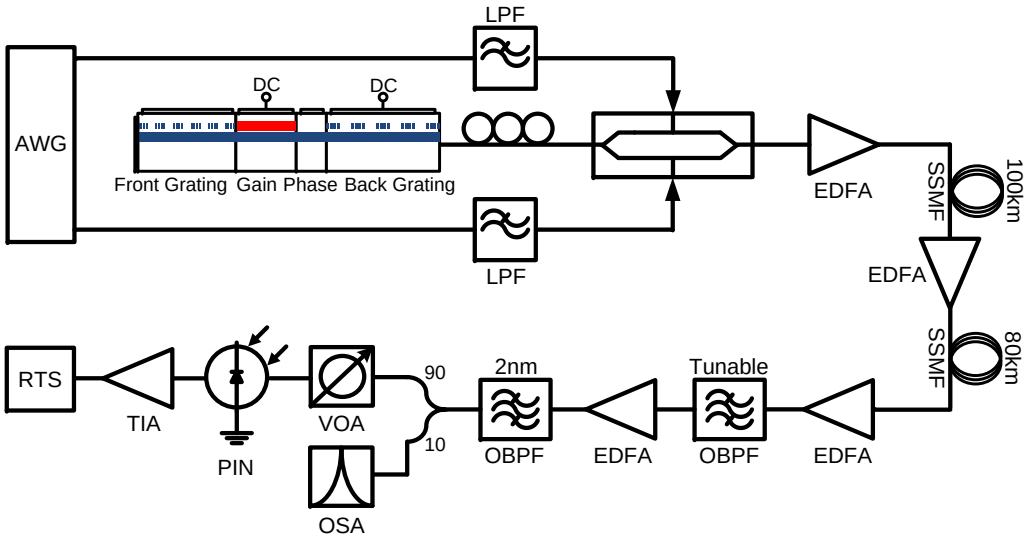

Figure 5.9: Experimental setup for transmission over 180km of SSB and DSB OFDM signals.

In order to demonstrate the use of SSB–OFDM to overcome dispersive fading, an experimental set up similar to that used in 5.4.1 was used, but for simplicity the SG–DBR laser was not switched. The revised setup is shown in figure 5.9. The back section of the laser was biased with a constant current and so remained static at 1554.05nm. The output power from the laser was 3dBm and the modulated optical launch power (after the transmitter EDFA) was set to 6dBm in order to ensure that fibre nonlinearities were not encountered. The signal was transmitted through 100km of SSMF before being amplified by an in–line EDFA and transmitted through a further 80km of SSMF. As before, a two stage EDFA re-

ceiver was used with the first OBPF set to have a wide bandwidth (100GHz). The optical power falling on the PIN photodiode was held constant at 0dBm. OFDM signal properties were the same as described in 5.1. Both DSB and SSB–OFDM signals were generated and used for transmission. SSB signals were output as described above in section 5.3 while the OFDM signal itself and its complement were used to drive the two arms of the modulator in order to generate the DSB signal.

5.5.2 Results and Discussion

In order to see the effects of dispersive fading it was necessary to transmit the OFDM signals through 180km of SSMF. Sections 3.5.3.4 and 4.4.2.3 show dispersive fading effects after 50km of SSMF. The reason why 180km is required in this case is due to the fact that the external modulator used in this experimental demonstration imparts far less frequency chirp across the OFDM signal band compared to the lasers in previous chapters, which were directly modulated by the OFDM signals [17]. As the phases of the OFDM subcarriers are largely unaffected at the input to the fibre, a greater length of SSMF is required for dispersive fading to occur at the frequencies occupied by the OFDM signal.

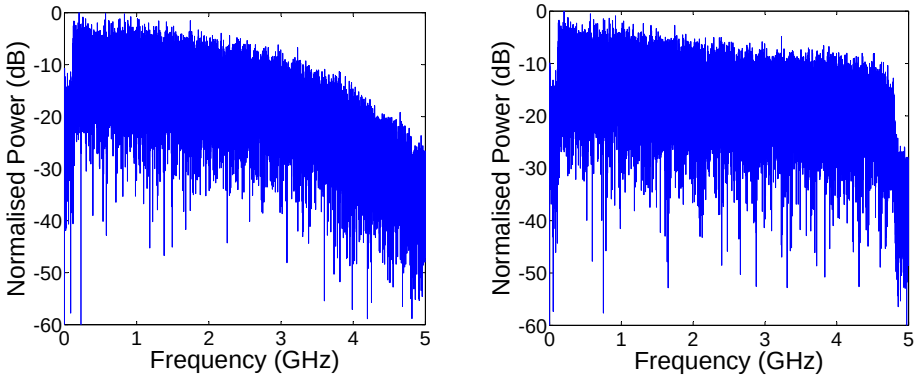

(a) (b)

Figure 5.10: Received DSB (a) and SSB (b) OFDM signals after 180km transmission.

Figures 5.10a and 5.10b show the received spectra of the DSB and SSB–OFDM signals respectively. The effects of dispersive fading are clear to see in figure 5.10a, with a severe roll off occurring after 2GHz. OFDM subcarrier powers fall to 20dB below maximum

values at 4GHz and -28dB below maximum values at the upper subcarrier limit of 4.85GHz. Figure 5.10b shows how the use of SSB–OFDM can overcome the effects of dispersive fading. The nulling effect is not exhibited in this case and the 10dB difference in subcarrier powers is due to the roll off of the electronics in the system; namely the AWG itself and the anti–aliasing filters used at the transmitter.

Having had its higher frequency subcarriers severely degraded by dispersive fading, the BER of the DSB signal was calculated to be 4.8×10^{-2}. The SSB signal gave a BER of 9.8×10^{-4} for the same received power of 0dBm. The received constellation diagrams of all channels for both the DSB and SSB signals are shown in figures 5.11b and 5.11b respectively. They exhibit an associated average EVM of 20.2% (DSB) and 14.97% (SSB). It is clear from figure 5.11b that while some subcarriers are demodulated correctly (giving a concentration of constellation points in the correct locations), the higher frequency subcarriers perform badly, indicated by a spread of received constellation points between ideal locations.

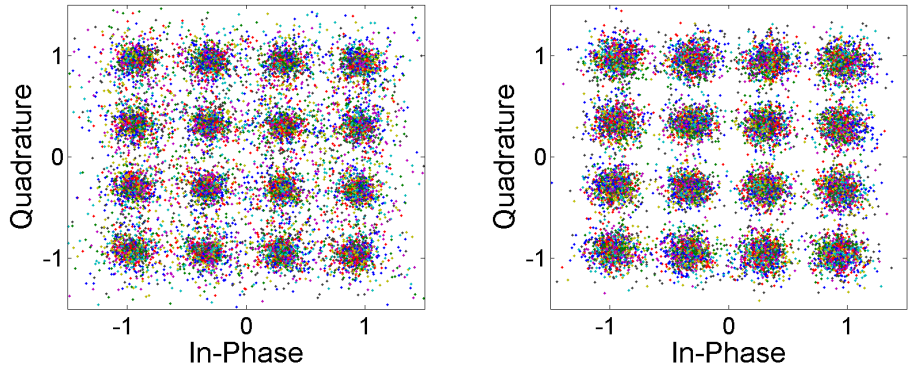

Figure 5.11: Received constellations of the DSB (a) SSB (b) OFDM signals after 180km transmission.

5.6 Conclusion

In this chapter, the application of OFDM in an OBS system using a single fast switching tuneable laser at the transmitter has been demonstrated. Furthermore, a DD–MZM is

exploited to generate SSB–OFDM, which is desirable for use in WDM networks as it increases spectral efficiency and, as the experimental work shows, can be used to mitigate effects of dispersive fading.

Results show how the placement of an OFDM Training Sequence within a data burst can affect system performance as the first OFDM symbol in the packet is degraded at delay times close to the start of the switch. The use of various filter profiles at the receiver shows how filter grid size governs not only the spectral efficiency, but the overall performance of SSB–OFDM. When using filter profiles compatible with 50GHz, 25GHz and 12.5GHz grids – as would be the case in future WDM based Metro networks – a performance limitation is exerted on the system due to frequency fluctuations after a switching event and the attenuation of higher frequency subcarriers. Additionally, the delay time between a switching event and the beginning of a data burst, required to achieve acceptable performance, is shown to vary depending on the type of WDM grid employed. Results presented where 12.5GHz grid filtering is employed show that a spectral efficiency of 1.2b/s/Hz is achieved with SSB–OFDM, comparing favourably with OOK, where around 0.4b/s/Hz could be attained. This high spectral efficiency, combined with the wavelength versatility offered by a tuneable SG–DBR laser, makes this technique a promising scheme for next generation Metro networks employing WDM.

References

[1] C. Qiao and M. Yoo, "Recommendation G.709/y.1331 (02/12)," , *Journal of High Speed Networks*, vol. 8, pp. 69–84, 1999.

[2] J. Kim, J. Cho, M. Jain, D. Gutierrez, L. Kazovsky, C.-F. Su, R. Rabbat, and T. Hamada, "Demonstration of 2.5Gbps optical burst switched WDM rings network," in *2006 Optical Fiber Communication Conference (OFC)*, 2006, p. PDP43.

[3] L. Kazovsky, "Burst-mode metro and access networks," in *2007 Optical Fiber Communication Conference (OFC)*, 2007, p. OWC1.

[4] J. Fernandez-Palacios, N. Gutierrez, G. Carrozzo, G. Bernini, J. Aracil, V. Lopez, G. Zervas, R. Nejabati, D. Simeonidou, M. Basham, and D. Christofi, "Metro architectures enabling subwavelengths: Rationale and technical challenges," in *Future Network and Mobile Summit*, 2010, pp. 1–8.

[5] J. Simsarian, J. Gripp, A. Gnauck, G. Raybon, and P. Winzer, "Fast-tuning 224Gb/s intradyne receiver for optical packet networks," in *2010 Optical Fiber Communication Conference (OFC)*, 2010, p. PDPB5.

[6] F. Smyth, C. Browning, K. Shi, F. Peters, B. Corbett, B. Roycroft, and L. Barry, "10.7Gbd DQPSK packet transmission using a widely tunable Slotted Fabry-Perot laser," in *36th European Conference and Exhibition on Optical Communication (ECOC)*, 2010, p. Mo.1.F.5.

[7] N. Cvijetic, D. Qian, and J. Hu, "100Gb/s optical access based on optical Orthogonal Frequency-Division Multiplexing," *IEEE Communications Magazine*, vol. 48, no. 7, pp. 70–77, July 2010.

[8] L. Anet Neto, A. Gharba, P. Chanclou, N. Genay, B. Charbonnier, M. Ouzzif, C. Aupetit-Berthelemot, and J. Le Masson, "High bit rate burst mode optical OFDM for next generation Passive Optical Networks," in *36th European Conference and Exhibition on Optical Communication (ECOC)*, 2010, p. Tu.3.B.5.

[9] L. Kahn, "Compatible Single Sideband," *Proceedings of the IRE*, vol. 49, no. 10, pp. 1503–1527, 1961.

[10] M. Schuster, B. Spinnler, C.-A. Bunge, and K. Petermann, "Spectrally efficient OFDM-transmission with Compatible Single-Sideband modulation for direct detection," in *33rd European Conference on Optical Communication (ECOC)*, 2007, pp. 1–2.

[11] A. Lowery, L. Du, and J. Armstrong, "Performance of optical OFDM in ultralong-haul WDM lightwave systems," *Journal of Lightwave Technology*, vol. 25, no. 1, pp. 131–138, 2007.

[12] M. Schuster, S. Randel, C.-A. Bunge, S. Lee, F. Breyer, B. Spinnler, and K. Petermann, "Spectrally efficient Compatible Single-Sideband modulation for OFDM transmission with direct detection," *IEEE Photonics Technology Letters*, vol. 20, no. 9, pp. 670–672, 2008.

[13] Z. Xu, M. O'Sullivan, and R. Hui, "OFDM system implementation using compatible SSB modulation with a dual-electrode MZM," *Optics Letters*, vol. 35, no. 8, pp. 1221–1223, 2010.

[14] K. Shi, D. Reid, L. Barry, Y. Yu, and F. Smyth, "Linewidth calibration of sg-dbr lasers," *Photonics Technology Letters, IEEE*, vol. 22, no. 23, pp. 1729–1731, 2010.

[15] Y. Yu and R. O'Dowd, "Influence of mode competition on the fast wavelength switching of an SG-DBR laser," *Journal of Lightwave Technology*, vol. 20, no. 4, pp. 700–704, 2002.

[16] E. Connolly, A. Kaszubowska-Anandarajah, and L. Barry, "Cross channel interference due to wavelength drift of tuneable lasers in DWDM networks," in *2006 International Conference on Transparent Optical Networks*, vol. 4, 2006, pp. 52–55.

[17] J. Tang and K. A. Shore, "30Gb/s signal transmission over 40km directly modulated DFB-laser-based single-mode-fiber links without optical amplification and dispersion compensation," *Journal of Lightwave Technology*, vol. 24, no. 6, p. 2318, Jun. 2006.

Chapter 6

Conclusion and Future Work

6.1 Conclusion

Increasing numbers of broadband connections means that total IP traffic continues to grow. The increased demand for new digital services means that internet service providers and governments alike are incentivised to invest in higher capacity optical networks in order to meet customer requirements. To realise these next generation optical networks, new advanced modulation formats and novel optical components, capable of providing high data rates and spectral efficiency, will have to be utilised. Furthermore, due to the nature of dynamic traffic patterns, future designs will be required to incorporate a higher level of reconfigurability so that an efficient use of the shared optical network can be provided.

The addition of Wavelength Division Multiplexing to optical networks has led to a more efficient use of optical fibres. However, as operators seek to further increase network capacity, more optical channels are required to allow for higher cumulative data rates and a greater number of users to be reached. This migration to increasingly smaller grid sizes can only be facilitated by the addition of more spectrally efficient modulation formats.

In access networks, a key advancement leading to the provision of higher speed connectivity will be the replacement of Hybrid Fibre Coaxial type networks with all optical access

networks – Fibre-to-the-Home. Overcoming this current traffic bottleneck presents a major challenge to network designers in terms of meeting the technical requirements of next generation access networks mentioned above in a cost effective manner.

In this thesis, Orthogonal Frequency Division Multiplexing is proposed as a modulation format, for both Access and Metropolitan Area Networks, capable of providing the data rates and spectral efficiencies needed for next generation designs. The use of OFDM in these network scenarios also provides a high tolerance to chromatic dispersion and potential for increased network reconfigurability. The application of OFDM to both of these network layers is experimentally investigated in this thesis and the main results are outlined below.

OFDM Passive Optical Networks

In Chapter 3, the transmission of directly modulated OFDM in a Passive Optical Network setup is demonstrated. The effects of nonlinearties introduced by the directly modulated laser are reduced by employing optical injection. This technique is performed using both an external laser and a novel two section monolithically integrated device which is suitable for use in PONS due to its low cost and footprint. A reduction of up to 10dB in the levels of IMD3 is shown, removing a performance limitation on the OFDM system. Improvement in BER from 2.4×10^{-3} to 3.25×10^{-5} when optical injection is used is shown over 50km of SSMF. Net data rates up to 15.5Gb/s are achieved with AM–OFDM when optical injection is employed.

The use of a novel Slotted Fabry–Pérot tuneable laser in a PON scenario is shown in chapter 4. The device is characterised and is found to have a tuning range of 14nm from 1557.68nm to 1571.72nm. Several of the available modes are used for transmission of AM–OFDM signals and raw data rates of 21.13Gb/s in the back-to-back case and 14.30Gb/s over 50km of SSMF are achieved. Dispersive fading is shown to exert a performance limitation for transmission over 50km of fibre.

Optical Burst Mode OFDM

Chapter 5 describes the use of OFDM in an Optical Burst Switched system. OBS systems are desirable where a ring network topology is utilised, as is the case in Metro networks. Work presented in chapter 5 demonstrates the use of Single Sideband OFDM with a single fast switching SG–DBR laser. SSB OFDM is shown to overcome the effects of dispersive fading. External modulation is used in order to achieve SSB modulation of 15Gb/s OFDM bursts, which are modulated onto one of two wavelengths provided by the switching source. Results are presented in terms of the performance of the OFDM packet at various delay times after a switching event, for WDM grid sizes of 50GHz, 25GHz and 12.5GHz. The various grid sizes are found to have an impact on the performance of the OFDM bursts to different degrees. In the case of 12.5GHz grid filtering, the total burst BER reduces below the FEC limit to 4.5×10^{-4} approximately 8ns after a switching event. For this WDM grid size a spectral efficiency of 1.2b/s/Hz is achieved.

6.2 Future Work

Work in this thesis has shown the potential of OFDM to meet many of the requirements for next generation optical networks. However, many areas directly related to this work remain in need of further investigation.

OFDM–PON Architectures

Many forms of PONs have been previously proposed, including light centralised PONs, reflective PONs and PONs capable of transmitting various modulation formats. The application to, and suitability of, OFDM to these different PON architectures could be investigated. In particular, the investigation of OFDM for PONs which are capable of carrying broadband user data as well as Radio-over–Fibre signals (RoF–PON) would be of interest, as current and next generation wireless radio standards such as WiMAX and LTE already specify the use of OFDM.

Increasing Throughput

With regard to the use of OFDM in metro networks, data rates per optical channel will soon migrate to 40Gb/s. To avoid the use of expensive high speed electronics, it is important to investigate new ways in which either greater OFDM bandwidths can be generated from existing electronics or performance can be improved – which would allow for higher order modulation formats to be used on OFDM subcarriers. Methods to achieve this which merit further exploration include, the use of a pilot tone to allow coherent detection in the RF domain and the development of new DSP to compensate for impairments introduced by optical components.

LC Algorithm for Nonlinear Applications

As described in chapter 3, the Levin–Campello algorithm which is used to produce a bit distribution for OFDM subcarriers cannot be considered to be optimal where the transmission channel exhibits high levels of nonlinearity, as is the case when direct modulation is used. A new version of the LC algorithm which factors in the levels nonlinearity introduced by direct modulation could be derived, thereby improving the bit distribution, leading to higher data rates/improved performance.

Appendix A

List of Publications Arising From This Work

A.1 Referred Journal Papers

1. K. Shi, F. Smyth, D. Reid, **C. Browning**, B. Roycroft, B. Corbett, F. Peters, and L. Barry, "Fast Switching Slotted Fabry-Perot Laser for Phase Modulated Transmission Systems," *Journal of Lightwave Technology*, vol. 28, pp. 3409–3416, 2010.

2. **C. Browning**, K. Shi, S. Latkowski, P.M. Anandarajah, F. Smyth, B. Cardiff, R. Phelan, and L.P. Barry, "Performance Improvement of 10Gb/s Direct Modulation OFDM by Optical Injection using Monolithically Integrated Discrete Mode Lasers," *Optics Express*, vol. 19, B289-B294, 2011.

3. K. Shi, R. Watts, D. Reid, T.N. Huynh, **C. Browning**, P.M. Anandarajah, F. Smyth and L.P. Barry, "Dynamic Linewidth Measurement Method via an Optical Quadrature Front End," *IEEE Photonics Technology Letters*, vol. 23, no. 21, pp. 1591–1593, Nov. 2011.

4. **C. Browning**, K. Shi, F. Smyth, B. Cardiff, P.M. Anandarajah, L.P. Barry, "Perform-

ance Enhancement of 10Gb/s Direct Modulation Optical OFDM by External Optical Injection", *Optics Communications*, Vol. 285, No. 2, pp. 136–139, Jan. 2012.

5. P.M. Anandarajah, S. Latkowski, **C. Browning**, Z. Rui, J. O'Carroll, R. Phelan, B. Kelly, J. O'Gorman and L.P. Barry, "Integrated Two-Section Discrete Mode Laser", *IEEE Photonics Journal*, vol. 4, no. 6, pp. 2085–2094, Dec. 2012.

6. **C. Browning**, K. Shi, S. Latkowski, P.M. Anandarajah, F. Smyth, B. Cardiff and L.P. Barry, "Increased Bit Rate Direct Modulation AMO-OFDM Transmission by Optical Injection Using Monolithically Integrated Lasers," *IEEE Photonics Technology Letters*, vol. 24, no. 11, pp.879–881, June 2012.

7. **C. Browning**, K. Shi, P.M. Anandarajah, R. Phelan, and L.P. Barry, "Direct Modulation of a Tuneable Slotted Fabry-Pérot Laser with Adaptive Modulation OFDM," *Optics Express*, vol. 20, B399-B404, 2012.

8. **C. Browning**, K. Shi, A.D. Ellis and L.P. Barry, "Optical Burst Switched SSB-OFDM using a Fast Switching SG-DBR Laser," *IEEE/OSA Journal of Optical Communications and Networking*, Under Review, June 2013.

A.2 Conference Papers

1. F. Smyth, **C. Browning**, K. Shi, F. Peters, B. Corbett, B. Roycroft and L.P. Barry, "10.7Gbd DQPSK Packet Transmission using a Widely Tunable Slotted Fabry-Pérot Laser," in *36th European Conference on Optical Communication (ECOC)*, paper Mo.1.F.5, Sept. 2010

2. **C. Browning**, K. Shi, F. Smyth, B. Cardiff, P. Anandarajah, and L. Barry, "Direct Modulation Optical OFDM Performance Enhancement by External Optical Injection," in *CLEO/Europe and EQEC 2011 Conference Digest, OSA Technical Digest*, paper CI15, Mar. 2011.

3. **C. Browning**, K. Shi, S. Latkowski, P. Anandarajah, F. Smyth, B. Cardiff, R. Phelan,

and L. Barry, “Performance Improvement of 10Gb/s Direct Modulation OFDM by Optical Injection using Monolithically Integrated Discrete Mode Lasers,” in *37th European Conference on Optical Communication (ECOC)*, paper We.10.P1.61., Sept. 2011

4. L.P. Barry, R. Watts, E. Martin, **C. Browning**, K. Merghem, C. Cal, A. Martinez, R. Rosales, and A. Ramdane, “Characterization of Optical Frequency Combs for OFDM based Optical Transmission Systems,” in *International Conference on Fibre Optics and Photonics, OSA Technical Digest*, paper W2A.2., 2012.

5. **C. Browning**, K. Shi, P. Anandarajah, R. Phelan, and L. Barry, “Direct Modulation of a Tuneable Slotted Fabry-Perot Laser with Adaptive Modulation OFDM,” in *38th European Conference on Optical Communication (ECOC)*, paper P6.10., Sept. 2012.

Appendix B

Gap–to–Capacity

Given a AWGN channel with noise power spectral density N_0 and an average transmit power of P watts, Shannon calculated that the maximum capacity of the channel C bits/s was [1]

$$C = B \times \log_2 \left(1 + \frac{P}{N_0} B\right) \tag{B.1}$$

where B is the channel bandwidth. Expressing this is terms of bits rather than bits/s yields

$$b = \log_2 \left(1 + \frac{E_s}{N_0}\right) \tag{B.2}$$

where b is the maximum achievable number of bits/symbol for the given channel SNR (E_s/N_0 is the energy per symbol to noise power spectral density). Given an expression for the probability of error of M–ary QAM in an AWGN channel [2] (Pg. 372) and then isolating b it is possible to derive a similar expression.

$$P_e \approx 2 \cdot \left(1 - \frac{1}{\sqrt{M}}\right) erfc \left(\sqrt{\frac{3}{2(M-1)} \cdot \frac{E_s}{N_0}}\right) \tag{B.3}$$

where M is the level of QAM being used. As QAM modulation has two dimensions (real and imaginary plane) the probability of error per dimension can be denoted Pe'

$$P_e' \approx \left(1 - \frac{1}{\sqrt{M}}\right) erfc\left(\sqrt{\frac{3}{2(M-1)} \cdot \frac{E_s}{N_0}}\right) \tag{B.4}$$

and since typically $\sqrt{M} \gg 1$,

$$P_e' \approx erfc\left(\sqrt{\frac{3}{2(M-1)} \cdot \frac{E_s}{N_0}}\right) \tag{B.5}$$

The number of bits/symbol b can be incorporated into the expression by noting that $M = 2^b$.

$$P_e' \approx erfc\left(\sqrt{\frac{3}{2(2^b-1)} \cdot \frac{E_s}{N_0}}\right) \tag{B.6}$$

Isolating b gives

$$\rightarrow b = \log_2\left(1 + \frac{E_s/N_0}{\frac{2}{3}(erfc^{-1}(P_e'))^2}\right) \tag{B.7}$$

For simplicity let

$$\Gamma \triangleq \frac{2}{3}(erfc^{-1}(P_e'))^2 \tag{B.8}$$

allowing equation B.7 to be rewritten as

$$\rightarrow b = \log_2\left(1 + \frac{1}{\Gamma} \cdot \frac{E_s}{N_0}\right) \tag{B.9}$$

Equation B.9 is almost identical to B.2 with the inclusion of an added Γ term which is known as the modulation 'gap to capacity' as it can be used to measure the proximity of data rates to the maximum theoretical value, the channel capacity expressed in equation B.1. It follows that when $\Gamma = 1$ the data rate is at its highest.

References

[1] S. Haykin, *Communication Systems, 4th Edition*. Wiley, 2001, ch. Fundamental Limits in Information Theory, p. 599.

[2] ——, *Communication Systems, 4th Edition*. Wiley, 2001, ch. Passband Data Transmission, p. 372.

Appendix C

Matlab Model

C.1 OFDM Transmitter and Receiver

```
%% QAM - OFDM optical system
clear all
close all
clc

%% Setup
Nbits=128;          %number of symbols
Nsamps=256;         %samples per FFT
N=Nbits*Nsamps;     %Total Number of data points
CPS=0.0625;         %size of cyclic prefix 6.25%

symrate=39.062500e6;
RFfreq=2.8e9;

dt=1/(symrate*Nsamps);
df=1/dt;
```

```
17 dt_sym = 1/symrate;
18 Nncp=N;
19 N=N*(1+CPS);
20 %define axes
21 time=(0:(Nsamps-1))*dt;
22 timecp=(0:(Nsamps-1)*(1+CPS))*dt;
23 freq=(-(Nsamps/2):(Nsamps/2-1))*1/(dt*Nsamps);
24 FREQ=(-(N/2):(N/2-1))*1/(dt*N);
25 TIME=(0:(N-1))*dt;
26 FREQncp=(-(Nncp/2):(Nncp/2-1))*1/(dt*Nncp);
27 TIMEncp=(0:(Nncp-1))*dt;
28 %Subcarrier arrangement
29 Numchans=74;
30 BufferLow=0;
31 BufferHigh=Nsamps-Numchans-BufferLow;
32 ChansPerSide=Numchans/2;
33 TP_number = 1;
34 Signal_Bandwidth = (2/max(timecp)) + ((Numchans-1)/max(time)
       );
35 %% OFDM Transmitter
36 order=32;
37 %bitstream
38 bits=randint(Numchans,Nbits,order,1);
39 SNRtotal = zeros(1,Numchans);
40 EVMavg_total = zeros(1,Numchans);
41 for loops = 1:150
42 %QAM Modulation
43 bitsqam=qammod(bits,order);
```

```
44 %Normalise
45 Con_Norm_Factor = sqrt(1/mean(mean(abs(bitsqam).^2)));
46 bitsqam=bitsqam*Con_Norm_Factor;
47 %Define Training Symbols
48 TP=(exp(1i*pi.*((1:Numchans).^2)/Numchans)).';
49 bitsqam(:,TP_number)=TP;
50 %Construct IFFT input
51 OFDMA=zeros(BufferLow/2,Nbits);
52 OFDMB=bitsqam((ChansPerSide+1):Numchans,:);
53 OFDMC=zeros(BufferHigh,Nbits);
54 OFDMD=bitsqam(1:ChansPerSide,:);
55 OFDME=zeros(BufferLow/2,Nbits);
56 OFDMfreq=[OFDMA;OFDMB;OFDMC;OFDMD;OFDME];
57 %IFFT
58 Ein=ifft(OFDMfreq);
59 %Add CP
60 CP=Nsamps*CPS;
61 Ein=[Ein((Nsamps-CP+1):Nsamps,:);Ein];
62 Ein=reshape(Ein,N,1);
63 %Iso I and Q
64 Iin=real(Ein);
65 Qin=imag(Ein);
66 %% RF Mixing up
67 ang=2*pi*RFfreq*(1:length(Iin))*dt;
68 RFsigin=Iin.*sin(ang')+Qin.*cos(ang');
69 RFsigin=RFsigin-mean(RFsigin);
70 RFsigin = (RFsigin./max(RFsigin));
71 %% Channel (Optical Source + Modulation + Fibre + Detector)
```

```
MyChan_DM_complete_LongSim
%% RF Mix down
Iout=RFsigout.*sin(ang');
Qout=RFsigout.*cos(ang');
Eout=Iout+1i*Qout;
%% OFDM Receiver
%remove CP
FrameCP=Nsamps*(1+CPS);
offs=round(0*Nsamps*CPS);
Esamp=reshape(Eout,FrameCP,Nbits);
Esamp=Esamp((CP+1-offs):(FrameCP-offs),:);
%FFT
Edata=fft(Esamp).';
%Extract data carrying subcarriers
HighSideOut=Edata(:,(BufferLow/2+1):((BufferLow/2+1)+
    ChansPerSide-1));
LowSideOut=Edata(:,(BufferLow/2+ChansPerSide+BufferHigh+1)
    :((BufferLow/2+ChansPerSide+BufferHigh+1)+ChansPerSide-1)
    );
Chanout=[LowSideOut HighSideOut];
Chanout=Chanout*sqrt(1/mean(mean(abs(Chanout).^2)));
%Extract training sequence
Tout=Chanout(TP_number,:);
ChanEst=Tout./TP.';
Chanout=Chanout(2:end,:);
Chanout_NoEQ = Chanout;
bitsqam=bitsqam(:,2:end);
TIMEncp=TIMEncp((Nsamps+1):end);
```

```
97 %% Equalisation
98 for m=1:Nbits-1,
99     Chanout(m,:)=Chanout(m,:)./ChanEst;
100 end
101 %% EVM
102 %Normalisation factor (Tx)
103 [S1,S2] = size(bitsqam);
104 Nbr_Tx_Symbols = S1*S2;
105 Tx_Total_Symbol_Pwr = sum(sum(abs(bitsqam).^2));
106 Tx_Avg_Symbol_Pwr = Tx_Total_Symbol_Pwr/Nbr_Tx_Symbols;
107 Norm_factor_Tx = sqrt(1/Tx_Avg_Symbol_Pwr);
108 %Normalisation factor (Rx)
109 [S1,S2] = size(Chanout);
110 Nbr_Rx_Symbols = S1*S2;
111 Rx_Total_Symbol_Pwr = sum(sum(abs(Chanout).^2));
112 Rx_Avg_Symbol_Pwr = Rx_Total_Symbol_Pwr/Nbr_Rx_Symbols;
113 Norm_factor_Rx = sqrt(1/Rx_Avg_Symbol_Pwr);
114 %calculate EVM
115 EVM_rms = ((sum(sum((abs((real(Chanout).*Norm_factor_Rx) - (
        real(bitsqam.').*Norm_factor_Tx)).^2) + (abs((imag(
        Chanout).*Norm_factor_Rx)- (imag(bitsqam.').*
        Norm_factor_Tx)).^2))))/Nbr_Rx_Symbols)^0.5;
116 EVM_graph = ((abs((real(Chanout).*Norm_factor_Rx) - (real(
        bitsqam.').*Norm_factor_Tx)).^2) + (abs((imag(Chanout).*
        Norm_factor_Rx) - (imag(bitsqam.').*Norm_factor_Tx)).^2)
        .^0.5).*100;
117 EVMavg = ((mean((abs((real(Chanout).*Norm_factor_Rx) - (real
        (bitsqam.').*Norm_factor_Tx)).^2) + (abs((imag(Chanout).*
```

```
        Norm_factor_Rx) - (imag(bitsqam.').*Norm_factor_Tx)).^2))
        ).^0.5).*100;
118 EVMstd=std(EVM_graph);
119 SNRpsc = (1./(EVMavg/100)).^2;
120 %Store Data
121 EVMavg_total = EVMavg + EVMavg_total;
122 SNRtotal = SNRpsc + SNRtotal;
123 loops
124 end
125 SNRtotal_avg = SNRtotal./loops;
126 EVMavg_total_avg = EVMavg_total./loops;
127 %% QAM Demodulation
128 bitsqam_test = (bitsqam.')/Con_Norm_Factor;
129 bitsqam_demod = qamdemod(bitsqam_test,order);
130 Chanout_test = Chanout/Con_Norm_Factor;
131 Chanout_demod = qamdemod(Chanout_test,order);
132 %reshape
133 bitsqam_demod = reshape(bitsqam_demod,(Nbits-1)*Numchans,1);
134 Chanout_demod = reshape(Chanout_demod,(Nbits-1)*Numchans,1);
135 %convert to binary
136 bitsqam_demod_bin = dec2bin(bitsqam_demod, log2(order));
137 Chanout_demod_bin = dec2bin(Chanout_demod, log2(order));
138 %Calculate BER
139 Errors = abs(bitsqam_demod_bin - Chanout_demod_bin);
140 BitErrors = sum(sum(Errors));
141 [BitsSizeA, BitsSizeB] = size(bitsqam_demod_bin);
142 TotalNbrBits = BitsSizeA*BitsSizeB;
143 BER_actual = 1/(TotalNbrBits/BitErrors);
```

```
144 %% Figures
145 %calculate spectra
146 Einf=abs(fftshift(fft(fftshift(Ein)))).^2;
147 Eoutf=abs(fftshift(fft(fftshift(Eout)))).^2;
148 FREQG=FREQ*1e-9;
149 ax=[min(FREQG) max(FREQG) -60 0];
150 %Plot Rx Constellation
151 figure(1)
152 plot(real(Chanout_NoEQ),imag(Chanout_NoEQ),'.')
153 title('Rx constellation: all channels')
154 axis square
155 %Plot Tx/Rx spectra
156 figure(2)
157 subplot(2,1,1), plot(FREQG,10*log10(RFsiginf/max(RFsiginf)))
158 title('Tx RF spectrum')
159 axis(ax)
160 subplot(2,1,2),plot(FREQG,10*log10(RFsigoutf/max(RFsigoutf))
      )
161 title('Rx RF spectrum')
162 axis(ax)
163 %% Performance Parameters
164 BW_ofdm = (2/max(timecp)) + ((Numchans-1)/max(time))
165 Data_Rate = symrate*Numchans*log2(order)
166 SNR = (1/EVM_rms)^2
167 SNRdB = 10*log10(SNR)
168 SER = EVM2SER(EVM_rms,BW_ofdm/(Numchans*symrate),order)
169 SER_best = EVM2SER(EVM_rms_Best,BW_ofdm/(Numchans*symrate),
      order);
```

```
170 SER_worst = EVM2SER(EVM_rms_Worst,BW_ofdm/(Numchans*symrate)
        ,order);
171 BER_actual
```

C.2 Optical Channel

```
1  %% Direct Modulation Optical Channel Parameters
2  amp = 15e-3;  %A
3  bias = 50e-3; %A
4  time_neg = (-N/2:N/2-1)*dt;
5  %Send signal to rate equations
6  Power = RateEQII(time_neg,RFsigin,amp,bias);
7  Intensity = Power;
8  U = transpose(Intensity);
9  %% Propagatstion Parameters
10 LaunchP=5;       %Power (dBm)
11 lambda=1550;     %Wavelength (nm)
12 L=50;            %Distance (km)
13 dz=0.001;        %Calculation step size
14 %Send to NLSE propagatgation Model
15 U=PropSMF(U,LaunchP,'FREQ',L,dz,lambda, TIME);
16 U=U.';
17 %% Reciever (optional EDFA pre-amplification)
18 %Optical Pre-Amplifier
19 % Gain = 5; %dB
20 % Noise_Fig = 3; %dB
21 % U = optamplifier(U,Gain,Noise_Fig,TIME);
22 % Power_Amp_ip_dB = mean(10*log10(abs(U).^2))
23
```

```
%Optical Amplifier
% Gain = 25; %dB
% Noise_Fig = 3; %dB
% U = optamplifier(U,Gain,Noise_Fig,TIME);
% Power_det_ip_dB = mean(10*log10((abs(U).^2)))

%% Photo Detector (Optional RF amplifier)
SBe = 40e9; %Detector response
SGorder=10;
S_filterfunc=exp(-2^(SGorder)*log(2)*(FREQ/SBe).^SGorder);
%send to detector model
RFsigout=Pindetector_NonSeeded(U,S_filterfunc',
    Signal_Bandwidth);

%RF amplifier (AC coupled)
% RFsigout=RFsigout-mean(RFsigout);
% GainRF = 0; %dB
% NFRF = 0.9; %dB
% RFsigout = RFamp(RFsigout, GainRF, NFRF, TIME);
```

C.3 NLSE Propagation Function

```
function Et=propagate(Et1,w,alpha,gamma,beta2,beta3,L,dz,
    TIME)
%Input Electric Field
Et=Et1;

if beta2==0,      %for 0 dispersion
    It=abs(Et).^2;
```

```
7       %Calculate nonlinearity and loss
8       Et = Et.*exp(L*(-alpha/2+1i*gamma*(abs(Et)).^2));
9   elseif gamma==0, %for 0 nonlinearity
10      %Frequency domain
11      Ef = fftshift(fft(fftshift(Et)));
12      %calculate just dispersion and loss
13      Ef = Ef.*exp(L*(-alpha/2+(1i/2)*beta2*w.^2-(1i/6)*beta3*
            w.^3));
14      %Time domain
15      Et = fftshift(ifft(fftshift(Ef)));
16  else
17      z=0;            %set current propagation length
18      Nbr_Span = 0; %set current number of spans
19      while z<L,
20          It=abs(Et).^2;
21          if L-z<dz,
22              dz=L-z;
23          end
24          %NLSE
25          Ef = fftshift(fft(fftshift(Et)));
26          Ef = Ef.*exp(dz*(-alpha/2+(1i/2)*beta2*w.^2));
27          Et = fftshift(ifft(fftshift(Ef)));
28          Et = Et.*exp(dz*1i*gamma*(abs(Et)).^2);
29          %Update current length
30          z=z+dz;
31      end
32  end
```

Appendix D

Two Section Discrete Mode Laser Characterisation

D.1 Static Characterisation

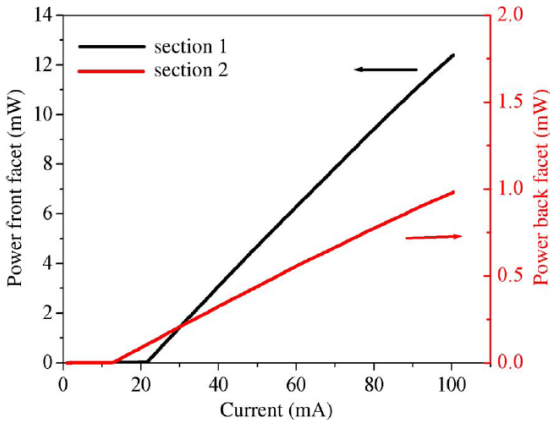

Figure D.1: Light-Current curve

Light-Current curves from the individually biased maser and slave lasers at 20°C. Threshold currents of 21 mA for the slave section and 12 mA for the master section have been extracted. The light from master section was measured out through the HR coated back facet.

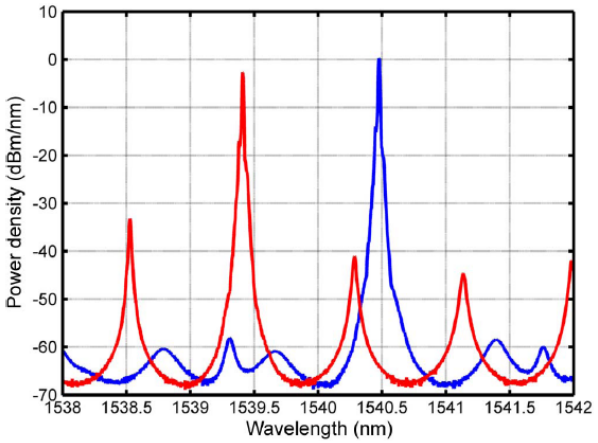

Figure D.2: CW optical spectra of the two-section monolithically integrated DM laser.

Figure D.2 shows the optical spectra of the two-section monolithically integrated DM laser. The red line corresponds to the spectrum when only the slave laser is turned on while the blue line shows the spectrum for the case where both the slave and master lasers are turned on.

D.1.1 Relative Intensity Noise (RIN)

The averaged RIN (0.6 to 10 GHz) for the case where only the slave section was turned on was about -129.3 dB/Hz. In this case, the slave section was biased at 45.6 mA, and the master was biased at 0 mA. The averaged RIN (0.6 to 10 GHz) for the second scenario where both the master and slave sections were turned on was measured to be -142.6 dB/Hz. Here, again, the slave section bias is maintained at 45.6 mA, while the master section bias was set at 50 mA.

D.2 Dynamic Characterisation

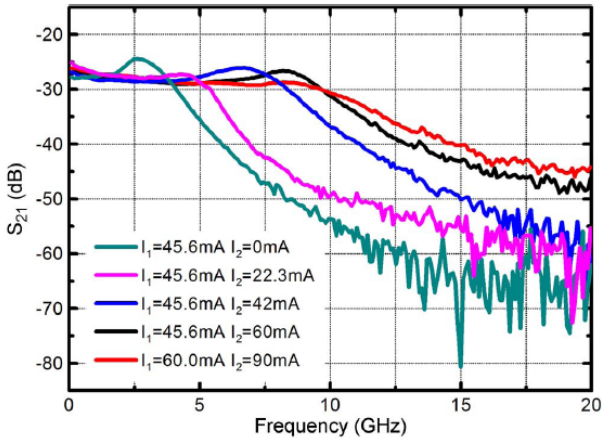

Figure D.3: Frequency response at various bias currents.

Frequency response of the two-section monolithically integrated DM laser. The different colours correspond to different bias scenarios (currents on the slave and master sections of the laser).

Appendix E

Discrete Mode Tuning Maps

Shown below are additional SMSR and wavelength tuning maps to that given in section 4.3.1. The graphs are generated by varying the bias current to both sections of the tuneable SFP device between 20mA and 80mA while the output wavelength and SMSR is monitored.

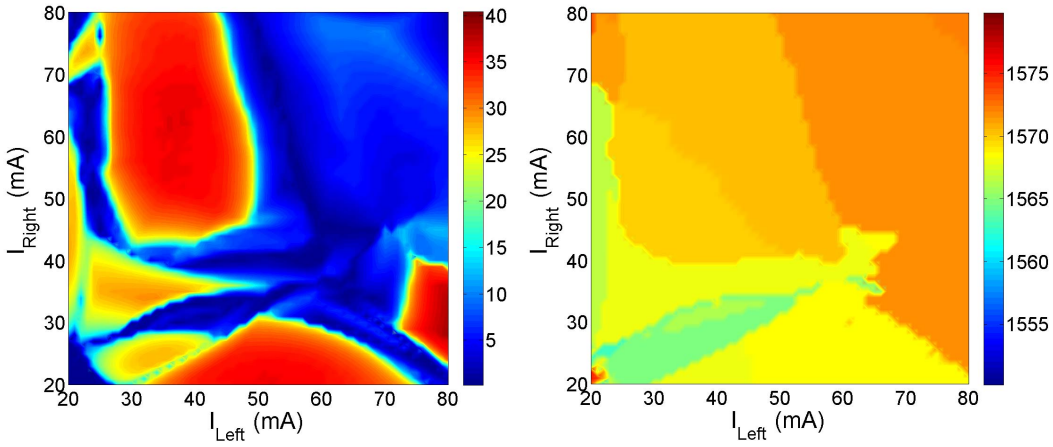

(a) (b)

Figure E.1: SMSR (a) and wavelength (b) tuning maps at 22.5°C.

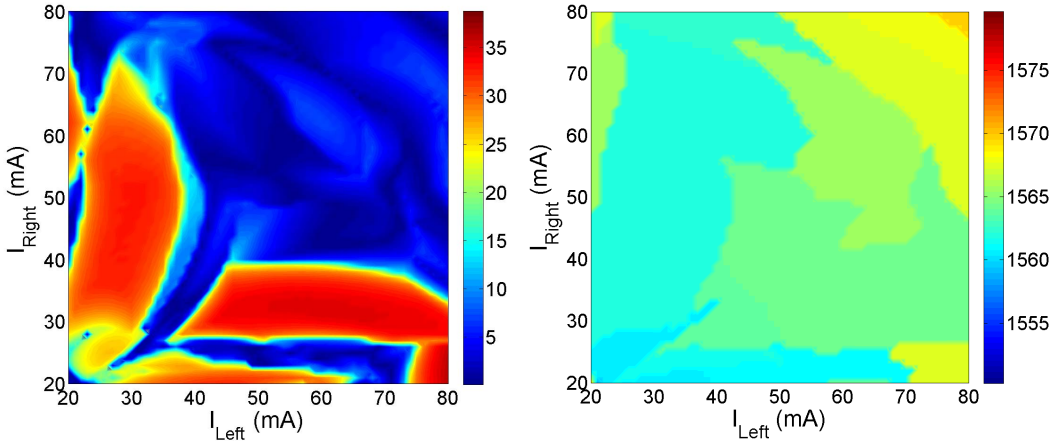

(a) (b)

Figure E.2: SMSR (a) and wavelength (b) tuning maps at 8°C.

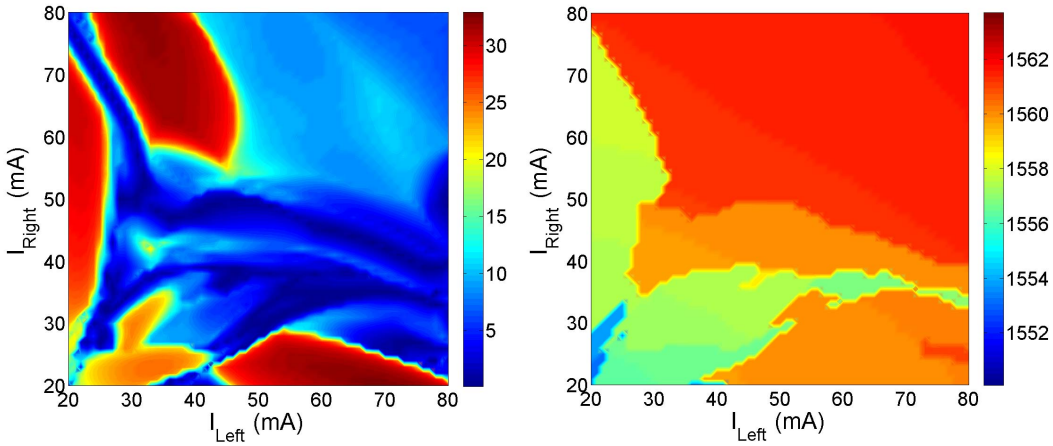

(a) (b)

Figure E.3: SMSR (a) and wavelength (b) tuning maps at 2.5°C.